

Deanship of Graduate Studies  
AL - Quds University



Estimation of Noisy Multichannel Autoregressive  
Processes Using Optimal Filters

Nidal A. Shakarneh

M.Sc. Thesis

Jerusalem - Palestine

May, 2009



---

# Estimation of Noisy Multichannel Autoregressive Processes Using Optimal Filters

By

Nidal A. Shakarneh

B.Sc.:Electrical Engineering, Birzeit University,  
Palestine

A thesis submitted in partial fulfillment of the requirements for the degree of Master of Electronic and Computer Engineering, Faculty of Engineering

Supervisor: Dr. Ali Jamoos

Co-supervisor: Dr. Hanna Abdel Nour

Al-Quds University

May, 2009

---

Electronic and Computer Engineering Master Program  
Faculty of Engineering  
Al-Quds University

Thesis Approval

Estimation of Noisy Multichannel Autoregressive Processes Using Optimal  
Filters

By

Student Name: Nidal Ali Shakarneh  
Reg. No: 20611276

Supervisor: Dr. Ali Jamoos  
Co-supervisor: Dr. Hanna Abdel Nour

Master thesis submitted and accepted.

Date: \_\_\_\_\_

The names and signatures of the examining committee members are as follows:

1- Dr. Ali Jamoos	: Head of Committee	Signature: _____
2- Dr. Hanna Abdel Nour	: Member of Committee	Signature: _____
3- Dr. Samer Bali	: Internal Examiner	Signature: _____
4- Dr. Allam Musa	: External Examiner	Signature: _____
5- Dr. Eric Grivel	: External Examiner	Signature: _____

## Dedication

*I dedicate this work to my grand-dad,  
who supports and encourages me in my life,  
my parents, brother and sisters*

## Declaration

I certify that this thesis submitted for the degree of Master is the result of my own research, except where otherwise acknowledged, and that this thesis (or any part of the same) has not been submitted for higher degree to any other university or institution.

Signed:.....

Nidal Ali Shakarneh

Date:.....

## Acknowledgements

I would like to thank Dr. Ali Jamoos for his guidance, encouragement, advices and insightful comments during my work period. In addition, I would like to thank him for providing me with the important references (books, scientific magazine and IEEE papers).

I would like to thank Dr. Hanna Abdel Nour for his guidance, encouragement, advices, insightful comments and for reviewing my report and slides.

## Abstract

Multichannel Autoregressive (M-AR) parametric model has been recently used to model multichannel processes arise in many applications such as in sonar, radar, speech processing, biomedical engineering and wireless communications.

In the framework of wireless communications, each carrier in multicarrier systems ( e.g., Orthogonal Frequency Division Multiplexing (OFDM) ) is usually affected by time-varying fading. The fading processes over all carriers are often correlated and corrupted by Additive White Gaussian Noise (AWGN). In this application, the fading processes are usually modeled by M-AR model which can be combined with optimal filters such as Kalman or  $H_\infty$  filter for processes estimation from noisy observations. This requires the estimation of M-AR model parameters which is the key issue to be addressed in this thesis.

Several M-AR parameter estimation methods have been proposed in the literature and can be classified as either off-line or on-line estimation techniques.

The off-line methods can be used when all observations are available for the estimation process. Off-line techniques such as Noise-Compensated Yule-Walker (NCYW) equations, Yule-Walker equations combined with Newton-Raphson, Improved Least Square for Vector (ILSV) processes and Errors-In-Variables (EIV) based method are all of interest. However, their computational costs are very high or some of them may diverge. In addition, these techniques are not suitable for on-line applications.

Using on-line techniques such as Kalman filter applied directly to the noisy observations results in biased parameter estimates. To avoid this problem, joint estimation of the process and its parameters based on Extended Kalman Filter (EKF) and Sigma Point Kalman Filter (SPKF) can be addressed. However, the size of the state vector to be estimated is quite high. To reduce the size and the resulting computational costs, we propose to use two cross-coupled optimal filters. Thus, we propose to extend to the multichannel case the so-called two cross-coupled Kalman or  $H_\infty$  filters initially introduced for the single channel case. We carry out a comparative simulation study between our methods and several other methods. This study is based either on synthetic M-AR process or M-AR process corresponds to fading channels. The results we obtained showed that our approach corresponds to a compromise between the computational cost and the performance in terms of parameter estimation accuracy.





# List of Tables

1.1	Simulation of correlated fading channels based on vector AR model [Bad04].	22
2.1	Hassan's method for M-AR parameter estimation from noisy observations [Has03]. . . . .	35
2.2	Kalman algorithm for M-AR process estimation. . . . .	38
2.3	$H_\infty$ algorithm for M-AR process estimation. . . . .	41
2.4	Kalman algorithm for parameters estimation of M-AR process. . . . .	43
2.5	$H_\infty$ algorithm for parameters estimation of M-AR process. . . . .	43
2.6	CC-Kalman filtering algorithm. . . . .	47
2.7	CC- $H_\infty$ filtering algorithm. . . . .	50
3.1	The true and estimated parameters at SNR=10dB based on 300 samples. .	55
3.2	The true and estimated poles at SNR=10dB based on 300 samples. . . . .	56
3.3	MSE of modulus and argument of the estimated poles at SNR=10dB based on 300 samples. . . . .	56
3.4	The true and estimated parameters at SNR=10dB based on 2000 samples.	59
3.5	The true and estimated poles at SNR=10dB based on 2000 samples. . . . .	59
3.6	MSE of modulus and argument of the estimated poles at SNR=10dB based on 2000 samples. . . . .	61
3.7	The MSE of the arguments and the modulus of pole#1 for different $\beta^{(i)}$ based on 1024 samples and SNR=[10,5]dB. . . . .	63
3.8	The true and estimated parameters at SNR=10dB based on 300 samples. .	67
3.9	The true and estimated poles at SNR=10dB based on 300 samples. . . . .	67
3.10	MSE of modulus and argument of the estimated poles at SNR=10dB based on 300 samples. . . . .	69
3.11	The true and estimated parameters at SNR=10dB based on 2000 samples.	70
3.12	The true and estimated poles at SNR=10dB based on 2000 samples. . . . .	70

3.13 MSE of modulus and argument of the estimated poles at SNR=10dB based on 2000 samples. . . . .	72
---	----

# List of Figures

1.1	Several applications where the observed signals can be modeled as M-AR process. . . . .	5
1.2	Stochastic model. . . . .	6
1.3	Transfer function of the ARMA model. . . . .	8
1.4	Transfer function of the MA model. . . . .	8
1.5	Transfer function of the AR model. . . . .	9
1.6	Multi-path fading in wireless mobile communication systems. . . . .	10
1.7	(a) PSD of multi-carrier DS-CDMA signal. (b) PSD of wide-band single-carrier DS-CDMA signal [Jam07a]. . . . .	11
1.8	Illustration of the Doppler effect [Jam07a]. . . . .	11
1.9	PDF for the Rayleigh envelope and phase. . . . .	13
1.10	The envelope and phase of Rayleigh fading process. . . . .	13
1.11	The envelope and phase of multichannel Rayleigh fading channels. . . . .	21
1.12	ACF and CCF of the of multichannel Rayleigh fading. . . . .	21
2.1	Transfer operator $\mathcal{T}$ . . . . .	39
2.2	SC-Kalman or SC- $H_\infty$ filters. . . . .	41
2.3	CC-Kalman or CC- $H_\infty$ filter for the estimation of M-AR process and its parameters. . . . .	44
3.1	The average estimated spectrum and poles averaged over 200 realizations of synthetic M-AR process, at SNR=10dB based on 300 observations using various estimation methods. . . . .	56
3.2	20 realizations for the estimated spectrum and poles of synthetic M-AR process, at SNR=10dB based on 300 observations. . . . .	57
3.3	The average estimated spectrum and poles for synthetic M-AR process, at SNR=10dB based on 2000 observations using various estimation methods. . . . .	58

3.4	20 realizations over 200 realizations of the estimated spectrum and poles of synthetic M-AR process, at SNR=10dB based on 2000 observations. . .	60
3.5	MSE of arguments and modulus for pole#1 based on different number of samples at SNR=10dB. True values of noise covariance matrices are used. .	62
3.6	MSE of arguments and modulus for pole#1 at different SNR based on 1000 samples. True values of noise covariance matrices are used. . . . .	62
3.7	Convergence of the estimated parameters of the first matrix: (a) using CC-Kalman filters, (b) CC- $H_\infty$ filters. . . . .	64
3.8	Convergence of the estimated parameters of the secondmatrix: (a) using CC-Kalman filters, (b) CC- $H_\infty$ filters. . . . .	64
3.9	The average estimated spectrum and poles of fading channels, at SNR=10dB based on 300 observations using various estimation methods. . . . .	66
3.10	20 realizations for the estimated spectrum and poles of multichannel fading processes, at SNR=10dB based on 300 observations. . . . .	68
3.11	The average estimated spectrum and poles of fading channels, at SNR=10dB based on 2000 observations using various estimation methods. . . . .	69
3.12	20 realizations for the estimated spectrum and poles of multichannel fading processes, at SNR=10dB based on 2000 observations. . . . .	71

# Contents

<b>Dedication</b>	<b>iii</b>
<b>Declaration</b>	<b>iv</b>
<b>Acknowledgments</b>	<b>v</b>
<b>Abstract</b>	<b>vi</b>
<b>List of Tables</b>	<b>ix</b>
<b>List of Figures</b>	<b>xi</b>
<b>Table of Contents</b>	<b>xiii</b>
<b>1 Introduction</b>	<b>1</b>
1.1 Motivation . . . . .	2
1.2 Parametric Models for Stochastic Processes . . . . .	6
1.2.1 Autoregressive Moving Average (ARMA) Model . . . . .	6
1.2.2 Moving Average (MA) Model . . . . .	7
1.2.3 Autoregressive (AR) Model . . . . .	8
1.3 Multichannel Mobile Fading Processes . . . . .	9
1.3.1 Fading Channel Description . . . . .	9
1.3.2 Correlated Mobile Fading Channels . . . . .	14
1.3.3 AR Modeling and Simulation of Fading Processes . . . . .	17
1.4 Aims of the Thesis . . . . .	22
1.5 Outlines of the Thesis . . . . .	23
<b>2 Parameter Estimation of Multichannel AR (M-AR) Processes</b>	<b>25</b>
2.1 State-of-the-Art . . . . .	26

2.2	Problem Formulation . . . . .	29
2.3	Off-line Parameter Estimation Methods . . . . .	30
2.3.1	Yule-Walker Equations . . . . .	30
2.3.2	Noise-Compensated Yule-Walker Equations . . . . .	32
2.3.3	Hassan's Method . . . . .	32
2.3.4	Other Off-line Estimation Techniques . . . . .	35
2.4	On-line M-AR Process Estimation Based on Optimal Filters . . . . .	36
2.4.1	Kalman Vs $H_\infty$ for M-AR Process Estimation . . . . .	36
2.4.1.1	Kalman Estimation Algorithm . . . . .	37
2.4.1.2	$H_\infty$ Estimation Algorithm . . . . .	38
2.4.2	Parameter Estimation Directly from the Noisy Observations . . . . .	41
2.4.2.1	Parameter Estimation Using Kalman Filter . . . . .	42
2.4.2.2	Parameter Estimation using $H_\infty$ Filter . . . . .	42
2.4.3	Joint Process and Parameter Estimations . . . . .	44
2.4.3.1	Two Cross-Coupled Kalman Filters . . . . .	44
2.4.3.2	Two Cross-Coupled $H_\infty$ Filters . . . . .	48
<b>3</b>	<b>Simulation Results</b>	<b>51</b>
3.1	Simulation Protocols . . . . .	52
3.2	Parameter Estimation of Synthetic M-AR Process . . . . .	54
3.2.1	Small Sample Size . . . . .	54
3.2.2	Large Sample Size . . . . .	55
3.2.3	Comparative Study Between the CC-Kalman and CC- $H_\infty$ Estimators	61
3.2.3.1	Using True Values of the Noise Covariance Matrices . . . . .	61
3.2.3.2	Using Estimated Noise Covariance Matrices . . . . .	61
3.2.3.3	Convergence Speed . . . . .	65
3.3	Parameter Estimation of Mobile Fading Channels . . . . .	65
3.3.1	Small Sample Size . . . . .	65
3.3.2	Large Sample Size . . . . .	66
<b>4</b>	<b>Conclusions and Future Work</b>	<b>73</b>
4.1	Conclusions . . . . .	74
4.2	Future Work . . . . .	75
	<b>Acronyms and Abbreviations</b>	<b>77</b>

Notations	79
Appendix A	83
Appendix B	84
Appendix C	85
Bibliography	91

# Chapter 1

## Introduction

### Contents

---

1.1	Motivation . . . . .	2
1.2	Parametric Models for Stochastic Processes . . . . .	6
1.3	Multichannel Mobile Fading Processes . . . . .	9
1.4	Aims of the Thesis . . . . .	22
1.5	Outlines of the Thesis . . . . .	23

---

## 1.1 Motivation

Stochastic signals are generated in real-world and can be classified as either discrete or continuous signals [Zei98]. In both cases, the signals may be pure, coming directly from the source to the destination, or corrupted by the noise, which is the case in most applications.

Modeling the stochastic signals is an important issue. Indeed, it forms the theoretical description of a signal processing systems, which can be used to process the signals so as to provide a desired outputs [Hay96]. Moreover, the model make it possible to learn much about the signal source. This means that we can simulate the real-world signal without the necessity to have the actual signal source, mainly, when the cost of getting signals from the actual source is high [Rab89]. The most important reason why using signal models is that, they often work well in practice such as in prediction, recognition and identification systems.

Different models have been used in the literature, depending on the type of signals to be modeled. These models can be either deterministic such as the sum-of-sinusoids and sum-of-exponential, or stochastic models such as the Autoregressive Moving Average (ARMA), the Moving Average (MA) and the Autoregressive (AR) models [Hay96]. The stochastic model represents the signal using a few number of parameter, and characterize the signal by its statistical properties. These models can be used for modeling both single channel and multichannel signals.

Multichannel Autoregressive (M-AR) model appears in wide range of applications (see 1.1). In these applications, different types of stochastic quantities are firstly measured. Then, they are transformed into electrical signals. For example, in the sonar systems, the ultrasound waves reflected from the objects to the receiver are random and can be modeled by M-AR model. By studying these signals we can determine the existence of obstacles in the sea [Bek06]. Also, tracking the marine mammal in the deep seas is possible, by modeling their sounds using M-AR model [Per04].

Many symptoms and diseases affect the human can be discovered and known through measuring the heart, brain and breathing signals. Measuring these signals involves using sensors and electronic devices connected by wires. For example, when measuring the heart signals known as ElectroCardioGram(ECG) and brain signals known as ElectroEncephaloGram(EEG), several poles are placed on the human body and their outputs can be modeled as M-AR model. By analyzing the spectrum of these signals, the doctor can understand the person state and the disease [Arn98] [Gul01] [Ube08].

In radar systems, there is a wide variety of applications in both civil and military

areas where the reflected signals can be modeled by M-AR model. Analyzing these signals, allows to track the targets and determine the position, velocity and acceleration [Pet09a]. Radar is used in Terrain Aided Navigation (TAN) system, it is used to periodically correct the error accumulation of Inertial Navigation System (INS). An imaging laser radar is used to transmit signals to scan the land surfaces, then receives the reflected signals from the terrains to compute the distance and correct the INS [Gon06].

In satellite navigation system such as in the Global Position System (GPS) the transmitted signal from the satellite to the receiver on the earth hits many obstacle and reflects in different directions to reach the receiver. These resulting multipath signal can be modeled by M-AR model. Then, it can be used to estimate the position coordinates on the earth. The autoregressive model can effectively characterize both seasonal and instrumental variations in ice sheet elevation time series constructed from satellite radar or laser altimeter data [Fer04].

In the framework of wireless mobile communication, the transmitted signal scatters from many objects and arrive at the receiver from different paths. These signal paths are added constructively or destructively results in what is called signal fading. In addition, the relative motion between the transmitter and the receiver results in time-varying fading [Jak94]. The fading channels can be modeled by M-AR model for the purpose of estimation or simulation [Che04] [Bad04].

In all of the above applications, we need to estimate the M-AR parameters using the received observations, which are usually correlated and corrupted by the additive noise. Several methods have been studied in order to estimate the parameter of the M-AR process from the noisy observations. These methods can be classified as either off-line or on-line techniques.

The off-line methods can be used when all noisy observations are available for the estimation process such as the Yule-Walker (YW) equations, it has been used widely in the M-AR parameter estimations. However, it provides biased estimates. To overcome this problem, one can use the Noise-Compensated Yule-Walker (NCYW) equations, which however require the preliminary estimation of the additive noise variances. Various off-line estimation methods have been proposed to estimate the noise variances and the M-AR parameters. Thus, Hassan [Has03] has proposed to combine YW equations for parameter estimation with Newton-Raphson method for noise variances estimation. This method might diverge in some cases. In addition, it might result in unstable system. To overcome these drawbacks, the Improved Least Square for Vector (ILSV) processes has been introduced in [Mah08]. It solves a system of linear equations to estimate the additive noise

variances, then applying the YW equations to estimate the M-AR parameters. However, it doesn't work properly at low Signal to Noise Ratio (SNR). To avoid this problem, the author in [Pet09b] proposed Errors-In-Variables (EIV) based approach initially proposed in [Bob07] for speech enhancement. In this method, the noisy observations autocorrelation matrix compensated by a specific diagonal block matrix and whose kernel is defined by the M-AR parameter matrices. However, it has high computational cost.

The computational costs of the off-line methods are very high and some of them may diverge. In addition, these techniques are not suitable for on-line applications. Using on-line techniques such as Kalman filter applied directly to the noisy observations results in biased parameter estimates [Arn98]. To avoid this problem, joint estimation of the process and parameters based on Extended Kalman Filter (EKF) or Sigma Point Kalman Filter (SPKF) can be addressed. However, the size of the state vector to be estimated is quite high. Thus, results in high computational cost. To reduce the size of the state vector and the resulting computational costs, we propose to use two cross-coupled optimal filters. Thus, we propose to extend to the multichannel case the so-called two cross-coupled Kalman (CC-Kalman) filters initially introduced for the single channel case [Lab06]. However, Kalman filter is based on restrictive Gaussian assumptions. To relax them, we also propose to extend to the multichannel case the so-called two cross-coupled  $H_\infty$  filters initially proposed in [Lab07] and used for fading channel estimation in [Jam08].

We carry out a comparative simulation study between our methods and several other methods [Jam09]. The results we obtained showed that our approach corresponds to a compromise between the computational cost and the performance in terms of parameter estimation accuracy.

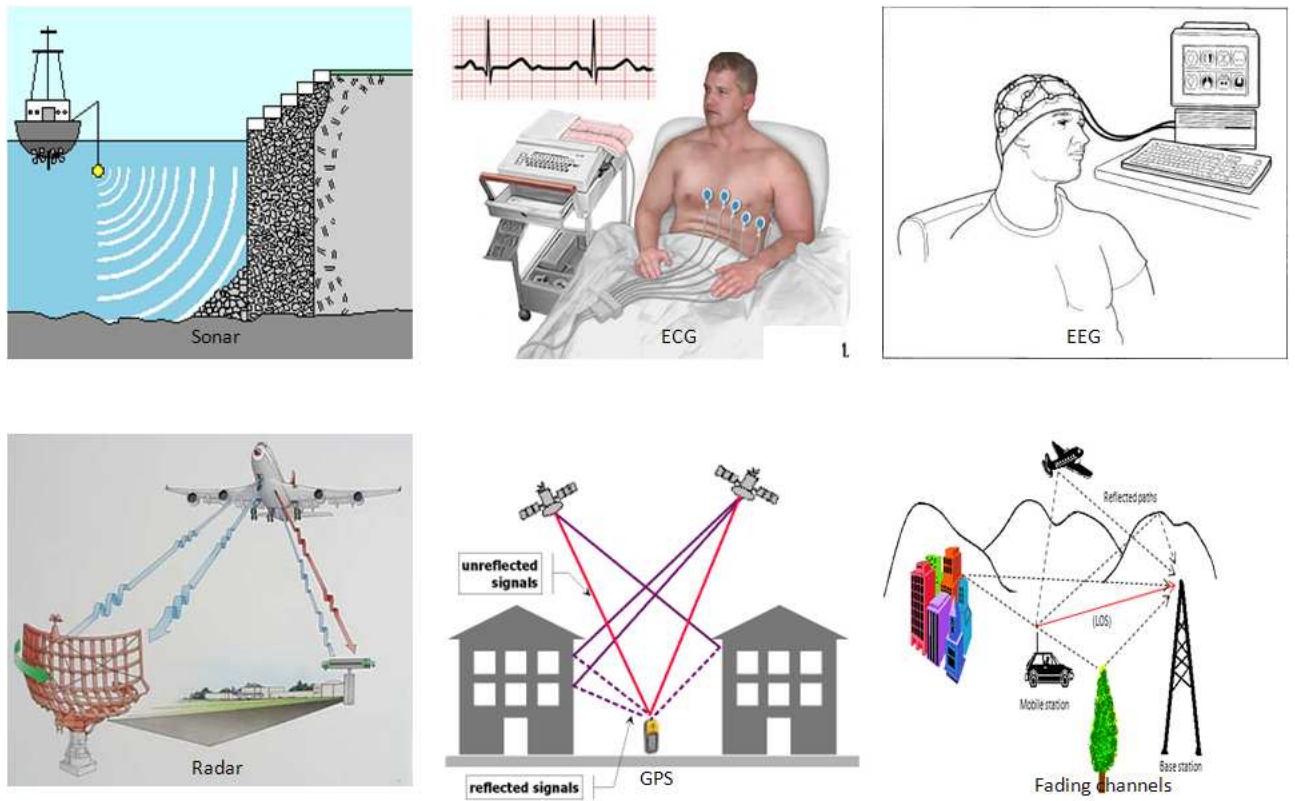


Figure 1.1: Several applications where the observed signals can be modeled as M-AR process.

## 1.2 Parametric Models for Stochastic Processes

A signal corresponds to a physical quantity that varies with time, space, etc.. A wide range of quantities in physics are converted to electrical signals. These signals may be broadly classified into deterministic or stochastic. Deterministic signal is one that may be reproduced exactly with repeated measurements, it can be studied using transformation such as Fourier transform [Zei98].

The stochastic signal is a signal that is not repeatable in a predictable manner. It posses a measure of uncertainty in their values at any instant of time, and their behavior are generally described by probabilistic and statistical averages such as mean, variance and correlation, and ensemble averages such as autocorrelation and autocovariance [Hay96].

These signals can be studied using parametric models such as ARMA, MA and AR with few numbers of parameters [Hay02]. They are simple and helps in estimating and analyzing the stochastic signals.

The term *model* is used to describe any hypothesis that may be applied to explain or describe the hidden laws that are supposed to govern or constrain the generation of physical data of interest. Figure 1.2 shows a block diagram of a general model. In this model  $u(k)$  and  $y(k)$  are the input and the output, respectively.

The representation of a stochastic process by a model dates back to an idea by Yule in 1927. At the end of the 1930s, Wold's decomposition theorem states that any regular and stationary process can be expressed as the sum of two orthogonal processes, one deterministic and the other random.

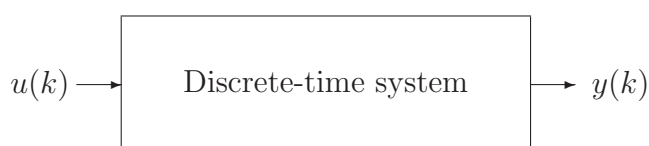


Figure 1.2: Stochastic model.

### 1.2.1 Autoregressive Moving Average (ARMA) Model

The ARMA model is one of the models that can be used to model a random process of correlated data. Consider an analog signal  $y(t)$  represented by  $p+1$  samples corresponding

to time instants  $kT_s, (k-1)T_s, \dots, (k-p)T_s$  as  $\left\{ y(k), y(k-1), \dots, y(k-p) \right\}$  where  $T_s$  is the sampling period.

Suppose that this signal is generated using a white process  $u(t)$  and characterized by  $q+1$  samples as:

$$\left\{ u(k), u(k-1), \dots, u(k-q) \right\}$$

A discrete linear model of the signal can be defined as a linear combination between the samples and the white process as follows:

$$a_0y(k) + \dots + a_py(k-p) = b_0u(k) + \dots + b_qu(k-q) \quad (1.1)$$

This makes the ARMA model, which is said to be of order  $(p, q)$ , where  $\{a_l\}_{l=0, \dots, p}$  and  $\{b_l\}_{l=0, \dots, q}$  are called the transversal parameters. We can note the importance of the ARMA model in (1.1) as it only uses a finite number of parameters and allows for the construction of the signal using these parameters.

Substituting  $a_0 = 1$  in (1.1), one obtain the following equation:

$$y(k) = - \sum_{l=1}^p a_ly(k-l) + \sum_{l=0}^q b_lu(k-l) \quad (1.2)$$

The bilateral  $z$ -transform  $Y(z)$  of  $y(k)$  is defined by:

$$Y(z) = \sum_{k=-\infty}^{+\infty} y(k)z^{-k} \quad (1.3)$$

where  $z$  is a complex variable.

By using the  $z$ -transform, the ARMA model can be written as follows:

$$Y(z) + \dots + a_pY(z) = b_0U(z) + \dots + b_qU(z) \quad (1.4)$$

Then, the transfer function  $H(z)$  of the ARMA model can be expressed as:

$$H(z) = \frac{Y(z)}{U(z)} = \frac{b_0 + b_1z^{-1} + \dots + b_qz^{-q}}{1 + a_1z^{-1} + \dots + a_pz^{-p}} = \frac{B(z)}{A(z)} \quad (1.5)$$

This transfer function is shown in Figure 1.3. The ARMA model is characterized by its poles and zeros, where the poles are the roots of  $A(z)$  and the zeros are the roots of  $B(z)$ .

## 1.2.2 Moving Average (MA) Model

The MA is a special case of (1.2), when the  $\{a_l\}_{l=1, \dots, p}$  are all zeros. Then the MA model is written in time-domain as:

$$y(k) = \sum_{l=0}^q b_lu(k-l) \quad (1.6)$$

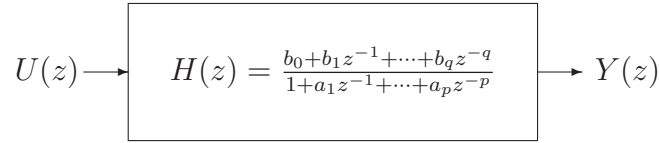


Figure 1.3: Transfer function of the ARMA model.

and the transfer function of the MA model is given by:

$$H(z) = \frac{Y(z)}{U(z)} = b_0 + b_1 z^{-1} + \dots + b_q z^{-q} = B(z) \quad (1.7)$$

From (1.7), one can note that  $H(z) = B(z)$  and  $A(z) = 1$ , which means the MA model is characterized by its zeros only. Thus, this model is named all-zeros model and shown in Figure 1.4

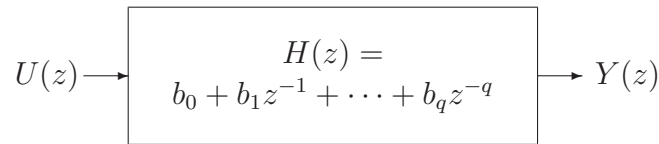


Figure 1.4: Transfer function of the MA model.

### 1.2.3 Autoregressive (AR) Model

The AR model is obtained when the transversal parameters  $\{b_l\}_{l=1,\dots,q}$  are zeros and  $b_0 = 1$ . It can be expressed in time-domain as follows:

$$y(k) = - \sum_{l=1}^p a_l y(k-l) + u(k) \quad (1.8)$$

The transfer function of AR model can be written as follows:

$$H(z) = \frac{Y(z)}{U(z)} = \frac{1}{1 + a_1 z^{-1} + \dots + a_p z^{-p}} = \frac{1}{A(z)} \quad (1.9)$$

This means that the AR model is characterized by the roots of  $A(z)$  which represents the poles of the AR model.

The AR model is highly popular as it can be used to model many processes such as speech signals [Lab07], EEG and ECG signals [Arn98], fading channels [Bad05], etc. .

The AR model can be used to model correlated multichannel processes as in the case of multichannel mobile fading processes [Bad04]. The transfer function of the AR model is shown in Figure 1.5.

$$U(z) \longrightarrow \boxed{H(z) = \frac{1}{1+a_1z^{-1}+\dots+a_pz^{-p}}} \longrightarrow Y(z)$$

Figure 1.5: Transfer function of the AR model.

### 1.3 Multichannel Mobile Fading Processes

Any communication system consists of three main parts: the transmitter, the channel and the receiver. The channel is the physical medium between the transmitter and the receiver.

For most practical channels, where signal propagation takes place in the atmosphere and near the ground, the free space model is inadequate to describe the channel and predict system performance. In wireless mobile communication system the transmitted signal fades along distance. The fading can be large scale over long distances, or small scale over short distances.

In the following section, a description of the mobile fading channels is provided, followed by an explanation of the correlated multichannel mobile fading processes. Then, a procedure on how to simulate these channels is presented.

#### 1.3.1 Fading Channel Description

The multiple reflected signals arrives at the receiver have different amplitude, phase and angle of arrival. These multiple paths arise due to reflection, diffraction and scattering of the electromagnetic wave from objects such as trees, hills, buildings, etc. [Sk197]. See Figure 1.6. When all the multi-paths arrive at the receiver within the symbol duration, the resulting fading is called frequency non-selective fading or flat fading. In the case of frequency selective fading, different frequencies will experience different gains and phase shifts, which spreads the transmitted signal in time leading to Inter Symbol Interference (ISI).

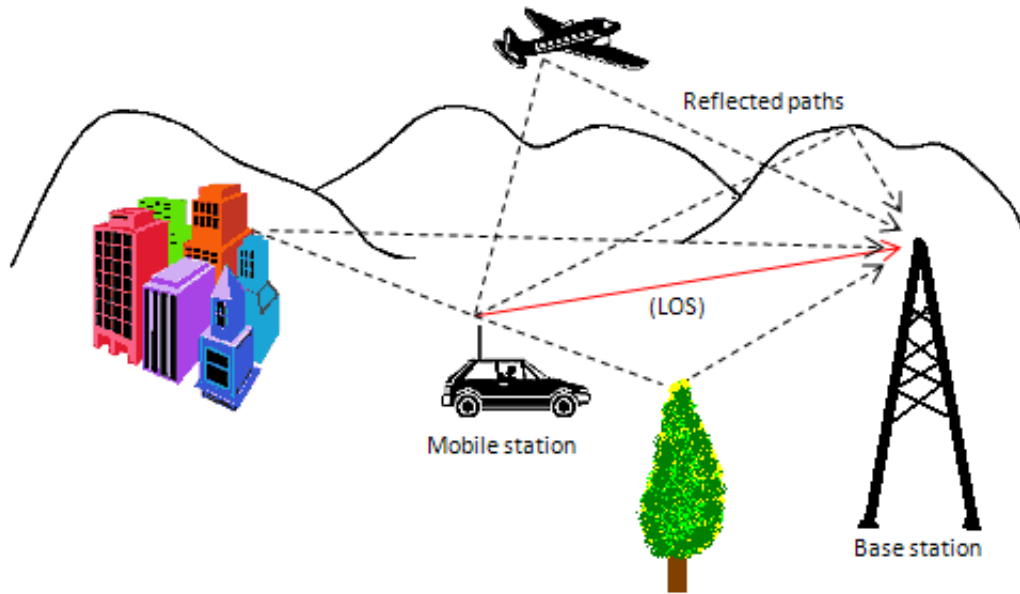


Figure 1.6: Multi-path fading in wireless mobile communication systems.

The maximum delay spread, denoted by  $T_m$  is a parameter describes the fading channel and defined as the range of values over which the power delay profile is non-zero. The channel coherence bandwidth  $B_c$  is the width of the band of frequencies which are similarly affected by the channel. The channel coherence bandwidth is inversely proportional to the channel maximum delay spread:

$$B_c \approx \frac{1}{T_m} \quad (1.10)$$

$B_c$  can be used to decide if the channel is frequency selective or not. If the transmitted signal bandwidth  $W$  is much greater than  $B_c$ , then the channel is frequency selective, and the channel is non-selective when  $W < B_c$ .

The frequency selective channel can be transformed into frequency non-selective channels, by dividing the wide frequency band which is greater than  $B_c$  into narrow frequency bands each with bandwidth less than  $B_c$ . For example, in multi-carrier modulation, a wide-band Direct Sequence-Code Division Multiple Access (DS-SS) signal can be replaced by several narrow-band DS-SS signals, as shown in Figure 1.7 [Jam07a].

The relative motion between the base station and the mobile station is another factor that affects the received signals as shown in Figure 1.8 [Jam07a]. The car is moving with a constant speed  $v$  making angle  $\varphi$  with the direction of propagation. This relative motion

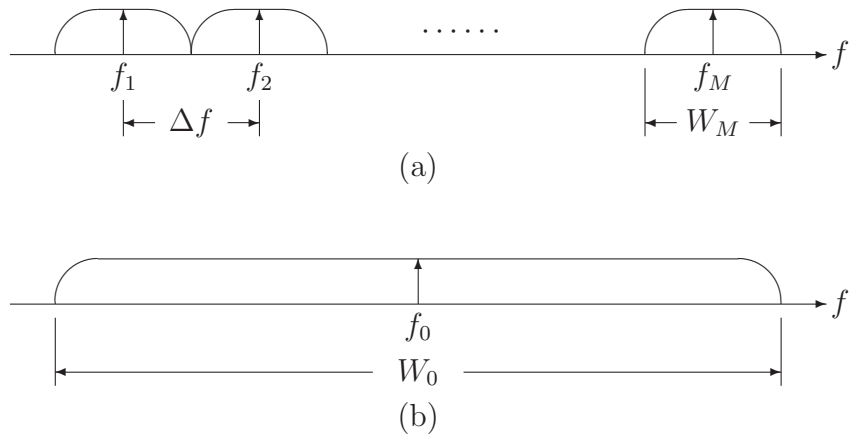


Figure 1.7: (a) PSD of multi-carrier DS-CDMA signal. (b) PSD of wide-band single-carrier DS-CDMA signal [Jam07a].

results in channel time variation due to Doppler shift  $f_D$  which is given by:

$$f_D = \frac{vf_c}{c} \cos(\varphi) \quad (1.11)$$

where  $f_c$  is the carrier frequency and  $c$  is the speed of light.

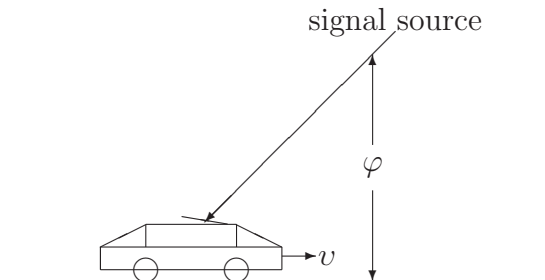


Figure 1.8: Illustration of the Doppler effect [Jam07a].

The maximum Doppler spread or frequency denoted as  $f_d$  can be computed using (1.11) when  $\varphi = 0$  as follows:

$$f_d = \frac{vf_c}{c} \quad (1.12)$$

Depending on the relative motion between the transmitter and the receiver, the channel can be classified as fast or slow fading. In slow fading, the impulse response changes slower than the signal, this occurs when the coherence time of the channel  $T_c$  is larger than the symbol duration  $T_s$  (i.e.  $T_s < T_c$ ). Otherwise, fast fading results when the channel impulse response changes rapidly compared to the signal (i.e.  $T_s > T_c$ ).

In multi-path fading channel, the transmitted signal arrives at the receiver along  $L_p$  resolvable paths. Each path is a superposition of a large number  $L_s$  of local uncor-

related scatters that arrive at the receiver within the symbol duration. Each scatter is characterized by its own random amplitude and phase.

According to Jack's model, the frequency non-selective fading process is given by:

$$h_m(t) = \sum_{l=1}^{L_s} g_{ml} e^{j(2\pi f_d t \cos \varphi_{ml} + \vartheta_{ml})} = |h_m(t)| e^{j\phi_m(t)} \quad (1.13)$$

where  $g_{ml}$ ,  $\varphi_{ml}$  and  $\vartheta_{ml}$  are the random scatterer amplitude, angle of arrival and initial phase for  $m^{\text{th}}$  carrier and  $l^{\text{th}}$  scatterer.

Based on the Central Limit Theorem (CLT) and for large number of scatterer,  $h(t)$  can be approximated as a complex Gaussian process. When there is a dominant Line-Of-Sight (LOS) path between the transmitter and the receiver, then the envelope of the fading process is Rician distributed. While in most cases of mobile communications, there is no direct LOS between the transmitter and the receiver. In this case, the envelope is Rayleigh distributed. In Rayleigh fading channels, the phase  $\phi(t)$  has the uniform distribution over  $[0, 2\pi)$  and the envelope  $\bar{h} = |h_m(t)|$  has the Rayleigh Probability Density Function (PDF) defined as follows:

$$f_{\bar{h}}(\bar{h}) = \begin{cases} \frac{\bar{h}}{\sigma_{h_m}^2} e^{-\bar{h}^2/2\sigma_{h_m}^2}, & \text{if } \bar{h} \geq 0 \\ 0, & \text{otherwise} \end{cases} \quad (1.14)$$

where  $\sigma_{h_m}^2 = E[|h_m(t)|^2]$  is the average power of the fading process.

Figure 1.9 shows a plot of the PDF of the envelope and phase while Figure 1.10 shows the envelope and phase of a fading process.

The value (1.13) can be used to compute the fading process Auto Correlation Function (ACF) as follows:

$$R_{hh}(\tau) = E[h_m(t + \tau)h_m^*(t)] \quad (1.15)$$

$$R_{hh}(\tau) = \sum_{l=1}^{L_s} \sum_{i=1}^{L_s} E[g_{ml} e^{j(2\pi f_d(t+\tau) \cos(\varphi_{ml}) + \vartheta_{ml})} g_{mi}^* e^{-j(2\pi f_d(t+\tau) \cos(\varphi_{mi}) + \vartheta_{mi})}] \quad (1.16)$$

and  $\tau$  the time shift.

Assuming WSS fading process, the different scatterers are uncorrelated:

$$E[g_{ml}g_{mi}] = \begin{cases} E[g_{ml}^2], & \text{if } l = i \\ 0, & \text{otherwise} \end{cases} \quad (1.17)$$

Hence, the ACF can be written as follows:

$$R_{hh}(\tau) = \sum_{l=1}^{L_s} E[g_{ml}^2] E[e^{j2\pi f_d \tau \cos \varphi_{ml}}] \quad (1.18)$$

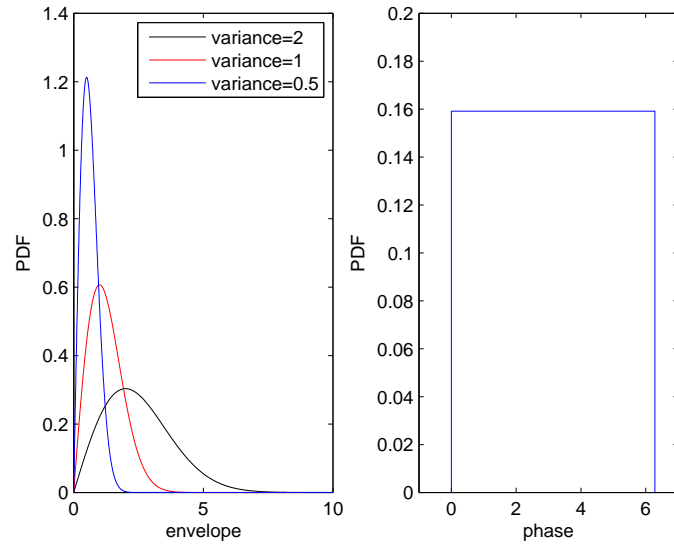
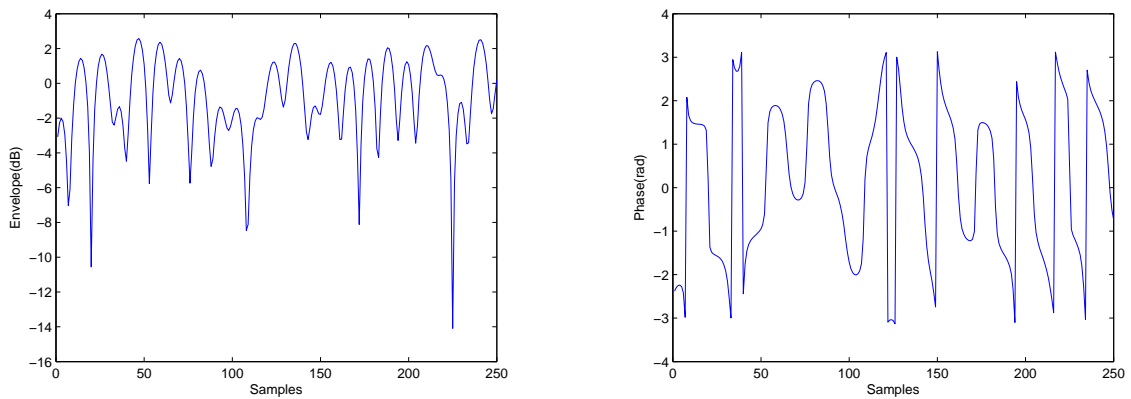


Figure 1.9: PDF for the Rayleigh envelope and phase.



(a) Rayleigh envelop of the fading process.

(b) Phase of the fading process.

Figure 1.10: The envelope and phase of Rayleigh fading process.

If the angle of arrival of each scatter has the same probability of the others, then the ACF becomes:

$$R_{hh}(\tau) = \frac{\sigma_h^2}{2\pi} \int_0^{2\pi} e^{j2\pi f_d \tau \cos \varphi_{ml}} d\varphi_{ml} = \sigma_h^2 J_0(2\pi f_d \tau) \quad (1.19)$$

where  $J_0(\cdot)$  is the zero-order Bessel function, and  $\sigma_h^2 = \sum_{l=1}^{L_s} E[g_{ml}]$ .

The right side of (1.19) is the sum of the ACF of the real and imaginary parts of the complex fading channel. They are not correlated. In addition, they have the same autocorrelation function as follows:

$$R_{h_m^{(R)} h_m^{(R)}} = R_{h_m^{(I)} h_m^{(I)}} = \frac{\sigma_h^2}{2} J_0(2\pi f_d \tau) \quad (1.20)$$

$$R_{h_m^{(I)} h_m^{(R)}} = R_{h_m^{(R)} h_m^{(I)}} = 0 \quad (1.21)$$

By taking the Fourier transform of (1.20), we obtain the Doppler power spectrum as follows:

$$\Psi(f) = \begin{cases} \frac{\sigma_h^2}{\pi f_d \sqrt{1-(f/f_d)^2}}, & \text{if } |f| \leq f_d \\ 0, & \text{otherwise} \end{cases} \quad (1.22)$$

According to (1.22), increasing Doppler frequency results in wider band limited spectrum between  $+f_d$  and  $-f_d$ .

The discrete-time Rayleigh process can be obtained when sampling the continuous signal at sampling rate  $1/T_b$  as follows:

$$h_m(k) = \sum_{l=1}^{L_s} g_{ml} e^{j(2\pi f_d T_b k \cos \varphi_{ml} + \vartheta_{ml})} \quad (1.23)$$

and the ACF is given by:

$$R_{hh}(k) = \sigma_h^2 J_0(2\pi f_d T_b k) \quad (1.24)$$

### 1.3.2 Correlated Mobile Fading Channels

The Rayleigh channel follows from the Gaussian WSS uncorrelated scattering fading assumption. This fading channel is characterized by its ACF which depends on the propagation geometry, the velocity of the mobile and the antenna characteristic [Bad05]. In Orthogonal Frequency-Division Multiplexing (OFDM) systems, the fading among the narrow-band sub-carriers is often assumed to be uncorrelated. However, when operating in channels having a large coherence bandwidth, the faded envelope of a large number of sub-carriers might have cross-correlation coefficient of 0.5 and above [Sor06]. If two

carriers are transmitted from the base station at slightly different frequencies, then their statistical properties, as observed at mobile antenna, are dependent if the frequency separation is not large enough. The frequency separation for which the signals are still strongly correlated is called the coherence bandwidth. In addition, in many real radio environment, signals that are received by any two antennas are found to be correlated spatially. This is mainly due to the insufficient physical separation between the antennas and/or lack of rich scattering environment [Xu09].

To deal with correlated channels we have to study the ACF and the Cross-Correlation Function (CCF) between these channels.

Define the  $p^{th}$  order multichannel fading vector of size  $M \times 1$  at time instant  $k$  as follows:

$$\mathbf{h}(k) = \begin{bmatrix} h_1(k) & h_2(k) & \cdots & h_M(k) \end{bmatrix}^T \quad (1.25)$$

The M-AR model of the fading vector is given by:

$$\mathbf{h}(k) = - \sum_{l=1}^p \mathbf{A}^{(l)} \mathbf{h}(k-l) + \mathbf{u}(k) \quad (1.26)$$

the fading vector at time  $k+l$  is given by:

$$\mathbf{h}(k+l) = \begin{bmatrix} h_1(k+l) & h_2(k+l) & \cdots & h_M(k+l) \end{bmatrix}^T \quad (1.27)$$

where  $\mathbf{u}(k)$  is the driving processes and  $(\cdot)^T$  denote the matrix transpose.

To formulate the ACF and CCF, compute the covariance matrix  $\mathbf{R}_{hh}(l)$  at lag  $l$  as follows:

$$\begin{aligned} \mathbf{R}_{hh}(l) &= E[\mathbf{h}(k)\mathbf{h}^H(k+l)] \\ &= E \begin{pmatrix} h_1(k)h_1(k+l) & h_1(k)h_2(k+l) & \cdots & h_1(k)h_M(k+l) \\ h_2(k)h_1(k+l) & h_2(k)h_2(k+l) & \cdots & h_2(k)h_M(k+l) \\ \vdots & \vdots & \ddots & \vdots \\ h_M(k)h_1(k+l) & h_M(k)h_2(k+l) & \cdots & h_M(k)h_M(k+l) \end{pmatrix} \end{aligned} \quad (1.28)$$

where  $(\cdot)^H$  denotes the Hermitian operator.

One can rewrite the above formula in terms of autocorrelation and cross-correlation between the channels as follows:

$$\mathbf{R}_{hh}(l) = \begin{pmatrix} R_{h_1h_1}(l) & R_{h_1h_2}(l) & \cdots & R_{h_1h_M}(l) \\ R_{h_2h_1}(l) & R_{h_2h_2}(l) & \cdots & R_{h_2h_M}(l) \\ \vdots & \vdots & \ddots & \vdots \\ R_{h_Mh_1}(l) & R_{h_Mh_2}(l) & \cdots & R_{h_Mh_M}(l) \end{pmatrix} \quad (1.29)$$

where  $R_{h_r h_s}(l)$  is the correlation between the channels  $r, s$  for  $r = 1, \dots, M$  and  $s = 1, \dots, M$ .

$R_{h_r h_s}(l)$  in (1.29) is general, it depends on the application. In [Jak94], the author considered the scenario where all complex Gaussian random processes with Rayleigh envelopes have equal power  $\sigma_h^2$  and derived the correlation properties between random processes as function of both time and frequency separation. Assume that  $h_r(k)$  and  $h_s(k+l)$  are the channels  $r$  and  $s$  at instants  $k$  and  $k+l$ , respectively. Since, these channels are complex, they can be written in rectangular form as follows:

$$h_r(k) = h_r^{(R)}(k) + jh_r^{(I)}(k) \quad (1.30)$$

$$h_s(k) = h_s^{(R)}(k) + jh_s^{(I)}(k) \quad (1.31)$$

where  $(R)$ ,  $(I)$  refers to the real and imaginary components. By definition, the covariance between the real and the imaginary parts of  $h_r(k)$  and  $h_s(k+l)$  are:

$$\begin{aligned} R_{h_r^{(R)} h_s^{(R)}}(l) &\triangleq E[h_r^{(R)} h_s^{(R)}], & R_{h_r^{(I)} h_s^{(I)}}(l) &\triangleq E[h_r^{(I)} h_s^{(I)}] \\ R_{h_r^{(R)} h_s^{(I)}}(l) &\triangleq E[h_r^{(R)} h_s^{(I)}], & R_{h_r^{(I)} h_s^{(R)}}(l) &\triangleq E[h_r^{(I)} h_s^{(R)}] \end{aligned} \quad (1.32)$$

Those covariance matrices have been derived in [Jak94] as follows:

$$\begin{aligned} R_{h_r^{(R)} h_s^{(R)}}(l) &= R_{h_r^{(I)} h_s^{(I)}}(l) = \frac{\sigma_h^2 J_0(2\pi f_m l)}{2[1 + (\Delta w_{rs} \sigma_\tau)^2]} \\ R_{h_r^{(R)} h_s^{(I)}}(l) &= -R_{h_r^{(I)} h_s^{(R)}}(l) = -\Delta w_{rs} \sigma_\tau R_{h_r^{(R)} h_s^{(R)}}(l) \end{aligned} \quad (1.33)$$

where  $f_m = f_d T_b$  is the Doppler rate,  $\sigma_h^2$  is the variance ( $\sigma_h^2/2$  is the variance per dimension),  $\sigma_\tau$  is the delay spread of the wireless channel, and  $\Delta w_{rs}$  is the angular frequency separation between the processes at frequencies  $f_r, f_s$  given by:

$$\Delta w_{rs} = 2\pi(f_r - f_s) \quad (1.34)$$

The general formula for the correlation between the channel  $h_r(k)$  and  $h_s(k+l)$  is given by:

$$R_{h_r h_s}(l) = [R_{h_r^{(R)} h_s^{(R)}}(l) + R_{h_r^{(I)} h_s^{(I)}}(l)] - j[R_{h_r^{(R)} h_s^{(I)}}(l) - R_{h_r^{(I)} h_s^{(R)}}(l)] \quad (1.35)$$

Substituting (1.33) in (1.35), it follows that:

$$R_{h_r h_s}(l) = \frac{\sigma_h^2 J_0(2\pi f_m l)}{[1 + (\Delta w_{rs} \sigma_\tau)^2]} - j\Delta w_{rs} \sigma_\tau \frac{\sigma_h^2 J_0(2\pi f_m l)}{[1 + (\Delta w_{rs} \sigma_\tau)^2]} = \frac{\sigma_h^2 J_0(2\pi f_m l)}{[1 + (\Delta w_{rs} \sigma_\tau)^2]} [1 - j\Delta w_{rs} \sigma_\tau] \quad (1.36)$$

For  $r = s$ , implies  $f_r = f_s$ , which leads to ( $\Delta w_{rs} = 0$ , by substitution this result in (1.36) produce  $R_{h_r h_s}(m) = \sigma_h^2 J_0(2\pi f_m m)$ ).

Equation (1.36) is used in [Bul98] to model Rayleigh fading channels and implement a diversity receiver for OFDM systems.

The fading correlation can be given as a function of spatial separation in antenna arrays [Bad04] [Tra05], [Xu09]. See appendix A for an example of spatial correlation [Bad04] for Multi Input Multi Output (MIMO) systems.

### 1.3.3 AR Modeling and Simulation of Fading Processes

Several models have been used to model fading channels depending on (1.23). These models are very important to simulate the wireless mobile fading channels, because they make system tests and evaluations less expensive and more reproducible than field trials. Many different techniques have been proposed for the modeling and simulation of mobile radio channels. Among them, are the sum-of-sinusoids models and the autoregressive models [Hay02].

To simplify the model described by (1.23), several authors used different assumptions of the amplitude  $g_{ml}$ , angle of arrival  $\varphi_{ml}$  and the phase  $\vartheta_{ml}$ .

Clarke in [Cla68] used  $g_{ml} = \frac{1}{\sqrt{L_s}}$  and the angle of arrival and the phase shift are random uniformly distributed over  $[-\pi, \pi)$  for all  $l$ , and they are mutually independent. This model is commonly considered as a computationally inefficient model compared to Jakes' Rayleigh fading simulator.

Jake used  $g_{ml} = \frac{1}{\sqrt{L_s}}$ ,  $\varphi_{ml} = \frac{2\pi l}{L_s}$ ,  $l = 1, \dots, L_s$  and  $\vartheta_{ml} = 0$ . These assumption make the simulator deterministic and wide-sense non-stationary [Pop01].

Based on Clarke's model, Pop et al. [Pop01] developed a class of WSS Rayleigh fading simulator. In this model, the author assume  $\varphi_{ml} = \frac{2\pi l}{L_s}$  and random phase shift. The draw back of this model is that it may model some higher order statistical properties inaccurately.

Recently, an improvement has been investigated in [Xia06] for Rayleigh fading channels simulators, based on the statistical analysis of Clarke's model and Pop-Beaulieu simulator. In this model, the author modified the angle of arrival to be the sum of Clarke's and Pop-Beaulieu assumptions, i.e.,  $\varphi_{ml} = \frac{2\pi l + \omega_l}{L_s}$ , where  $\omega_l$  is uniformly distributed variable, independent from the phase shift.

Although, the sum-of-sinusoids simulators are suitable for simulating fading channels, they can't be used in the design of channel estimation algorithms as they are non-linear models. In addition, three parameters have to be defined for each scatter ( $g_{ml}$ ,  $\varphi_{ml}$  and  $\vartheta_{ml}$ ) which means a large number of parameters to be estimated for large value of

$L_s$ . Moreover, the estimation of these parameters is not an easy task [Jam07a].

Generation of multichannel mobile fading processes has been studied by different authors and different algorithms have been proposed. Some of these methods are dedicated to generate two correlated fading channels with equal power. Other methods generate any number of channels but they are applicable for equal power fading channels. Two recent algorithms have been investigated by Chung [Tra05] and Sorooshyari [Sor06] based on filtering a white Gaussian noise variates. These are general algorithms for generating any number of channels with any desired channel variances. They depend on producing coloring matrix and then multiplying it by a white Gaussian noise to obtain the desired fading processes. The coloring matrix obtained by factorizing the covariance matrix, which has to be positive semi-definite. The shortcoming of these methods comes from the last condition. It can be solved by forcing the non-positive semi-definite matrix to positive semi-definite.

The main difference between these methods appears in the type of decomposition they used. In [Tra05], the eigen decomposition is considered, while the Cholesky decomposition is used in [Sor06]. The output sequences of the previous fading channel simulators are restricted to have cross-correlation statistics that have the same functional form as component autocorrelation function.

To overcome the previous disadvantage, more general algorithm, based on the autoregressive modeling of the mobile fading channels has been proposed in [Bad04]. It is suitable for the simulation and estimation of correlated fading channels and provides accurate fitting of the theoretical fading channels statistics such as (ACF, CCF, etc.).

Here, we adopt Baddour algorithm [Bad04] for the generation of multichannel fading processes which is based on the multichannel autoregressive (M-AR) model.

Thus, the multichannel fading processes can be modeled as a  $p^{th}$  order M-AR model:

$$\mathbf{h}(k) = - \sum_{l=1}^p \mathbf{A}^{(l)} \mathbf{h}(k-l) + \mathbf{u}(k) \quad (1.37)$$

where  $\mathbf{h}(k) = [h_1(k) \ h_2(k) \ \dots \ h_M(k)]^T$  is the multichannel vector, and  $\mathbf{u}(k) = [u_1(k) \ u_2(k) \ \dots \ u_M(k)]^T$  is a complex Gaussian white vector with zero-mean and covariance matrix  $\mathbf{Q}_u = E[\mathbf{u}(k)\mathbf{u}^H(k)]$ .  $\{\mathbf{A}^{(l)}\}_{l=1,\dots,p}$  are  $M \times M$  matrices containing the M-AR model coefficients as follows:

$$\mathbf{A}^{(l)} = \begin{pmatrix} a_{11}^{(l)} & \dots & a_{1M}^{(l)} \\ \vdots & \ddots & \vdots \\ a_{M1}^{(l)} & \dots & a_{MM}^{(l)} \end{pmatrix} \quad (1.38)$$

where  $(\cdot)^H$  denotes the Hermitian operator (i.e. the conjugate transpose).

Define the vector  $\underline{\mathbf{h}}(k)$  as follows:

$$\underline{\mathbf{h}}(k) = \left[ \mathbf{h}(k-1)^T \quad \mathbf{h}(k-2)^T \quad \cdots \quad \mathbf{h}(k-p)^T \right]^T \quad (1.39)$$

Then, the model covariance matrix  $\mathbf{R}_{hh}$  of dimension  $Mp \times Mp$  is defined as follows:

$$\mathbf{R}_{hh} = E[\underline{\mathbf{H}}(k)\underline{\mathbf{H}}^H(k)] \quad (1.40)$$

The relationship between the desired  $\mathbf{R}_{hh}$  and the M-AR model parameters is given by the multichannel Yule-Walker equations:

$$\underbrace{\begin{pmatrix} \mathbf{R}_{hh}(0) & \mathbf{R}_{hh}(-1) & \cdots & \mathbf{R}_{hh}(-p+1) \\ \mathbf{R}_{hh}(1) & \mathbf{R}_{hh}(0) & \cdots & \mathbf{R}_{hh}(-p+2) \\ \vdots & \vdots & \ddots & \vdots \\ \mathbf{R}_{hh}(p-1) & \mathbf{R}_{hh}(p-2) & \cdots & \mathbf{R}_{hh}(0) \end{pmatrix}}_{\mathbf{R}_{hh}} \underbrace{\begin{pmatrix} \mathbf{A}^{(1)H} \\ \mathbf{A}^{(2)H} \\ \vdots \\ \mathbf{A}^{(p)H} \end{pmatrix}}_{\mathbf{A}} = - \underbrace{\begin{pmatrix} \mathbf{R}_{hh}(1) \\ \mathbf{R}_{hh}(2) \\ \vdots \\ \mathbf{R}_{hh}(p) \end{pmatrix}}_{\mathbf{V}} \quad (1.41)$$

where the sub-matrices in  $\mathbf{R}_{hh}$  are the  $M \times M$  Toeplitz matrices  $\mathbf{R}_{hh}(l) = E[\mathbf{h}(k+l)\mathbf{h}^H(k)]$ , satisfying the following property:

$$\mathbf{R}_{hh}(-l) = \mathbf{R}_{hh}^H(l) \quad (1.42)$$

Once the  $\mathbf{A}^{(l)}$  coefficient matrices have been determined, the  $M \times M$  covariance matrix of the driving noise vector process can be computed as follows:

$$\mathbf{Q}_u = \mathbf{R}_{hh}(0) + \sum_{l=1}^p \mathbf{R}_{hh}(-l)\mathbf{A}^{(l)H} = \mathbf{R}_{hh}(0) + \mathbf{V}^T \mathbf{A} \quad (1.43)$$

After obtaining  $\mathbf{Q}_u$ , the realization of the driving noise process  $\mathbf{u}(k)$  can be accomplished by factorizing  $\mathbf{Q}_u$  as follows:

$$\mathbf{Q}_u = \mathbf{G}\mathbf{G}^H \quad (1.44)$$

The Cholesky decomposition can be used here. The driving process is then generated as follows:

$$\mathbf{u}(k) = \mathbf{G}\underline{\mathbf{z}}(k) \quad (1.45)$$

where  $\underline{\mathbf{z}}(k)$  is an  $M \times 1$  vector of independent zero-mean complex Gaussian variates with unit variance.

For high order M-AR process, the determinant of the matrix  $\mathbf{R}_{hh}$  is very small, which means that  $\mathbf{R}_{hh}$  is close to singular resulting in an ill-conditioned matrix. The numerical

problems arise in this case can be resolved by approximating any band-limited processes by adding a very small positive bias  $\epsilon$  to the zero<sup>th</sup> lag of their corresponding ACFs [Bad05]. If the ill-conditioning is ignored, then the algorithm produces a meaningless solution with either a covariance matrix  $\mathbf{Q}_u$  that are not realizable or a multichannel Infinite-Impulse Response (IIR) filter that is unstable.

If the matrix  $\mathbf{R}_{hh}$  is positive semi-definite, then the eigenvalues either positive or zeros. The added bias  $\epsilon$  can be selected to be the smallest value of the eigenvalues. But if  $\mathbf{R}_{hh}$  is not positive semi-definite, then a technique described in [Sor06] can be used to approximate the desired  $\mathbf{R}_{hh}$  with the nearest resizable positive semi-definite matrix in Frobenius sense.

The correlation between any two channels  $h_r(k)$  and  $h_s(k+l)$  in this algorithm can be computed as follows:

$$R_{h_r h_s}(l) = \begin{cases} J_0(2\pi f_m |l|), & \text{if } r = s \\ \rho_{rs} J_0(2\pi f_m |l|), & \text{if } r \neq s \end{cases} \quad (1.46)$$

where  $\rho_{rs}$  is the cross-correlation coefficient between channels  $h_r$  and  $h_s$ . In general,  $\rho_{rs} \neq \rho_{sr}$ .

In the case of Jakes model [Jak94], the cross-correlation  $\rho_{rs}$  is given from (1.36) as follows:

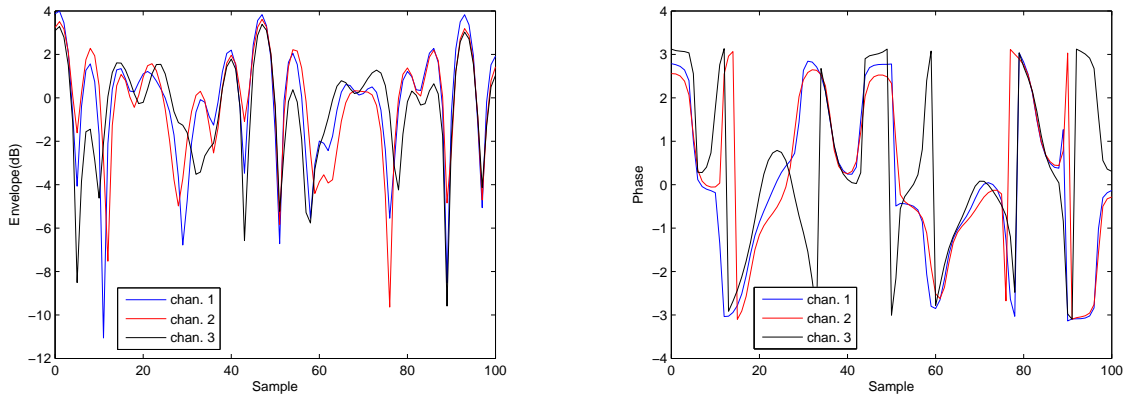
$$\rho_{rs} = \frac{1 - j\Delta w_{rs}\sigma_\tau}{1 + (\Delta w_{rs}\sigma_\tau)^2} \quad (1.47)$$

The formula of  $\rho_{rs}$  depends on the practical cases, for example we can use (1.36) in the case of OFDM systems.

A simulation using the vector AR method [Bad04] to generate multiple correlated band-limited Rayleigh processes is provided. In this example, we consider  $M=3$ ,  $\text{AR}(6)$ ,  $f_m = 0.1$ , and given the correlation coefficients  $\rho_{12} = \rho_{21} = 0.95$ ,  $\rho_{13} = \rho_{31} = 0.8$  and  $\rho_{23} = \rho_{32} = 0.6$ . Figure 1.11 shows the envelope and the phase of the generated channels, while the ACF is shown in Figure 1.12. We can note that the theoretical ACF is very close to the practical ACF for lags up to the process order.

When the correlation coefficients  $\rho_{rs} = \rho_{sr}$ , the resulting parameter matrices  $\{\mathbf{A}\}_{l=1,\dots,p}^{(l)}$  are diagonal:

$$\mathbf{A}^{(l)} = \begin{pmatrix} a_{11}^{(l)} & 0 & \cdots & 0 \\ 0 & a_{22}^{(l)} & 0 & 0 \\ \vdots & \vdots & \ddots & \vdots \\ 0 & \cdots & 0 & a_{MM}^{(l)} \end{pmatrix} \quad (1.48)$$



(a) Envelope of the multichannel fading processes. (b) Phase of the multichannel fading processes.

Figure 1.11: The envelope and phase of multichannel Rayleigh fading channels.

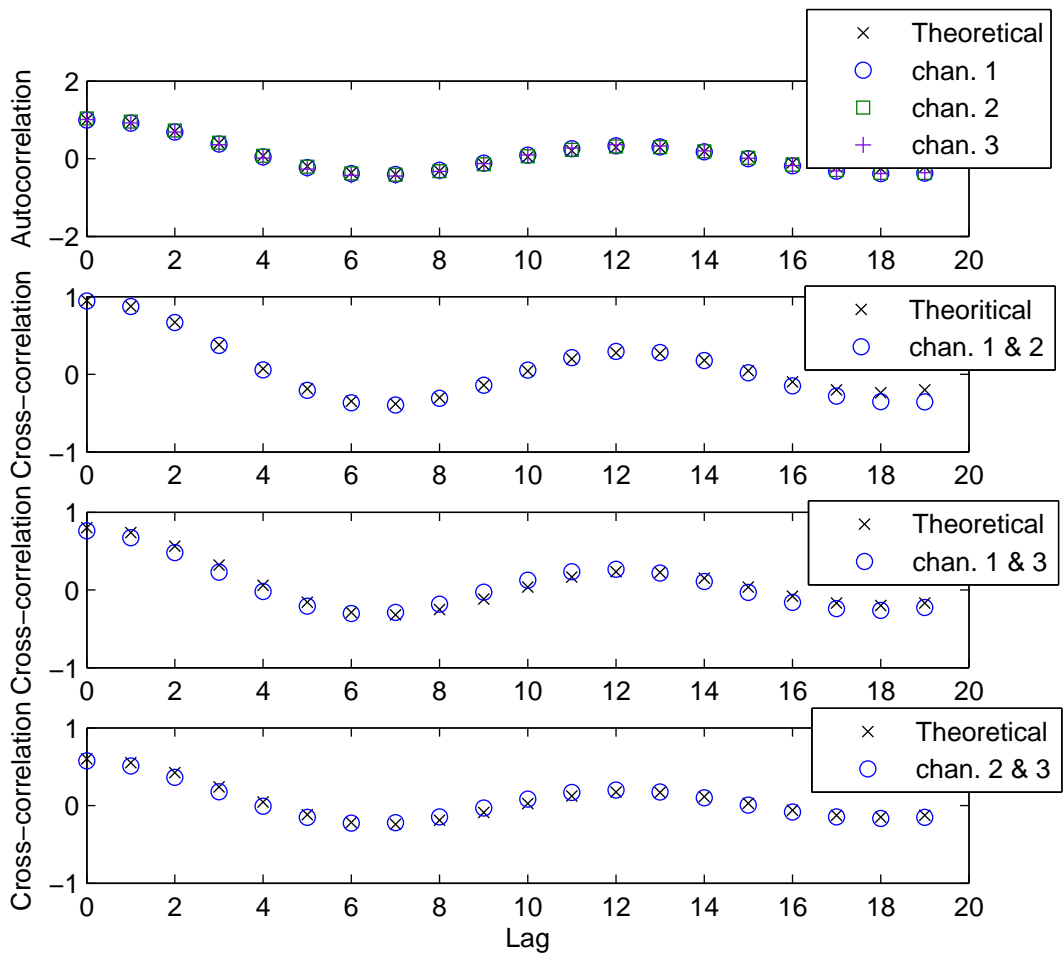


Figure 1.12: ACF and CCF of the of multichannel Rayleigh fading.

Table 1.1: Simulation of correlated fading channels based on vector AR model [Bad04].

- 1- Compute  $\mathbf{R}_{hh}(l)$  for  $l = -p + 1, \dots, 0, \dots, p$  based on 1.46.
- 2- Build the covariance matrix  $\mathbf{R}_{hh}$  using the sub-matrices in step 1.
- 3- Build the cross-correlation matrix  $\underline{\mathbf{V}}$  using the sub-matrices in step 1.
- 4- Compute  $\underline{\mathbf{A}}$  using (1.41).
- 5- Compute the driving processes covariance matrix  $\mathbf{Q}_u$  using (1.43).
- 6- Perform the factorization  $\mathbf{Q}_u = \mathbf{G}\mathbf{G}^T$ .
- 7- Generate the independent zero-mean complex Gaussian variates with unit variance  $\mathbf{z}(k)$ .
- 8- Compute  $\mathbf{u}(k) = \mathbf{G}\mathbf{z}(k)$  using the results from step 6.
- 9- Generate the M-AR fading process by using 1.37.

In this case, the correlation between the channels result from the driving noise processes  $\mathbf{u}(k)$ . The proof of this fact for first order M-AR process is provided in appendix B.

The single channel fading process can be generated as a special case of multichannel fading processes when  $M=1$  [Bad05].

Table 1.1 summarize the algorithm of vector AR method for the generation of M-AR fading process [Bad04].

## 1.4 Aims of the Thesis

Multichannel processes appears in different applications such as in biomedical engineering, Radar, satellite navigation and wireless mobile communications. In these applications, the channels can be modeled as M-AR model, which is defined using a few number of parameters. The M-AR process is usually contaminated by AWGN. Our purpose is to estimate the parameters of the M-AR process from noisy observations.

Different approaches have been studied to estimate the parameters of M-AR process from noisy observations. The YW equations results in biased estimates, as it does not account for the additive noise. To avoid the biased estimation problem, the NCYW can be used. It requires a priori knowledge of the additive noise variances. However, the additive noise variances are usually unknown in practice. Thus, different algorithms have been studied to solve this problem such as Hassan's method [Has03], ILSV method [Mah08] and EIV based approach [Pet09b].

The above estimation methods are off-line requiring all observations to be used in the estimation. This is not applicable in the on-line applications, where only one sample is available at a time. Several on-line estimation techniques have been studied in the

literature such as the methods based on Kalman or  $H_\infty$  filters.

When Kalman or  $H_\infty$  filters are applied directly on the noisy observations, the estimated AR parameters are biased [Arn98] [Cai04]. To avoid this problem, we propose to extend to the multichannel case the two cross-coupled Kalman (CC-Kalman) filters and two cross-coupled  $H_\infty$  (CC- $H_\infty$ ) filters initially proposed for parameter estimation in single channel AR process [Lab06] [Lab07].

## 1.5 Outlines of the Thesis

In chapter 1, a motivation of the work is firstly presented. In Section 2, the parametric models (ARMA, MA and AR) are presented. In section 3, a description of correlated multichannel fading processes is provided followed by presenting a method for the simulation of correlated M-AR fading processes based on VAR modeling.

In chapter 2, a survey about the estimation of single channel AR process and M-AR process is firstly presented. The formulation of the problem of M-AR process estimation is presented in section 2. In section 3, off-line parameters estimation of M-AR process are explained. In section 4, on-line parameter estimation techniques based on optimal filters are introduced. Finally, we present our extension of CC-Kalman filters and CC- $H_\infty$  filters to the multichannel case.

In chapter 3, we provide a comparative simulation study between the various parameter estimation methods based either on synthetic M-AR process or correlated multichannel fading processes.

Conclusion and recommendations for future works are drawn in chapter 4.



# Chapter 2

## Parameter Estimation of Multichannel AR (M-AR) Processes

### Contents

---

2.1	State-of-the-Art . . . . .	26
2.2	Problem Formulation . . . . .	29
2.3	Off-line Parameter Estimation Methods . . . . .	30
2.4	On-line M-AR Process Estimation Based on Optimal Filters	36

---

## 2.1 State-of-the-Art

The single channel AR model has been widely used in digital signal processing applications as it is simple and contains few parameters that can be easily estimated [Hay02]. Examples of these applications are speech coding enhancement [Gib74] and smoothing [Lab07], medical imaging [Che99]. In radar applications, the interest is to determine the position, velocity and acceleration of a plane or objects in the sky [Gon06]. In mechanical systems [Pro00] and vehicle navigation, the purpose is to determine position, velocity and acceleration [Pie04]. In the framework of mobile communications, the aim is to simulate [Bad05] and estimate the AR process and parameters [Cai04] [Jam08]. In all AR applications, the aim is to estimate the AR process and its parameters from the received noisy observations. The noise is a part of the nature that can't be avoided and is usually added to the desired signal. The noise sources may be internal from the system ( i.e., the thermal noise due to the random motion of the electrons in the conductor ). The other sources of noise are external to the system ( e.g., atmospheric noise, galactic noise and man-made noise ) [Hay00].

The effect of the additive noise on the signal was studied by Steven Kay in [Kay79]. He showed that the additive noise results in smoothing the AR spectrum. This smoothing results from the introduction of spectral zeros due to the noise.

The estimation methods of single channel AR process can be classified into either off-line or on-line. Off-line methods such as ARFIT [Neu01] and YW equations [Kay80] provide unbiased estimates when the observations are free of noise. However, they provide biased estimates when the estimation is from the noisy observations, mainly for low SNR. To contract the effect of disturbance noise, Kay in [Kay80] introduced the NCYW equations; by including the additive noise variance in the main diagonal of the autocorrelation matrix. It provides accurate parameter estimates. However, it requires that the noise variance to be a priori known which is not the case in most applications. To overcome this problem, Davila in [Dav01] proposed a method for estimating the noise variance and the parameter using YW equations.

The off-line estimation methods can't be used in the applications where only one observation is available at a time or when the sample size is limited. Thus, different techniques have been investigated to estimate the AR parameters using the on-line observations. Such as the Least Mean Square (LMS) algorithm, Recursive Least Square (RLS) algorithm and two serially-connected Kalman (SC-Kalman) filters [Arn98] [Jam07a]. However, applying these techniques directly to the noisy observations results in biased esti-

mation of the AR parameters.

To avoid the bias of estimation problem, a wide variety of Kalman filters have now been developed such as the EKF, SPKF and the Uncented Kalman Filter (UKF) [Hay02]. The UKF has slightly better performance than the EKF [Pie04]. The size of the state vector to be estimated is quite high. To reduce this size and the resulting computational cost, the CC-Kalman filters has been investigated. In this arrangement, one filter is used to estimate the process, while the other filter estimates the parameters from the estimated process [Lab06] [Jam07b]. This arrangement provides consistent estimation of the AR parameters from noisy observations.

Kalman filter is optimal in the  $H_2$  sense providing that the initial state, the driving process and measurement noise are independent, white and Gaussian with known variances. However, these assumptions may no longer be satisfied in real cases. To relax them,  $H_\infty$  filter has been investigated [Has93] [She97] [Hay02] [Cai04].

The CC- $H_\infty$  filters has been investigated in different applications, such as speech enhancement [Lab07], and fading channel estimation [Jam08]. They provide consistent and robust estimation of the AR parameter.

Some applications have more than one AR process, and each process is treated individually from the other processes. In these cases, the estimation of the AR parameters are addressed ignoring the correlation between channels. Treating each process individually in the case of multichannel applications returns to two main reasons: the first is the simplicity of the existing estimation algorithms for single channel, the other returns to difficulty of generating correlated processes such as the correlated fading channels [Sor06]. To take into account the correlation between channels, the M-AR model have to be considered [Bad04].

The correlated channels arise in different multichannel applications such as the EEG and EEG signals [Arn98]. In the framework of mobile communications the correlation between the channels over each carrier in OFDM systems has to be considered in order to estimate the M-AR process and its parameters accurately [Sor06].

Off-line approaches such as the ARFIT algorithm is used to estimate the M-AR parameters based on eigenmodes decomposition [Neu01]. The YW equations can be used to estimate the parameters of M-AR process. However, they provide biased estimates. As the case of single channel AR process, the effect of the additive noise can be reduced by using NCYW equations. In this method, the noise variances are subtracted from the main diagonal of the model covariance matrix. The NCYW equations requires a priori knowledge of the noise covariance matrix which is usually not known.

To estimate the noise covariance matrix and the M-AR parameter, several techniques have been addressed. Thus, in [Has03], the authors proposed an iterative algorithm that combining the YW equations and Newton-Raphson algorithm to estimate the noise covariance matrix and the AR parameters. Hassan's method has high computational complexity due to solving the non-linear equations. In addition, it diverges in some cases and requires diagonal noise covariance matrix.

To avoid the drawbacks of Hassan's method, the ILSV approach based on the least square method has been recently investigated [Mah08]. This approach solves linear equations to estimate the noise covariance matrix with lower number of iterations. Therefore, it requires less computation cost. In addition, it doesn't assume independent additive noise. However, it doesn't work properly at low SNR ( e.g.,  $SNR < 4$  ). To avoid this drawback, EIV based method has been recently proposed [Pet09b]. In this method, the noisy observations autocorrelation matrix compensated by a specific diagonal block matrix and whose kernel is defined by the M-AR parameter matrices must be positive semi-definite. However, it has high computational cost.

The off-line methods require all observations to be available. In addition, they have high computational cost. Moreover, some of them go divergence in some cases or provide estimated parameters that result in unstable systems. To overcome these drawbacks, several on-line methods based on Kalman or  $H_\infty$  filters have been investigated.

In the last years, different methods and algorithms have been investigated for multichannel autoregressive processes estimation. Some of these methods are an extension to the estimation method of single channel. An extension of two serially-connected Kalman filter, from single channel AR process to M-AR process was applied in the biomedical engineering for analyzing the spectrum of EEG and ECG signals [Arn98]. The maximum likelihood has been investigated by Nissila as application in the multi-path fading channels estimation [Nis04]. However, these methods provide biased estimates; as the estimation is directly from the noisy observations.

In order to estimate the M-AR parameters consistently, we propose to extend the CC-Kalman filters [Lab06] from single channel to the multichannel case. However, Kalman filter require the driving processes and the additive noise to be white, Gaussian and a priori known. To avoid these assumptions, we propose to extend the CC- $H_\infty$  filters [Lab07] from single channel to the multichannel case.

## 2.2 Problem Formulation

In multichannel applications, the  $p^{\text{th}}$  order M-AR process  $\mathbf{h}(k)$  satisfies:

$$\mathbf{h}(k) = \begin{pmatrix} h_1(k) \\ \vdots \\ h_M(k) \end{pmatrix} = - \sum_{l=1}^p \mathbf{A}^{(l)} \mathbf{h}(k-1) + \mathbf{u}(k) \quad (2.1)$$

where  $\{\mathbf{A}^{(l)}\}_{l=1,\dots,p}$  are the  $M \times M$  parameter matrices which can be written as follows:

$$\mathbf{A}^{(l)} = \begin{pmatrix} a_{11}^{(l)} & \cdots & a_{1M}^{(l)} \\ \vdots & \ddots & \vdots \\ a_{M1}^{(l)} & \cdots & a_{MM}^{(l)} \end{pmatrix} \quad (2.2)$$

and  $\mathbf{u}(k) = [u_1(k) \ u_2(k) \ \cdots \ u_M(k)]^T$  is a zero-mean white driving vector whose autocorrelation matrix  $\Sigma_u$  satisfies:

$$\Sigma_u = E[\mathbf{u}(k)\mathbf{u}^T(k)] = \text{diag}(\left[ \sigma_{u_1}^2 \ \cdots \ \sigma_{u_M}^2 \right]) \quad (2.3)$$

where  $\text{diag}(\cdot)$  denotes a diagonal matrix.

In addition, the M-AR parameter matrices  $\{\mathbf{A}^{(l)}\}_{l=1,\dots,p}$  are constrained so that the roots  $\{p_i\}_{i=1,\dots,Mp}$  of:

$$\det(\mathbf{A}_p(z)) = 0 \quad (2.4)$$

lie inside the unit circle in the  $z$ -plane, where:

$$\mathbf{A}_p(z) = \mathbf{I}_M + \mathbf{A}^{(1)}z^{-1} + \cdots + \mathbf{A}^{(p)}z^{-p} \quad (2.5)$$

In (2.5),  $z^{-1}$  denotes the backward shift operator and  $\mathbf{I}_M$  is the  $M \times M$  identity matrix.

Let the M-AR process  $\mathbf{h}(k)$  be disturbed by an additive zero-mean white noise vector  $\mathbf{v}(k) = [v_1(k) \ \cdots \ v_M(k)]^T$  uncorrelated with  $\mathbf{u}(k)$ , and with the following correlation matrix:

$$\Sigma_v = E[\mathbf{v}(k)\mathbf{v}^T(k)] = \text{diag}(\left[ \sigma_{v_1}^2 \ \cdots \ \sigma_{v_M}^2 \right]) \quad (2.6)$$

Thus, the noisy observation vector  $\mathbf{y}(k)$  is written as follows:

$$\mathbf{y}(k) = \begin{bmatrix} y_1(k) \\ \vdots \\ y_M(k) \end{bmatrix} = \mathbf{h}(k) + \mathbf{v}(k) \quad (2.7)$$

The purpose of the M-AR parameter estimation methods is to estimate the parameter matrices  $\{\mathbf{A}^{(l)}\}_{l=1,\dots,p}$  from the noisy vector  $\mathbf{y}(k)$ .

Single channel system can be obtained as a special case of the multichannel system when substituting  $M = 1$  in (2.1) and (2.7) as follows:

$$h(k) = - \sum_{l=1}^p a_l h(k-l) + u(k) \quad (2.8)$$

$$y(k) = h(k) + v(k) \quad (2.9)$$

The YW equations, NCYW equations and Hassan's method are explained in section 3 as off-line approaches. In section 4, the separate estimation of M-AR process and its parameters using Kalman or  $H_\infty$  filters is presented. Finally, we introduce the joint estimation of the M-AR process and its parameters using CC-Kalman filters and CC- $H_\infty$  filters as an extension to [Lab06] [Lab07].

## 2.3 Off-line Parameter Estimation Methods

In this section, we describe some of the off-line parameters estimation methods for the system represented by (2.1) and (2.7) showing their advantages and disadvantages.

### 2.3.1 Yule-Walker Equations

The M-AR parameter matrices  $\mathbf{A} = \begin{bmatrix} \mathbf{A}^{(1)} & \cdots & \mathbf{A}^{(p)} \end{bmatrix}$  can be estimated by solving the following YW equations:

$$\mathbf{A}\mathbf{R}_{yy} = -\mathbf{V} \quad (2.10)$$

where the autocorrelation matrix  $\mathbf{R}_{yy}$  is given by:

$$\mathbf{R}_{yy} = \begin{pmatrix} \mathbf{R}_{yy}(0) & \cdots & \mathbf{R}_{yy}(p-1) \\ \vdots & \ddots & \vdots \\ \mathbf{R}_{yy}(-p+1) & \cdots & \mathbf{R}_{yy}(0) \end{pmatrix} \quad (2.11)$$

the cross correlation matrix  $\mathbf{V}$  is given by:

$$\mathbf{V} = \begin{bmatrix} \mathbf{R}_{yy}(1) & \cdots & \mathbf{R}_{yy}(p) \end{bmatrix} \quad (2.12)$$

The sub-matrices  $\{\mathbf{R}_{yy}(m)\}_{m=0,\dots,p}$  represents the correlation matrix of the vector  $\mathbf{y}(k)$  in (2.7) and given by:

$$\mathbf{R}_{yy}(m) = E[\mathbf{y}(k)\mathbf{y}^H(k-m)] \quad (2.13)$$

Using (2.7), we can express  $\mathbf{R}_{yy}(m)$  in terms of  $\mathbf{h}(k)$  and  $\mathbf{v}(k)$  as follows:

$$\mathbf{R}_{yy}(m) = E[(\mathbf{h}(k) + \mathbf{v}(k))(\mathbf{h}(k-m) + \mathbf{v}(k-m))^H] \quad (2.14)$$

$$\mathbf{R}_{yy}(m) = E[\mathbf{h}(k)\mathbf{h}^H(k-m)] + E[\mathbf{h}(k)\mathbf{v}^H(k-m)] + E[\mathbf{v}(k)\mathbf{h}^H(k-m)] + E[\mathbf{v}(k)\mathbf{v}^H(k-m)] \quad (2.15)$$

Assuming that the M-AR process and the measurement noise are independent, then equation (2.15) reduces to:

$$\mathbf{R}_{yy}(m) = \begin{cases} \mathbf{R}_{hh}(m) + \Sigma_v, & \text{if } m = 0 \\ \mathbf{R}_{hh}(m), & \text{if } m \neq 0 \end{cases} \quad (2.16)$$

In the case of mobile fading channels, the autocorrelation matrix  $\mathbf{R}_{yy}$  is close to singular for high order M-AR model and has no inverse. To solve this problem, Baddour et al. [Bad05] suggests to add a small bias to the elements of the main diagonal in the case of single channel AR process. The same principle is applicable in M-AR process [Bad04].

When the auto-correlation matrices are prepared, we can use (2.10) to compute the matrix  $\mathbf{A}$  as follows:

$$\mathbf{A} = -\mathbf{V}\hat{\mathbf{R}}_{yy}^{-1} \quad (2.17)$$

where  $\hat{\mathbf{R}}_{yy}^{-1}$  is the inverse of the estimate of  $\mathbf{R}_{yy}$ .

Using (2.16),  $\mathbf{R}_{yy}$  can be expressed as follows:

$$\mathbf{R}_{yy} = \mathbf{R}_{hh} + \Sigma_v \otimes \mathbf{I}_p \quad (2.18)$$

where  $\otimes$  denotes the matrices Kronecker product.

The YW equations provide biased estimates of  $\mathbf{A}$  due to the right most term in (2.18).

In some applications the correlation between the processes can be formulated. For example, the correlation in the case of fading processes is a zero-order Bessel function of the first kind. In the case of finite set of observations with unknown correlation function we can use the following estimate:

$$\hat{\mathbf{R}}_{yy}(m) = \frac{1}{N} \sum_{i=1}^{N-m} \mathbf{y}(i+m)\mathbf{y}^H(i) \quad (2.19)$$

where  $N$  is the number of samples. In general, the autocorrelation matrix  $\mathbf{R}_{yy}$  is Hermitian, i.e.,  $\mathbf{R}_{yy}(m) = \mathbf{R}_{yy}^H(-m)$ .

YW provide high performance for free of noise observations, while it provides biased estimates in the case of noisy observations. To avoid this drawback, NCYW equations can be used as explained in the next subsection.

### 2.3.2 Noise-Compensated Yule-Walker Equations

Since the noisy observations are used in the estimation process, the autocorrelation matrices have to be modified to compensate for the additive noise as explained later in this subsection.

Equation (2.16) can be arranged as follows:

$$\mathbf{R}_{hh}(m) = \begin{cases} \mathbf{R}_{yy}(m) - \Sigma_v, & \text{if } m = 0 \\ \mathbf{R}_{yy}(m), & \text{if } m \neq 0 \end{cases} \quad (2.20)$$

The autocorrelation matrix  $\mathbf{R}_{hh}$  of the vector  $\mathbf{h}(k)$  can be obtained by replacing submatrices in (2.11) by (2.20) as follows:

$$\mathbf{R}_{hh} = \begin{pmatrix} \mathbf{R}_{yy}(0) - \Sigma_v & \cdots & \mathbf{R}_{yy}(p-1) \\ \vdots & \ddots & \vdots \\ \mathbf{R}_{yy}(-p+1) & \cdots & \mathbf{R}_{yy}(0) - \Sigma_v \end{pmatrix} \quad (2.21)$$

From the above equation we note that the modification on the autocorrelation matrix obtained by subtracting the noise covariances from the elements of the main diagonal.

Thus, the parameter matrix  $\mathbf{A}$  can be estimated as follows:

$$\mathbf{A} = -\mathbf{V} \hat{\mathbf{R}}_{hh}^{-1} \quad (2.22)$$

where  $\hat{\mathbf{R}}_{hh}^{-1}$  is the inverse of the estimated  $\mathbf{R}_{hh}$

The NCYW method is preferable when the measurement noise covariance matrix is a priori known. However, it is usually unknown in most applications. Thus, several techniques have been studied to estimate the M-AR parameters and the noise covariance matrix. Examples of these methods are Hassan's method [Has03], ILSV approach [Mah08] and EIV based method [Pet09b].

### 2.3.3 Hassan's Method

Hassan's method [Has03] is based on solving iteratively and alternatively a set of linear and non-linear equations. Thus, the Newton-Raphson iteration is used to estimate the unknown noise variances by solving a set of non-linear equations, while the M-AR parameters matrices are estimated by solving the YW equations.

If the noisy observations in (2.7) are filtered by the inverse system  $\mathbf{A}_p(z)$  of  $\mathbf{H}(z)$ , then the output  $\mathbf{z}(k)$  is given by:

$$\mathbf{z}(k) = \mathbf{y}(k) + \sum_{l=1}^p \mathbf{A}^{(l)} \mathbf{y}(k-1) \quad (2.23)$$

By substituting (2.1) and (2.7) into (2.23), it follows that:

$$\mathbf{z}(k) = \mathbf{v}(k) + \mathbf{u}(k) + \sum_{l=1}^p \mathbf{A}^{(l)} \mathbf{v}(k-1) \quad (2.24)$$

Compute the autocorrelation matrix  $\mathbf{R}_{zz}(1) = E[\mathbf{z}(k)\mathbf{z}^T(k-1)]$  of  $\mathbf{z}(k)$  at lag  $k = 1$  we obtain the following:

$$\mathbf{R}_{zz}(1) = \sum_{l=1}^p \mathbf{A}^{(l)} \boldsymbol{\Sigma}_v \mathbf{A}^{(l-1)T} \quad (2.25)$$

Here,  $\boldsymbol{\Sigma}_v$  has to be diagonal.

We can use (2.25) to write the  $i^{\text{th}}$  element of the main diagonal of  $\mathbf{R}_{zz}(1)$  for  $i = 1, \dots, M$  as below:

$$R_{zz}(1)_{ii} = \sigma_{vi}^2 a_{ii}^{(1)} + \sum_{l=2}^p \sum_{m=1}^M \sigma_{vm}^2 a_{im}^{(l)} a_l^{(l-1)} \quad (2.26)$$

The system of linear equations constructed from (2.26) can be written in matrix form as follows:

$$\mathbf{C} \mathbf{d} = \mathbf{D} \quad (2.27)$$

where  $\mathbf{d}$  has the same elements as the main diagonal of the noise covariance matrix  $\boldsymbol{\Sigma}_v$ ,  $\mathbf{D}$  is a column vector contains the main diagonal of the matrix  $\mathbf{R}_{zz}(1)$  and  $\mathbf{C}$  is  $M \times M$  matrix. They are given as follows:

$$\mathbf{d} = \begin{pmatrix} \sigma_{v1}^2 \\ \vdots \\ \sigma_{vM}^2 \end{pmatrix}, \mathbf{D} = \begin{pmatrix} R_{zz}(1)_{11} \\ \vdots \\ R_{zz}(1)_{MM} \end{pmatrix}, \mathbf{C} = \begin{pmatrix} C_{11} & \cdots & C_{1M} \\ \vdots & \ddots & \vdots \\ C_{M1} & \cdots & C_{MM} \end{pmatrix}$$

where  $C_{ij}$  can be computed by the following formula:

$$C_{ij} = \begin{cases} a_{ij}^{(1)} + a_{ij}^{(2)} a_{ij}^{(1)} + \cdots + a_{ij}^{(p)} a_{ij}^{(p-1)}, & \text{if } i = j; \\ a_{ij}^{(2)} a_{ij}^{(1)} + \cdots + a_{ij}^{(p)} a_{ij}^{(p-1)}, & \text{if } i \neq j; \end{cases} \quad (2.28)$$

From the above formula, we can express  $\mathbf{C}$  in terms of the parameter matrices as follows:

$$\mathbf{C} = \mathbf{A}^{(1)} \cdot \mathbf{I} + \mathbf{A}^{(2)} \cdot \mathbf{A}^{(1)} + \cdots + \mathbf{A}^{(p)} \cdot \mathbf{A}^{(p-1)} \quad (2.29)$$

where  $(\cdot)$  is the matrices dot product, i.e., multiply each element in the first matrix by the corresponding element in the second matrix.

As the noise variances are unknown we can substitute  $\boldsymbol{\alpha} = \text{diag}(\alpha_1, \alpha_2, \dots, \alpha_M)$  for  $\boldsymbol{\Sigma}_v$  in (2.17) to estimate the parameter matrix  $\mathbf{A} = \begin{bmatrix} \mathbf{A}^{(1)} & \mathbf{A}^{(2)} & \cdots & \mathbf{A}^{(p)} \end{bmatrix}$ . Then, the estimated parameters are substituted in (2.27) to estimate  $\mathbf{d}$ .

Since  $\sigma_{vi}^2$  depends on  $\alpha_i$ , we can write  $\bar{\sigma}_{vi}^2 = f_i(\alpha_1, \alpha_2, \dots, \alpha_M)_{i=1, \dots, M}$ , and the aim is to match  $\alpha_i$  with  $\sigma_i^2$  simultaneously.

At matching conditions for each  $i$  we can write:

$$\alpha_i - \bar{\sigma}_{vi}^2 = 0 \quad (2.30)$$

i.e.,

$$\alpha_i - f_i(\alpha_1, \alpha_2, \dots, \alpha_M) = F_i(\alpha_1, \alpha_2, \dots, \alpha_M) = 0 \quad (2.31)$$

In order to solve the nonlinear  $M$  equations formed using (2.31) simultaneously, we can expand the function  $F_i$  as a Taylor series expansion about the point  $(\alpha_1^{(0)}, \alpha_2^{(0)}, \dots, \alpha_M^{(0)})$ . Using the first two terms and truncating the others, it follows that:

$$\sum_{j=1}^M \frac{\partial F_i}{\partial \alpha_j} (\Delta \alpha_j) = -F_i(\alpha_1, \alpha_2, \dots, \alpha_M) \quad (2.32)$$

We can write the system of equation formed by (2.32) in matrix form as follows:

$$\begin{pmatrix} \frac{\partial F_1}{\partial \alpha_1} & \dots & \frac{\partial F_1}{\partial \alpha_M} \\ \vdots & \ddots & \vdots \\ \frac{\partial F_M}{\partial \alpha_1} & \dots & \frac{\partial F_M}{\partial \alpha_M} \end{pmatrix} \begin{pmatrix} \Delta \alpha_1 \\ \vdots \\ \Delta \alpha_M \end{pmatrix} = - \begin{pmatrix} F_1 \\ \vdots \\ F_M \end{pmatrix} \quad (2.33)$$

Starting from (2.31), one can derive the formula for  $\frac{\partial F_i}{\partial \alpha_j}$  as follows:

$$F_i(\alpha_1, \alpha_2, \dots, \alpha_M) = \alpha_i - f_i(\alpha_1, \alpha_2, \dots, \alpha_M) \quad (2.34)$$

where the partial derivative of  $F_i$  with respect to  $\alpha_j$  is given by:

$$\frac{\partial F_i}{\partial \alpha_j} = \frac{\partial F_i(\alpha_1, \alpha_2, \dots, \alpha_M)}{\partial \alpha_j} \quad (2.35)$$

By substituting (2.34) in (2.35), it follows that:

$$= \frac{\partial(\alpha_i - f_i(\alpha_1, \alpha_2, \dots, \alpha_M))}{\partial \alpha_j} = \frac{\partial \alpha_i}{\partial \alpha_j} - \frac{\partial f_i(\alpha_1, \alpha_2, \dots, \alpha_M)}{\partial \alpha_j} \quad (2.36)$$

The above formula can be written as follows:

$$\frac{\partial F_i}{\partial \alpha_j} = \begin{cases} 1 - \frac{\partial f_i(\alpha_1, \alpha_2, \dots, \alpha_M)}{\partial \alpha_j}, & \text{if } i = j \\ -\frac{\partial f_i(\alpha_1, \alpha_2, \dots, \alpha_M)}{\partial \alpha_j}, & \text{if } i \neq j \end{cases} \quad (2.37)$$

When the function  $f_i$  in the above formula is not known, we can use the following equation:

$$\frac{\partial F_i}{\partial \alpha_j} = \begin{cases} 1 - \frac{[f_i(\alpha_1 + \delta, \alpha_2 + \delta, \dots, \alpha_M + \delta) - f_i(\alpha_1, \alpha_2, \dots, \alpha_M)]}{\delta}, & \text{if } i = j \\ -\frac{[f_i(\alpha_1 + \delta, \alpha_2 + \delta, \dots, \alpha_M + \delta) - f_i(\alpha_1, \alpha_2, \dots, \alpha_M)]}{\delta}, & \text{if } i \neq j \end{cases} \quad (2.38)$$

Table 2.1: Hassan’s method for M-AR parameter estimation from noisy observations [Has03].

<ol style="list-style-type: none"> <li>1- Initialize <math>(\alpha_1^{(0)}, \alpha_2^{(0)}, \dots, \alpha_M^{(0)})</math>.</li> <li>2- Compute <math>[\mathbf{A}^{(1)} \dots \mathbf{A}^{(p)}]</math> at <math>(\alpha_1^{(k)}, \alpha_2^{(k)}, \dots, \alpha_M^{(k)})</math> using (2.17).</li> <li>3- Compute <math>\bar{\sigma}_{v_i}^2</math> for <math>i = 1, \dots, M</math> at <math>(\alpha_1^{(k)}, \alpha_2^{(k)}, \dots, \alpha_M^{(k)})</math> using (2.27).</li> <li>4- Compute <math>F_i = \alpha_1^{(i)} - \bar{\sigma}_{v_i}^2</math> at <math>(\alpha_1^{(k)}, \alpha_2^{(k)}, \dots, \alpha_M^{(k)})</math>.</li> <li>5- Compute <math>[\mathbf{A}^{(1)} \dots \mathbf{A}^{(p)}]</math> at <math>(\alpha_1^{(k)} + \delta, \alpha_2^{(k)} + \delta, \dots, \alpha_M^{(k)} + \delta)</math> using (2.17).</li> <li>6- Compute <math>\bar{\sigma}_{v_i}^2</math> for <math>i = 1, \dots, M</math> at <math>(\alpha_1^{(k)} + \delta, \alpha_2^{(k)} + \delta, \dots, \alpha_M^{(k)} + \delta)</math> using (2.27).</li> <li>7- Compute the partial derivatives <math>\frac{\partial F_i}{\partial \alpha_j}</math> for <math>i = 1, \dots, M</math> and <math>h = 1, \dots, M</math>, using (2.38) and the values obtained in steps 3 and 6.</li> <li>8- Compute <math>(\Delta\alpha_1, \Delta\alpha_2, \dots, \Delta\alpha_M)</math> using (2.33) and the values in step 4 and 7.</li> <li>9- Compute <math>\alpha_i^{(k+1)} = \alpha_i^{(k)} + \Delta\alpha_i</math>, for <math>i = 1, \dots, M</math>.</li> <li>10- Repeat steps 2 to 9 until <math>F_1, F_2, \dots, F_M</math> converge simultaneously to zero.</li> </ol>
--

Hassan’s algorithm requires large number of iterations to converge. In addition, this algorithm might diverge in some cases: mainly for complex valued data, few samples and low SNR [Mah08].

Table 2.1 summarizes Hassan’s algorithm for the estimation of noise variances and M-AR parameters matrices.

### 2.3.4 Other Off-line Estimation Techniques

To avoid the drawbacks of Hassan’s method, some approaches has been recently investigated. Such as ILSV approach [Mah08], which is an extension of Zheng’s method [Zhe05] to the multichannel case. The ILSV solves a set of linear equation to estimate the observation noise covariance matrix, and estimate the parameter using YW equations. This method converges within a few iterations. In addition, it is more general method, which doesn’t assume diagonal noise covariance matrix. Moreover, it is applicable for any driving and additive noise distribution. Nevertheless, this method is no longer reliable when the SNR becomes lower than 10dB. In addition, it may lead to a set of AR parameter matrix estimates corresponding to unstable system [Pet09b].

The method proposed in [Pet09b] estimates the M-AR parameter matrices and the covariance matrices of the additive noise and the driving process from noisy observations based on an EIV approach. In this method, the noisy observations autocorrelation matrix compensated by a specific diagonal block matrix whose kernel is defined by the M-AR parameter matrices must be positive semi-definite. Hence, the parameter estimation con-

sists in searching every diagonal block matrix that satisfies this property. This method is applicable even for low SNR (e.g.,  $SNR < 4dB$ ). However, it has high computational cost. To reduce the computational cost, we investigate the on-line estimation techniques in the next section.

## 2.4 On-line M-AR Process Estimation Based on Optimal Filters

The off-line estimation methods of M-AR process parameters are applicable when all observations are available. In addition, they require large sample size. Moreover, they are no longer valid for on-line applications, since only single observation is available at a time. Thus, on-line methods based on Kalman or  $H_\infty$  filters have been investigated for the estimation of M-AR process and its parameters.

### 2.4.1 Kalman Vs $H_\infty$ for M-AR Process Estimation

A requirement for the use of Kalman or  $H_\infty$  filters is that the system given by (2.1) and (2.7) has a representation in state-space form. Such a model consists of two linear equations: the state equation and the observation equation.

Let us first define the state vector  $\underline{\mathbf{h}}(k)$  as follows:

$$\underline{\mathbf{h}}(k) = \left[ \mathbf{h}(k) \quad \mathbf{h}(k-1) \quad \cdots \quad \mathbf{h}(k-p+1) \right]^T \quad (2.39)$$

Given the system represented by (2.1), (2.7) and the state vector  $\underline{\mathbf{h}}(k)$ , the state-space representation for the estimation of the state vector can be written as follows:

The state equation:

$$\underline{\mathbf{h}}(k) = \mathbf{\Phi}(k)\underline{\mathbf{h}}(k-1) + \mathbf{\Gamma}\mathbf{u}(k) \quad (2.40)$$

The observation equation:

$$\mathbf{y}(k) = \mathbf{H}\underline{\mathbf{h}}(k) + \mathbf{v}(k) \quad (2.41)$$

where the transition matrix  $\mathbf{\Phi}(k)$  with dimension  $Mp \times Mp$  is given by:

$$\mathbf{\Phi}(k) = \begin{pmatrix} -\mathbf{A}^{(1)} & -\mathbf{A}^{(2)} & \cdots & -\mathbf{A}^{(p)} \\ \mathbf{I}_M & \mathbf{0}_M & \cdots & \mathbf{0}_M \\ \vdots & \ddots & \ddots & \vdots \\ \mathbf{0}_M & \mathbf{0}_M & \mathbf{I}_M & \mathbf{0}_M \end{pmatrix} \quad (2.42)$$

and the matrices  $\mathbf{H}$  and  $\mathbf{\Gamma}$  satisfy:

$$\mathbf{H} = \mathbf{\Gamma}^T = \begin{bmatrix} \mathbf{I}_M & \mathbf{0}_M & \cdots & \mathbf{0}_M \end{bmatrix} \quad (2.43)$$

### 2.4.1.1 Kalman Estimation Algorithm

Given the state-space model (2.40) and (2.41), the Kalman estimator provides an estimation of the state vector by minimizing the mean square error:

$$J = E[\|\mathbf{e}(k)\|^2] = E[\|\underline{\mathbf{h}}(k) - \hat{\underline{\mathbf{h}}}(k)\|^2] \quad (2.44)$$

where  $\|\mathbf{e}(k)\|^2 = \mathbf{e}^T(k)\mathbf{e}(k)$  and  $\hat{\underline{\mathbf{h}}}(k)$  is the estimate of  $\underline{\mathbf{h}}(k)$ .

The a priori estimation  $\underline{\mathbf{h}}(k/k-1)$  of the state vector at instant  $k$  given  $k-1$  observations is given by:

$$\hat{\underline{\mathbf{h}}}(k/k-1) = \mathbf{\Phi}(k)\hat{\underline{\mathbf{h}}}(k-1/k-1) \quad (2.45)$$

The vector  $\mathbf{b}(k)$  is the white Gaussian innovation process with covariance matrix  $\mathbf{C}_b(k)$  given respectively as follows:

$$\mathbf{b}(k) = \mathbf{y}(k) - \mathbf{H}\hat{\underline{\mathbf{h}}}(k/k-1) \quad (2.46)$$

$$\mathbf{C}_b(k) = \mathbf{H}\mathbf{P}(k/k-1)\mathbf{H}^T + \mathbf{\Sigma}_v \quad (2.47)$$

Then, the aposteriori estimation of the state vector  $\underline{\mathbf{h}}(k/k)$  can be recursively estimated as follows:

$$\hat{\underline{\mathbf{h}}}(k/k) = \hat{\underline{\mathbf{h}}}(k/k-1) + \mathbf{K}(k)\mathbf{b}(k) \quad (2.48)$$

where  $\mathbf{K}(k)$  is the Kalman gain, given by:

$$\mathbf{K}(k) = \mathbf{P}(k/k-1)\mathbf{H}^T\mathbf{C}_b^{-1}(k) \quad (2.49)$$

In (2.49),  $\mathbf{P}(k/k-1)$  is the a priori error covariance matrix computed as follows:

$$\mathbf{P}(k/k-1) = \mathbf{\Phi}(k)\mathbf{P}(k-1/k-1)\mathbf{\Phi}(k)^T + \mathbf{\Gamma}\mathbf{\Sigma}_u\mathbf{\Gamma}^T \quad (2.50)$$

The aposteriori error covariance matrix  $\mathbf{P}(k/k)$  of the state vector is updated using the following Riccati equation:

$$\mathbf{P}(k/k) = \mathbf{P}(k/k-1) - \mathbf{K}(k)\mathbf{H}\mathbf{P}(k/k-1) \quad (2.51)$$

We need to initialize the state vector  $\underline{\mathbf{h}}(0)$  and the covariance matrix  $\mathbf{P}(0)$ . We can use  $\underline{\mathbf{h}}(0) = \mathbf{0}_{M \times 1}$  and  $\mathbf{P}(0) = \lambda\mathbf{I}_M$ , where  $\lambda$  is a scalar value.

The Kalman algorithm for M-AR process estimation is summarized in Table (2.2).

Table 2.2: Kalman algorithm for M-AR process estimation.

$\underline{\mathbf{h}}(0/0) = \underline{\mathbf{h}}_0$ $\mathbf{P}(0/0) = \mathbf{P}_0$
$\underline{\mathbf{h}}(k/k-1) = \mathbf{\Phi}(k)\underline{\mathbf{h}}(k-1/k-1)$ $\mathbf{P}(k/k-1) = \mathbf{\Phi}(k)\mathbf{P}(k-1/k-1)\mathbf{\Phi}^T(k) + \mathbf{\Gamma}\mathbf{\Sigma}_u\mathbf{\Gamma}^T$ $\mathbf{C}_b(k) = \mathbf{H}\mathbf{P}(k/k-1)\mathbf{H}^T + \mathbf{\Sigma}_v$ $\mathbf{K}(k) = \mathbf{P}(k/k-1)\mathbf{H}^T\mathbf{C}_b^{-1}(k)$ $\mathbf{b}(k) = \mathbf{y}(k) - \mathbf{H}\hat{\underline{\mathbf{h}}}(k/k-1)$ $\hat{\underline{\mathbf{h}}}(k/k) = \hat{\underline{\mathbf{h}}}(k/k-1) + \mathbf{K}(k)\mathbf{b}(k)$ $\mathbf{P}(k/k) = [\mathbf{I}_{M_p} - \mathbf{K}(k)\mathbf{H}]\mathbf{P}(k/k-1)$

### 2.4.1.2 $H_\infty$ Estimation Algorithm

The Kalman estimator assumes that the signal generating processes have known dynamics and that the noise sources have Gaussian known statistical properties. However, these assumptions may limit the application of the estimator since in many situations, only approximate signal model are available and the statistics of the noise sources are not fully known or unavailable. In addition, Kalman estimator may not be robust against parameter uncertainty of the signal models. To avoid these drawbacks, the  $H_\infty$  filter has been studied.

The optimal  $H_\infty$  estimator is designed to guarantee that the transfer operator relating the noise signals to the resulting estimation errors should provide an  $H_\infty$  norm less than a prescribed positive value. In the  $H_\infty$  estimator, the noise sources can be arbitrary signals with the only requirement of bounded noise. The  $H_\infty$  estimator aims to minimize the maximum transferred power from the disturbances to the output.

The concept of  $H_\infty$  filter is related to the game theory [She97]. Since  $H_\infty$  estimator involves the minimization of the worst possible amplification of the error signal, it can be viewed as a dynamic two-persons zero-sum game. In the game, the  $H_\infty$  filter (the designer) is a player prepared for the worst strategy that the other player (the nature) can provide. Thus, the goal of the filter is to provide a uniformly small estimation error for any process and measurement noises and any initial states. In this approach, a difference game is defined in which the state estimator and the disturbance signals (driving process, initial conditions and measurements noise) have the conflicting objectives of respectively, minimizing and maximizing the estimation error. The minimizer picks the optimal filter estimate, and the maximizer picks the worst case disturbance and initial conditions.

Unlike Kalman filter,  $H_\infty$  deals with the estimation of the linear combination of the state vector components  $\mathbf{z}(k)$  as follows:

$$\mathbf{z}(k) = \mathbf{L}\mathbf{h}(k) \quad (2.52)$$

where  $\mathbf{L}$  is a matrix whose value depends on the problem. Here, as the aim is to estimate the M-AR process, the matrix  $\mathbf{L}$  with dimension  $M \times Mp$  is defined as follows:

$$\mathbf{L} = \begin{bmatrix} \mathbf{I}_M & \mathbf{0}_M & \cdots & \mathbf{0}_M \end{bmatrix} \quad (2.53)$$

Define the estimation error as:

$$\underline{\mathbf{e}}(k) = \mathbf{z}(k) - \hat{\mathbf{z}}(k) = \mathbf{L}[\mathbf{h}(k) - \hat{\mathbf{h}}(k)] \quad (2.54)$$

Then, based on (2.40), (2.41) and (2.52), the  $H_\infty$  filter aims at minimizing the  $H_\infty$  norm of the transfer operator  $\mathcal{T}$  that maps the noise disturbances  $\mathbf{u}(k)$ ,  $\mathbf{v}(k)$  and the initial state error  $\mathbf{E}_0 = \mathbf{h}(0) - \hat{\mathbf{h}}(0)$  to the estimation error  $\underline{\mathbf{e}}(k)$  as follows:

$$J_\infty = \sup_{\mathbf{u}(k), \mathbf{v}(k), \mathbf{h}(0)} J \quad (2.55)$$

where

$$J = \frac{\sum_{k=0}^{N-1} \|\underline{\mathbf{e}}(k)\|^2}{\|\mathbf{E}_0\|_{\mathbf{P}_0^{-1}}^2 + \sum_{k=0}^{N-1} [\|\mathbf{u}(k)\|_{\mathbf{Q}_u^{-1}}^2 + \|\mathbf{v}(k)\|_{\mathbf{R}_v^{-1}}^2]} \quad (2.56)$$

with  $N$  the number of available data samples.  $\mathbf{P}_0^{-1} > 0$ ,  $\mathbf{Q}_u > 0$  and  $\mathbf{R}_v > 0$  are weighting matrices tuned by the designer to achieve the desired performance. They can be estimated during the estimation process. In addition,  $\|\mathbf{S}\|_Q^2 = \mathbf{S}^H \mathbf{Q} \mathbf{S}$ .

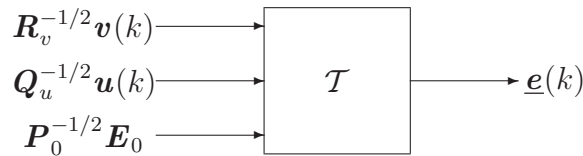


Figure 2.1: Transfer operator  $\mathcal{T}$ .

However, as a closed-form solution to the above optimal  $H_\infty$  estimation problem does not always exist, the following suboptimal design strategy is usually considered:

$$J_\infty < \gamma^2 \quad (2.57)$$

where  $\gamma$  is a prescribed level of noise attenuation.

Let  $\gamma > 0$ , then there exists an  $H_\infty$  filter if and only if there exists a stabilizing symmetric solution  $\underline{\mathbf{P}}(k) > \mathbf{0}$  to the following discrete-time Riccati-type equation:

$$\underline{\mathbf{P}}(k+1) = \Phi(k)\underline{\mathbf{P}}(k)\mathbf{C}^{-1}(k)\Phi^T(k) + \Gamma\mathbf{Q}_u\Gamma^T \quad (2.58)$$

where  $\mathbf{C}(k)$  is given by:

$$\mathbf{C}(k) = \mathbf{I}_{M_p} - \gamma^{-2}\mathbf{L}^T\mathbf{L}\underline{\mathbf{P}}(k) + \mathbf{H}^T\mathbf{R}_v^{-1}\mathbf{H}\underline{\mathbf{P}}(k) \quad (2.59)$$

This leads to the following constraint:

$$\underline{\mathbf{P}}(k)\mathbf{C}^{-1}(k) > \mathbf{0} \quad (2.60)$$

If the condition (2.60) is fulfilled, the  $H_\infty$  filter exist and is given by:

$$\hat{\underline{\mathbf{h}}}(k) = \Phi(k)\hat{\underline{\mathbf{h}}}(k-1) + \underline{\mathbf{K}}(k)\mathbf{b}(k) \quad (2.61)$$

where the innovation vector  $\mathbf{b}(k)$  and the  $H_\infty$  gain  $\underline{\mathbf{K}}(k)$  are respectively given as follows:

$$\mathbf{b}(k) = \mathbf{y}(k) - \mathbf{H}\Phi(k)\hat{\underline{\mathbf{h}}}(k-1) \quad (2.62)$$

$$\underline{\mathbf{K}}(k) = \Phi(k)\underline{\mathbf{P}}(k)\mathbf{C}^{-1}(k)\mathbf{H}^T\mathbf{R}_v^{-1} \quad (2.63)$$

It should be noted that the the matrix  $\underline{\mathbf{P}}(k)$  can be seen as the upper bound of the error covariance matrix in Kalman filter theory, i.e:

$$\underline{\mathbf{P}}(k) \geq \mathbf{P}(k) = E[(\underline{\mathbf{h}}(k) - \hat{\underline{\mathbf{h}}}(k))(\underline{\mathbf{h}}(k) - \hat{\underline{\mathbf{h}}}(k))^T] \quad (2.64)$$

If the weighting parameters  $\mathbf{Q}_u$ ,  $\mathbf{R}_v$  and  $\underline{\mathbf{P}}_0$  are respectively chosen to be  $\Sigma_u$ ,  $\Sigma_v$  and the initial error covariance matrix of  $\underline{\mathbf{h}}(k)$ , then the  $H_\infty$  filter reduces to the Kalman one when  $\gamma \rightarrow \infty$ .

The level attenuation factor  $\gamma$  must be carefully selected to satisfy the condition in (2.60):

$$\gamma^2 > \max(\text{eig}(\mathbf{L}^T\mathbf{L}[\underline{\mathbf{P}}^{-1}(k) + \mathbf{L}^T\mathbf{R}_v^{-1}\mathbf{L}]^{-1})) \quad (2.65)$$

where  $\max(\text{eig}[\mathbf{F}])$  is the maximum eigenvalue of  $\mathbf{F}$ . There are two strategies for selecting  $\gamma^2$ , either using a constant value for  $\gamma^2$  or updating it according to (2.65) as follows:

$$\gamma^2(k) = \zeta \max(\text{eig}(\mathbf{L}^T\mathbf{L}[\underline{\mathbf{P}}^{-1}(k) + \mathbf{L}^T\mathbf{R}_v^{-1}\mathbf{L}]^{-1})) \quad (2.66)$$

where  $\zeta > 2$

The  $H_\infty$  algorithm for M-AR process estimation is summarized in Table (2.3).

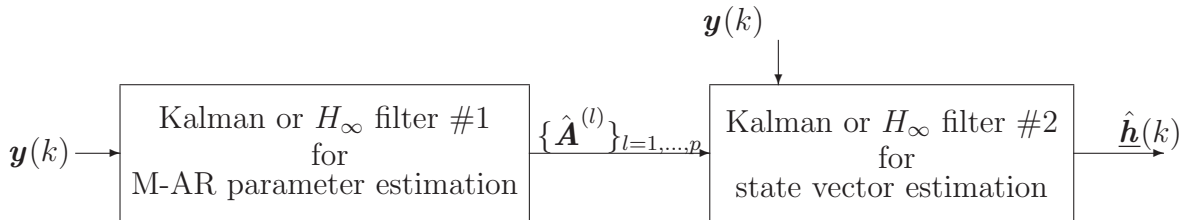
Table 2.3:  $H_\infty$  algorithm for M-AR process estimation.

<p><i>Initialization</i></p> $\underline{\mathbf{h}}(0) = \underline{\mathbf{h}}_0$ $\underline{\mathbf{P}}(0) = \underline{\mathbf{P}}_0$ <p><i>Filtering</i></p> $\mathbf{C}(k) = \mathbf{I}_{M_p} - \gamma^{-2} \mathbf{L}^T \mathbf{L} \underline{\mathbf{P}}(k) + \mathbf{H}^T \mathbf{R}_v^{-1} \mathbf{H} \underline{\mathbf{P}}(k)$ $\underline{\mathbf{K}}(k) = \underline{\Phi}(k) \underline{\mathbf{P}}(k) \mathbf{C}^{-1}(k) \mathbf{H}^T \mathbf{R}_v^{-1}$ $\mathbf{b}(k) = \mathbf{y}(k) - \mathbf{H} \underline{\Phi}(k) \hat{\underline{\mathbf{h}}}(k-1)$ $\hat{\underline{\mathbf{h}}}(k) = \underline{\Phi}(k) \hat{\underline{\mathbf{h}}}(k) + \underline{\mathbf{K}}(k) \mathbf{b}(k)$ $\underline{\mathbf{P}}(k+1) = \underline{\Phi}(k) \underline{\mathbf{P}}(k) \mathbf{C}^{-1}(k) \underline{\Phi}^T(k) + \Gamma \mathbf{Q}_u \Gamma^T$
--

### 2.4.2 Parameter Estimation Directly from the Noisy Observations

In the previous section we present the Kalman and  $H_\infty$  filters for the estimation of M-AR process. In this section, we address the estimation of M-AR process parameters directly from the noisy observations using Kalman or  $H_\infty$  filters.

Two serially-connected Kalman (SC-Kalman) or  $H_\infty$  (SC- $H_\infty$ ) filters [Arn98] [Cai04] can be used in the estimation of M-AR process and its parameters as shown in Figure 2.2.


 Figure 2.2: SC-Kalman or SC- $H_\infty$  filters.

Define the vector  $\mathbf{Y}_\theta(k)$  which contains the last  $p$  observations as the following:

$$\mathbf{Y}_\theta(k) = \begin{bmatrix} -\mathbf{y}^T(k) & -\mathbf{y}^T(k-1) & \cdots & -\mathbf{y}^T(k-p+1) \end{bmatrix}^T \quad (2.67)$$

By stacking the columns of the matrix  $\boldsymbol{\psi} = \begin{bmatrix} \mathbf{A}^{(1)} & \cdots & \mathbf{A}^{(p)} \end{bmatrix}^T$  on top of each others, the resulting  $M^2 p \times 1$  state vector can be expressed as:

$$\boldsymbol{\theta}(k) = \begin{bmatrix} [a_{11}^{(1)} \cdots a_{1M}^{(1)}] \cdots [a_{11}^{(p)} \cdots a_{1M}^{(p)}] \\ \cdots [a_{M1}^{(1)} \cdots a_{MM}^{(1)}] \cdots [a_{M1}^{(p)} \cdots a_{MM}^{(p)}] \end{bmatrix}^T \quad (2.68)$$

By combining the M-AR model (2.1) with the observation equation (2.7), one can obtain:

$$\mathbf{y}(k) = \mathbf{H}_\theta(k)\boldsymbol{\theta}(k) + \mathbf{v}_\theta(k) \quad (2.69)$$

where

$$\mathbf{v}_\theta(k) = \mathbf{u}(k) + \mathbf{v}(k) + \sum_{l=1}^p \mathbf{A}^{(l)}\mathbf{v}(k-l) \quad (2.70)$$

and

$$\mathbf{H}_\theta(k) = \mathbf{I}_M \otimes \mathbf{Y}_\theta^T(k) \quad (2.71)$$

with  $\otimes$  denotes the matrix Kronecker product.

When the M-AR process is assumed stationary, the AR parameters are time-invariant and, hence, satisfy the following relationship:

$$\boldsymbol{\theta}(k) = \boldsymbol{\theta}(k-1) \quad (2.72)$$

Thus, equations (2.69) and (2.72) define the state-space representation for the estimation of the AR parameters using Kalman or  $H_\infty$  algorithms.

#### 2.4.2.1 Parameter Estimation Using Kalman Filter

Based on the state-space model (2.69) and (2.72), the parameter vector  $\boldsymbol{\theta}(k)$  can be estimated as follows:

$$\hat{\boldsymbol{\theta}}(k) = \hat{\boldsymbol{\theta}}(k-1) + \mathbf{K}_\theta(k)[\mathbf{y}(k) - \mathbf{H}_\theta(k)\hat{\boldsymbol{\theta}}(k-1)] \quad (2.73)$$

where the Kalman gain  $\mathbf{K}_\theta(k)$  and the error covariance matrix  $\mathbf{P}_\theta(k/k)$  are respectively given by:

$$\mathbf{K}_\theta(k) = \mathbf{P}_\theta(k/k-1)\mathbf{H}_\theta^T(k)[\mathbf{H}_\theta(k)\mathbf{P}_\theta(k/k-1)\mathbf{H}_\theta^T(k) + \mathbf{R}_\theta(k)]^{-1} \quad (2.74)$$

and

$$\mathbf{P}_\theta(k/k) = [\mathbf{I}_{M^2p} - \mathbf{K}_\theta(k)\mathbf{H}_\theta(k)]\mathbf{P}_\theta(k/k-1) \quad (2.75)$$

where  $\mathbf{R}_\theta(k)$  is the covariance matrix of  $\mathbf{v}_\theta(k)$ .

Table 2.4 summarizes the estimation of M-AR parameters using Kalman algorithm.

#### 2.4.2.2 Parameter Estimation using $H_\infty$ Filter

Based on the state-space model (2.69) and (2.72), the  $H_\infty$  filter provides an estimation of the parameter vector  $\boldsymbol{\theta}(k)$  as follows:

$$\hat{\boldsymbol{\theta}}(k) = \hat{\boldsymbol{\theta}}(k-1) + \underline{\mathbf{K}}_\theta(k)[\mathbf{y}(k) - \mathbf{H}_\theta(k)\hat{\boldsymbol{\theta}}(k-1)] \quad (2.76)$$

Table 2.4: Kalman algorithm for parameters estimation of M-AR process.

<i>Initialization</i> $\boldsymbol{\theta}(0) = \boldsymbol{\theta}_0$ $\mathbf{P}_\theta(0/0) = \mathbf{P}_{\theta 0}$
<i>Filtering</i> $\mathbf{P}_\theta(k/k-1) = \mathbf{P}_\theta(k-1/k-1)$ $\mathbf{Y}_\theta(k) = \begin{bmatrix} -\mathbf{y}^T(k) & -\mathbf{y}^T(k-1) & \cdots & -\mathbf{y}^T(k-p+1) \end{bmatrix}^T$ $\mathbf{H}_\theta(k) = \mathbf{I}_M \otimes \mathbf{Y}_\theta^T(k)$ $\mathbf{K}_\theta(k) = \mathbf{P}_\theta(k/k-1) \mathbf{H}_\theta^T(k) [\mathbf{H}_\theta(k) \mathbf{P}_\theta(k/k-1) \mathbf{H}_\theta^T(k) + \mathbf{R}_\theta(k)]^{-1}$ $\hat{\boldsymbol{\theta}}(k) = \hat{\boldsymbol{\theta}}(k-1) + \mathbf{K}_\theta(k) [\mathbf{y}(k) - \mathbf{H}_\theta(k) \hat{\boldsymbol{\theta}}(k-1)]$ $\mathbf{P}_\theta(k/k) = [\mathbf{I}_{M^2p} - \mathbf{K}_\theta(k) \mathbf{H}_\theta(k)] \mathbf{P}_\theta(k/k-1)$

 Table 2.5:  $H_\infty$  algorithm for parameters estimation of M-AR process.

<i>Initialization</i> $\boldsymbol{\theta}(0) = \boldsymbol{\theta}_0$ $\underline{\mathbf{P}}_\theta(0) = \underline{\mathbf{P}}_{\theta 0}$
<i>Filtering</i> $\mathbf{Y}_\theta(k) = \begin{bmatrix} -\mathbf{y}^T(k) & -\mathbf{y}^T(k-1) & \cdots & -\mathbf{y}^T(k-p+1) \end{bmatrix}^T$ $\mathbf{H}_\theta(k) = \mathbf{I}_M \otimes \mathbf{Y}_\theta^T(k)$ $\mathbf{C}_\theta(k) = \mathbf{I}_{M^2p} - \gamma_\theta^{-2} \underline{\mathbf{P}}_\theta(k) + \mathbf{H}_\theta^T(k) \mathbf{R}_{v_\theta}^{-1} \mathbf{H}_\theta(k) \underline{\mathbf{P}}_\theta(k)$ $\underline{\mathbf{K}}_\theta(k) = \underline{\mathbf{P}}_\theta(k) \mathbf{C}_\theta^{-1}(k) \mathbf{H}_\theta^T(k) \mathbf{R}_{v_\theta}^{-1}$ $\hat{\boldsymbol{\theta}}(k) = \hat{\boldsymbol{\theta}}(k-1) + \underline{\mathbf{K}}_\theta(k) [\mathbf{y}(k) - \mathbf{H}_\theta(k) \hat{\boldsymbol{\theta}}(k-1)]$ $\underline{\mathbf{P}}_\theta(k+1) = \underline{\mathbf{P}}_\theta(k) \mathbf{C}_\theta^{-1}(k)$

where the  $H_\infty$  gain

$$\underline{\mathbf{K}}_\theta(k) = \underline{\mathbf{P}}_\theta(k) \mathbf{C}_\theta^{-1}(k) \mathbf{H}_\theta^T(k) \mathbf{R}_v^{-1} \quad (2.77)$$

and

$$\underline{\mathbf{P}}_\theta(k+1) = \underline{\mathbf{P}}_\theta(k) \mathbf{C}_\theta^{-1}(k) \quad (2.78)$$

$$\mathbf{C}_\theta(k) = \mathbf{I}_{M^2p} - \gamma_\theta^{-2} \underline{\mathbf{P}}_\theta(k) + \mathbf{H}_\theta^T(k) \mathbf{R}_{v_\theta}^{-1} \mathbf{H}_\theta(k) \underline{\mathbf{P}}_\theta(k) \quad (2.79)$$

where  $\mathbf{R}_{v_\theta}$  is a weighing matrix.

The  $H_\infty$  algorithm for M-AR parameter estimation is summarized in Table 2.5.

According to (2.70) Kalman or  $H_\infty$  filters applied directly to the noisy observations provide biased estimates, since the noise  $\mathbf{v}_\theta$  is colored. To avoid this drawback, we propose to extend the CC-Kalman filters [Lab06] and CC- $H_\infty$  filters [Lab07] to the multichannel case.

### 2.4.3 Joint Process and Parameter Estimations

The structure of SC-Kalman or SC- $H_\infty$  filters provides biased estimates as mentioned previously. To avoid this problem, we suggest using mutually-interactive Kalman or  $H_\infty$  filters as shown in Figure 2.3.

As a new observation is available the first filter is used to estimate the M-AR process; where as the second filter uses the estimated M-AR process to update the M-AR parameters. This structure jointly estimate the M-AR process and its parameters. It provides consistent estimation of the parameter matrices as they are estimated from the estimated M-AR process [Lab06].

This structure, firstly developed for the estimation of single channel AR process [Lab06] [Lab07], is here extended to account for multichannel AR processes.

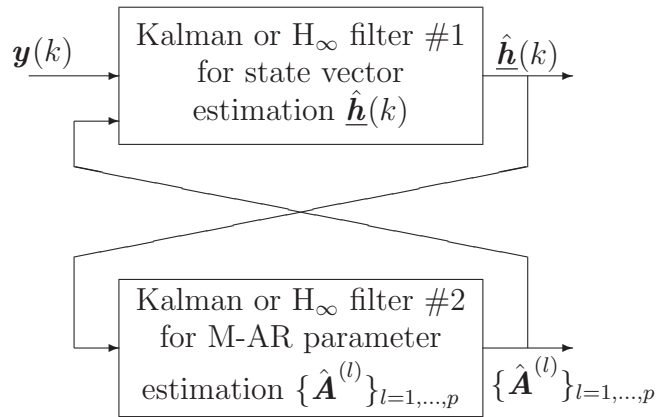


Figure 2.3: CC-Kalman or CC- $H_\infty$  filter for the estimation of M-AR process and its parameters.

#### 2.4.3.1 Two Cross-Coupled Kalman Filters

To avoid the bias estimation issue, we propose to extend to the multichannel case, the two cross-coupled Kalman filters, initially developed for the estimation of single channel AR process and its parameters [Lab06].

##### **A. Estimation of M-AR Process:**

Based on the state-space model in (2.40) and (2.41), the M-AR process can be estimated as summarized in Table 2.2. The estimated vector  $\hat{\mathbf{h}}(k)$  is used in the second filter to estimate the M-AR parameters.

If the covariance matrices  $\Sigma_u$  and  $\Sigma_v$  are not known, they can be estimated during the estimation process as explained later.

***B. Estimation of the M-AR Parameters:***

The estimated process vector  $\hat{\mathbf{h}}(k)$  can be expressed in terms of the parameters vector. By combining (2.45) and (2.48) and multiplying the result by  $\mathbf{L}$ , one can obtain:

$$\hat{\mathbf{h}}(k/k) = \mathbf{H}_\theta(k)\boldsymbol{\theta}(k) + \mathbf{v}_\theta(k) \quad (2.80)$$

where  $\mathbf{H}_\theta(k)$  depends on the estimated state vector and is expressed as follows:

$$\mathbf{H}_\theta(k) = -\mathbf{I}_M \otimes \hat{\mathbf{h}}^T(k-1/k-1) \quad (2.81)$$

and  $\mathbf{v}_\theta(k)$  is given by:

$$\mathbf{v}_\theta(k) = \mathbf{L}\mathbf{K}(k)\mathbf{b}(k) \quad (2.82)$$

By combining (2.47) and (2.80), the covariance matrix  $\mathbf{R}_\theta(k)$  of  $\mathbf{v}_\theta(k)$  can be expressed as follows:

$$\mathbf{R}_\theta(k) = \mathbf{H}\mathbf{K}(k)\mathbf{C}_b(k)\mathbf{K}^T(k)\mathbf{H}^T(k) \quad (2.83)$$

The state vector  $\boldsymbol{\theta}(k)$  can be written as follows:

$$\boldsymbol{\theta}(k) = \left[ \begin{array}{ccc} [a_{11}^{(1)} & \cdots & a_{1M}^{(1)}] & \cdots & [a_{11}^{(p)} & \cdots & a_{1M}^{(p)}] \\ \cdots & [a_{M1}^{(1)} & \cdots & a_{MM}^{(1)}] & \cdots & [a_{M1}^{(p)} & \cdots & a_{MM}^{(p)}] \end{array} \right]^T \quad (2.84)$$

If the M-AR process is assumed to be stationary, then the parameter vector  $\boldsymbol{\theta}(k)$  satisfies (2.72).

A second Kalman filter can then be used to estimate the parameters.

***C. Estimation of Noise-Covariance Matrices:***

In some applications we don't know the driving process and measurement noise covariance matrices. They can be estimated during the estimation process as follows:

Substituting (2.50) into (2.51), it follows that:

$$\mathbf{P}(k/k) = \Phi(k)\mathbf{P}(k-1/k-1)\Phi^T(k) + \Gamma\Sigma_u\Gamma^T - \mathbf{K}(k)\mathbf{H}\mathbf{P}(k/k-1) \quad (2.85)$$

By multiplying both sides of (2.49) by  $\mathbf{C}_b(k)$  and transposing the result, one can obtain the following :

$$\mathbf{H}\mathbf{P}(k/k-1) = \mathbf{C}(k)\mathbf{K}^T(k) \quad (2.86)$$

since  $\mathbf{P}(k/k-1)$  is real and symmetric, we can write the following:

$$\mathbf{P}(k/k-1) = \mathbf{P}^T(k/k-1) \quad (2.87)$$

By combining (2.85) and (2.86),  $\Sigma_u$  can be expressed as follows:

$$\Sigma_u = \mathbf{D}[\mathbf{P}(k/k) - \Phi(k)\mathbf{P}(k-1/k-1)\Phi^T(k) + \mathbf{K}(k)\mathbf{C}(k)\mathbf{K}^T(k)]\mathbf{D}^T \quad (2.88)$$

where  $\mathbf{D} = (\Gamma^T\Gamma)^{-1}\Gamma^T$ .

The covariance matrix  $\Sigma_u$  can be estimated recursively as follows [Lab06]:

$$\hat{\Sigma}_u(k) = \frac{k-1}{k}\hat{\Sigma}_u(k-1) + \frac{1}{k}\mathbf{D}\mathbf{G}(k)\mathbf{D}^T \quad (2.89)$$

where  $\mathbf{G}(k)$  is given by:

$$\mathbf{G}(k) = \mathbf{P}(k/k) - \Phi(k)\mathbf{P}(k-1/k-1)\Phi^T(k) + \mathbf{K}(k)(\text{diag}(\mathbf{b}(k)))^2\mathbf{K}^T(k) \quad (2.90)$$

The measurements noise covariance matrix  $\Sigma_v(k)$  can be estimated recursively based on (2.47) as follows [Lab06]:

$$\hat{\Sigma}_v(k) = \frac{k-1}{k}\hat{\Sigma}_v(k-1) + \frac{1}{k}\mathbf{M}(k) \quad (2.91)$$

where  $\mathbf{M}(k)$  is given by:

$$\mathbf{M}(k) = (\text{diag}[\mathbf{b}(k) - \mathbf{H}(k)\mathbf{P}(k/k-1)\mathbf{H}^T(k)])^2 \quad (2.92)$$

#### ***D. Computational Complexity:***

The first filter in the CC-Kalman filters is used to estimate the  $Mp \times 1$  state vector, it results in computational complexity of the order of  $O((Mp)^3)$ . And the second filter is used to estimate the  $M^2p \times 1$  parameter vector, it results in computational complexity of the order of  $O((M^2p)^2)$ . Thus, the overall computational complexity of the CC-Kalman filters is of the order of  $O((M^2p)^2) + O((Mp)^3)$ . While in the case of the EKF and SPKF the computational complexity is higher. The dimension of the state vector to be estimated is  $(M^2p + Mp) \times 1$  which results in computational complexity of the order of  $O((M^2p + Mp)^3)$ .

#### ***E. CC-Kalman Algorithm:***

Table 2.6 summarizes the CC-Kalman filtering algorithm.

Table 2.6: CC-Kalman filtering algorithm.

<p><i>Initializing the first filter</i></p> $\hat{\mathbf{h}}(0/0) = \mathbf{h}_0$ $\mathbf{P}(0/0) = \mathbf{P}_0$ <p><i>Initializing the second filter</i></p> $\hat{\boldsymbol{\theta}}(0) = \boldsymbol{\theta}_0$ $\mathbf{P}_\theta(0/0) = \mathbf{P}_{\theta 0}$ <p><i>The first filter: M-AR process estimation</i></p> $\hat{\mathbf{h}}(k/k-1) = \boldsymbol{\Phi}(k)\hat{\mathbf{h}}(k-1/k-1)$ $\mathbf{P}(k/k-1) = \boldsymbol{\Phi}(k)\mathbf{P}(k-1/k-1)\boldsymbol{\Phi}^T(k) + \boldsymbol{\Gamma}\boldsymbol{\Sigma}_u\boldsymbol{\Gamma}^T$ $\mathbf{b}(k) = \mathbf{y}(k) - \mathbf{H}\hat{\mathbf{h}}(k/k-1)$ $\mathbf{C}_b(k) = \mathbf{H}\mathbf{P}(k/k-1)\mathbf{H}^T + \boldsymbol{\Sigma}_v$ $\mathbf{K}(k) = \mathbf{P}(k/k-1)\mathbf{H}^T\mathbf{C}_b^{-1}(k)$ $\hat{\mathbf{h}}(k/k) = \hat{\mathbf{h}}(k/k-1) + \mathbf{K}(k)\mathbf{b}(k)$ $\mathbf{P}(k/k) = [\mathbf{I}_{M_p} - \mathbf{K}(k)\mathbf{H}]\mathbf{P}(k/k-1)$ <p><i>The second filter: Parameters estimation</i></p> $\mathbf{H}_\theta(k) = -\mathbf{I}_M \otimes \hat{\mathbf{h}}^T(k-1/k-1)$ $\mathbf{v}_\theta = \mathbf{H}\mathbf{K}(k)\mathbf{b}(k)$ $\mathbf{R}_\theta(k) = \mathbf{H}\mathbf{K}(k)\mathbf{C}_b(k)\mathbf{K}^T(k)\mathbf{H}^T$ $\mathbf{P}_\theta(k/k-1) = \mathbf{P}_\theta(k-1/k-1)$ $\mathbf{K}_\theta(k) = \mathbf{P}_\theta(k/k-1)\mathbf{H}_\theta^T(k)[\mathbf{H}_\theta(k)\mathbf{P}_\theta(k/k-1)\mathbf{H}_\theta^T(k) + \mathbf{R}_\theta(k)]^{-1}$ $\hat{\boldsymbol{\theta}}(k) = \hat{\boldsymbol{\theta}}(k-1) + \mathbf{K}_\theta(k)\mathbf{v}_\theta(k)$ $\mathbf{P}_\theta(k/k) = [\mathbf{I}_{M^{2p}} - \mathbf{K}_\theta(k)\mathbf{H}_\theta(k)]\mathbf{P}_\theta(k/k-1)$ <p><i>Estimation of noise autocorrelation matrices</i></p> $\hat{\boldsymbol{\Sigma}}_u(k) = \frac{k-1}{k}\hat{\boldsymbol{\Sigma}}_u(k-1) + \frac{1}{k}\mathbf{D}\mathbf{L}(k)\mathbf{D}^T$ $\hat{\boldsymbol{\Sigma}}_v(k) = \frac{k-1}{k}\hat{\boldsymbol{\Sigma}}_v(k-1) + \frac{1}{k}\mathbf{M}(k)$
---

### 2.4.3.2 Two Cross-Coupled $H_\infty$ Filters

The Kalman filter requires that the driving process and the measurement noise to be Gaussian with known variances. These assumptions are rarely satisfied in reality. To relax these assumptions, we propose to extend the CC- $H_\infty$  filters [Lab07] to the multichannel case for joint M-AR process and parameters estimation.

#### **A. Estimation of M-AR process:**

Based on the state-space model in (2.40) and (2.41), the M-AR process can be estimated as summarized in Table 2.3. Here, the estimated vector  $\hat{\mathbf{h}}(k)$  is used in the second filter to estimate the M-AR parameters.

#### **B. Estimation of the M-AR Parameters:**

By combining (2.52) and (2.61), the estimated M-AR process  $\hat{\mathbf{h}}(k)$  can be written as follows:

$$\hat{\mathbf{h}}(k) = \mathbf{H}_\theta(k)\boldsymbol{\theta}(k) + \mathbf{v}_\theta(k) \quad (2.93)$$

where  $\mathbf{H}_\theta(k)$  and  $\mathbf{v}_\theta(k)$  are respectively given as follows:

$$\mathbf{H}_\theta(k) = -\mathbf{I}_M \otimes \hat{\mathbf{h}}^T(k-1) \quad (2.94)$$

$$\mathbf{v}_\theta(k) = \mathbf{L}\mathbf{K}(k)\mathbf{b}(k) \quad (2.95)$$

The state vector  $\boldsymbol{\theta}(k)$  is written as follows:

$$\boldsymbol{\theta}(k) = \left[ \begin{array}{ccc} [ a_{11}^{(1)} & \cdots & a_{1M}^{(1)} ] & \cdots & [ a_{11}^{(p)} & \cdots & a_{1M}^{(p)} ] \\ \cdots & [ a_{M1}^{(1)} & \cdots & a_{MM}^{(1)} ] & \cdots & [ a_{M1}^{(p)} & \cdots & a_{MM}^{(p)} ] \end{array} \right]^T \quad (2.96)$$

Assume stationary processes, then the parameters are time invariant satisfying the following relationship:

$$\boldsymbol{\theta}(k) = \boldsymbol{\theta}(k-1) \quad (2.97)$$

The equations (2.93) and (2.97) define a state-space representation for the estimation of the AR parameters. A second  $H_\infty$  filter can be used to recursively estimate  $\boldsymbol{\theta}(k)$ , where the AR parameter estimation error is defined as:

$$\mathbf{e}_\theta(k) = \mathbf{H}_\theta(k)[\boldsymbol{\theta}(k) - \hat{\boldsymbol{\theta}}(k)] \quad (2.98)$$

**C. Tuning the Parameters:**

The matrix  $\underline{\mathbf{P}}_\theta(k)$  and the initial state  $\boldsymbol{\theta}(k)$  can be respectively initialized as:

$$\underline{\mathbf{P}}_\theta(0) = \underline{\mathbf{P}}_0 = \mathbf{I}_{M^2p} \quad (2.99)$$

$$\boldsymbol{\theta}_\theta(0) = \boldsymbol{\theta}_0 = \mathbf{0}_{M^2p \times 1} \quad (2.100)$$

Equation (2.93) can be used to derive a formula to estimate  $\mathbf{R}_{v_\theta}$  as follows:

$$\mathbf{R}_{v_\theta} = \mathbf{L}\underline{\mathbf{K}}(k)\mathbf{b}(k)\mathbf{b}^H(k)\underline{\mathbf{K}}^H(k)\mathbf{L}^T \quad (2.101)$$

and  $\mathbf{Q}_u$  can be tuned recursively as follows:

$$\hat{\mathbf{Q}}_u(k) = \lambda \hat{\mathbf{Q}}_u(k-1) + (1-\lambda)\mathbf{L}\mathbf{M}(k)\mathbf{L}^T \quad (2.102)$$

where  $\lambda$  is the forgetting factor, and  $\mathbf{M}(k)$  is given by:

$$\mathbf{M}(k) = \underline{\mathbf{P}}(k) - \underline{\Phi}(k)\underline{\mathbf{P}}(k-1)\underline{\Phi}^T(k) + \underline{\mathbf{K}}(k)\mathbf{b}(k)\mathbf{b}^H(k)\underline{\mathbf{K}}(k) \quad (2.103)$$

**D. Computational Complexity:**

The computational complexity of the CC- $H_\infty$  is of the order of  $O((M^2p)^2) + O((Mp)^3)$  as in the case of CC-Kalman filters, with CC- $H_\infty$  filters has slightly more computational complexity due to (2.59). In addition, the CC- $H_\infty$  filters need need to select or update the level attenuation factor according to (2.65) or (2.66).

**E. CC- $H_\infty$  Algorithm:**

Table 2.7 summarizes the two cross-coupled  $H_\infty$  algorithm.

Table 2.7: CC- $H_\infty$  filtering algorithm.

<p><i>Initializing the first filter</i></p> $\hat{\underline{\mathbf{h}}}(0) = \underline{\mathbf{h}}_0$ $\underline{\mathbf{P}}(0) = \underline{\mathbf{P}}_0$ <p><i>Initializing the second filter</i></p> $\hat{\underline{\boldsymbol{\theta}}}(0) = \underline{\boldsymbol{\theta}}_0$ $\underline{\mathbf{P}}_\theta(0) = \underline{\mathbf{P}}_{\theta 0}$ <p><i>The first filter: processes estimation</i></p> $\underline{\mathbf{C}}(k) = \mathbf{I}_{M_p} - \gamma^{-2} \mathbf{L}^T \underline{\mathbf{L}} \underline{\mathbf{P}}(k) + \mathbf{H}^H \mathbf{R}_v^{-1} \mathbf{H} \underline{\mathbf{P}}(k)$ $\underline{\mathbf{K}}(k) = \underline{\mathbf{P}}(k) \underline{\mathbf{C}}^{-1}(k) \mathbf{H}^H \mathbf{R}_v^{-1}$ $\underline{\mathbf{b}}(k) = \mathbf{y}(k) - \mathbf{H} \hat{\underline{\mathbf{h}}}(k-1)$ $\hat{\underline{\mathbf{h}}}(k) = \underline{\Phi}(k) \hat{\underline{\mathbf{h}}}(k-1) + \underline{\mathbf{K}}(k) \underline{\mathbf{b}}(k)$ $\underline{\mathbf{P}}(k+1) = \underline{\Phi}(k) \underline{\mathbf{P}}(k) \underline{\mathbf{C}}^{-1}(k) \underline{\Phi}^T(k) + \Gamma \mathbf{R}_u^{-1} \Gamma^T$ <p><i>The second filter: parameters estimation</i></p> $\hat{\underline{\mathbf{h}}}(k) = \underline{\mathbf{L}} \hat{\underline{\mathbf{h}}}(k)$ $\mathbf{H}_\theta(k) = -\mathbf{I}_M \otimes \hat{\underline{\mathbf{h}}}(k-1)^T$ $\underline{\mathbf{C}}_\theta(k) = \mathbf{I}_{M^2 p} - \gamma_\theta^{-2} \mathbf{H}_\theta^H(k) \mathbf{H}_\theta(k) \underline{\mathbf{P}}_\theta(k) + \mathbf{H}_\theta^H(k) \mathbf{R}_{v_\theta}^{-1} \mathbf{H}_\theta(k) \underline{\mathbf{P}}_\theta(k)$ $\underline{\mathbf{K}}_\theta(k) = \underline{\mathbf{P}}_\theta(k) \underline{\mathbf{C}}_\theta^{-1}(k) \mathbf{H}_\theta^H(k) \mathbf{R}_{v_\theta}^{-1}$ $\underline{\mathbf{b}}_\theta(k) = \hat{\underline{\mathbf{h}}}(k) - \mathbf{H}_\theta(k) \hat{\underline{\boldsymbol{\theta}}}(k-1)$ $\hat{\underline{\boldsymbol{\theta}}}(k) = \hat{\underline{\boldsymbol{\theta}}}(k-1) + \underline{\mathbf{K}}_\theta(k) \underline{\mathbf{b}}_\theta(k)$ $\underline{\mathbf{P}}_\theta(k+1) = \underline{\mathbf{P}}_\theta(k) \underline{\mathbf{C}}_\theta^{-1}(k)$ <p><i>Tuning parameters</i></p> $\mathbf{R}_{v_\theta}(k) = \underline{\mathbf{L}} \underline{\mathbf{K}}(k) \underline{\mathbf{b}}(k) \underline{\mathbf{b}}^H(k) \underline{\mathbf{K}}^H(k) \underline{\mathbf{L}}^T$ $\underline{\mathbf{M}}(k) = \underline{\mathbf{P}}(k) - \underline{\Phi}(k) \underline{\mathbf{P}}(k-1) \underline{\Phi}^T(k) + \underline{\mathbf{K}}(k) \underline{\mathbf{b}}(k) \underline{\mathbf{b}}^H(k) \underline{\mathbf{K}}^H(k)$ $\hat{\underline{\mathbf{R}}}_u(k) = \lambda \hat{\underline{\mathbf{R}}}_u(k-1) + (1-\lambda) \underline{\mathbf{L}} \underline{\mathbf{M}}(k) \underline{\mathbf{L}}^T$
---

# Chapter 3

## Simulation Results

### Contents

---

3.1	Simulation Protocols . . . . .	52
3.2	Parameter Estimation of Synthetic M-AR Process . . . . .	54
3.3	Parameter Estimation of Mobile Fading Channels . . . . .	65

---

In this chapter, we carry out a comparative simulation study between several M-AR parameter estimation methods:

- 1- The YW equations.
- 2- The ARFIT [Neu01].
- 3- The SC-Kalman filters [Arn98].
- 4- The NCYW equations.
- 5- Hassan's algorithm [Has03].
- 6- The proposed CC-Kalman filters.
- 7- The proposed CC- $H_\infty$  filters.

These methods are compared in terms of the following:

- 1- The performance in the case of limited number of samples and small SNR.
- 2- The accuracy of the estimated M-AR process parameters.
- 3- The computational complexity.
- 4- The stability of the algorithm, i.e., the estimated parameters result in a stable system or not.
- 5- The uncertainty of the models and the lack of statistical information.

In the following section, we describe the simulation protocols. In section 2, we provide the simulation results in the case of a synthetic M-AR process. In section 3, we present the simulation results of the M-AR processes that corresponds to correlated fading channels.

### 3.1 Simulation Protocols

The simulations in the next two sections are performed for a correlated second order M-AR process with two channels. In this case, the M-AR process can be written as follows:

$$\mathbf{h}(k) = -\mathbf{A}^{(1)}\mathbf{h}(k-1) - \mathbf{A}^{(2)}\mathbf{h}(k-2) + \mathbf{u}(k) \quad (3.1)$$

where  $\mathbf{u}(k) = \begin{bmatrix} u_1(k) & u_2(k) \end{bmatrix}^T$  is the driving vector, and  $\mathbf{h}(k) = \begin{bmatrix} h_1(k) & h_2(k) \end{bmatrix}^T$  is the M-AR process vector.

The processes  $\mathbf{h}(k)$  are contaminated by an additive noise vector  $\mathbf{v}(k) = \begin{bmatrix} v_1(k) & v_2(k) \end{bmatrix}^T$  of zero-mean. Thus, the received observation vector  $\mathbf{y}(k)$  is given by:

$$\mathbf{y}(k) = \mathbf{h}(k) + \mathbf{v}(k) \quad (3.2)$$

The simulation is carried out to estimate the M-AR parameters using the noisy observations  $\mathbf{y}(k)$ .

We consider two simulation protocols:

### Simulation protocol#1: Synthetic M-AR process

A synthetic M-AR process is generated according to the simulation protocol in [Has03] with the following:

$$\mathbf{A}^{(1)} = \begin{pmatrix} -0.71 & 0.32 \\ -0.88 & -0.24 \end{pmatrix}, \mathbf{A}^{(2)} = \begin{pmatrix} 0.57 & -0.15 \\ -0.49 & -0.30 \end{pmatrix}$$

These matrices leads to four roots of  $\det(\mathbf{A}_2(z))$ :

$$Pole1 = 0.941 \times e^{j1.125}, Pole2 = 0.941 \times e^{-j1.125}, Pole3 = 0.599, Pole4 = -0.461$$

In this protocol, the driving process vector is assumed to be white Gaussian with zero-mean and diagonal covariance matrix  $\Sigma_u = \mathbf{I}_2$ .

### Simulation protocol#2: Correlated Mobile Fading Channels

In this protocol, we use the VAR method [Bad04] to generate correlated mobile fading channels. Two correlated fading channels of second order ( $p = 2$ ) are generated, with unit power of each channel  $\sigma_h^2 = 1$  and cross-correlation coefficient  $\rho_{12} = \rho_{21} = 0.6$  with maximum Doppler frequency  $f_d = 0.1$ . The generated M-AR parameter matrices  $\mathbf{A}^{(1)}$  and  $\mathbf{A}^{(2)}$ , and the driving process covariance matrix  $\mathbf{Q}_u$  are given below, respectively:

$$\mathbf{A}^{(1)} = \begin{pmatrix} -1.7625 & 0 \\ 0 & -1.7625 \end{pmatrix}, \mathbf{A}^{(2)} = \begin{pmatrix} 0.9503 & 0 \\ 0 & 0.9503 \end{pmatrix}$$

$$\mathbf{Q}_u = \mathbf{G}\mathbf{G}^H = \begin{pmatrix} 0.0178 & 0.0124 \\ 0.0124 & 0.0178 \end{pmatrix}$$

where  $\mathbf{G}$  is computed using the Cholesky decomposition as follows:

$$\mathbf{G} = \begin{pmatrix} 0.1334 & 0 \\ 0.0933 & 0.0952 \end{pmatrix}$$

The corresponding 4 poles due to these parameter matrices are as follows:

$$Pole1 = Pole3 = 0.9748e^{j0.4417}, Pole2 = Pole4 = 0.9748e^{-j0.4417}$$

The driving processes covariance matrix is not diagonal, while the parameter matrices are diagonal. This means that the correlation between the processes is due to the driving processes and not to the coefficient matrices.

After obtaining the estimated parameters we do the following:

- 1- Compute the estimated poles using the estimated parameters.
- 2- Compute the Mean Square Error (MSE) of the poles modulus and arguments.
- 3- Tabulate the results.
- 4- Plotting the estimated and the true poles and spectra.

The simulations are carried out on both synthetic M-AR process and M-AR process corresponds to mobile fading channels.

## 3.2 Parameter Estimation of Synthetic M-AR Process

In this section, simulation results are provided for correlated synthetic M-AR process, according to the simulation protocol#1. In following two subsections, the simulations are carried out for 300 and 2000 samples at SNR=10dB.

### 3.2.1 Small Sample Size

In this example, the simulation is carried out for 300 samples at SNR=10dB. The aim of this simulation is to compare the estimation performance at small samples size. This is usually the case in practice.

Table 3.1 shows the true and the estimated parameters values with their variances. According to this table, we can conclude that for small sample size, the SC-Kalman filters, YW equations and ARFIT provide biased estimates. While Hassan's algorithm provides better results than these methods, it is outperformed by the NCYW equations, CC-Kalman filters and CC- $H_\infty$  filters.

CC-Kalman filters and CC- $H_\infty$  filters have closed parameter estimates and slightly better than NCYW equations. This shows the relevance of our approach when small number of samples are available.

Table 3.2 contains the true and the estimated poles, using the various methods, while Table 3.3 includes the MSE of the modulus and arguments of the estimated poles. From Table 3.2 and Figure 3.1, the accuracy of the estimated poles and spectrum when using CC-Kalman and CC- $H_\infty$  estimators is better than that of Hassan's method. The estimated parameters using SC-Kalman filters, ARFIT and YW equations are biased.

The above remarks can be also deduced from Table 3.3. The MSE of the arguments and the modulus of the estimated poles are very small for NCYW, CC-Kalman and CC- $H_\infty$ . While they are larger when using the other methods. For all methods, the third pole

Table 3.1: The true and estimated parameters at SNR=10dB based on 300 samples.

	True	ARFIT [Neu01]	SC-Kalman [Arn98]	YW	Hassan [Has03]	NCYW	CC-Kalman	CC- $H_\infty$
$a_{11}^{(1)}$	-0.71	-0.4753 $\pm 0.0035$	-0.4808 $\pm 0.0035$	-0.4776 $\pm 0.0031$	-0.6112 $\pm 0.0091$	-0.7143 $\pm 0.0063$	-0.6730 $\pm 0.0046$	-0.6367 $\pm 0.0099$
$a_{12}^{(1)}$	0.32	0.3330 $\pm 0.0069$	0.3317 $\pm 0.0070$	0.3322 $\pm 0.0074$	0.3644 $\pm 0.0310$	0.3050 $\pm 0.0340$	0.3084 $\pm 0.0355$	0.3095 $\pm 0.0436$
$a_{21}^{(1)}$	-0.88	-0.6697 $\pm 0.0045$	-0.6725 $\pm 0.0043$	-0.6687 $\pm 0.0040$	-0.8195 $\pm 0.0147$	-0.9182 $\pm 0.0078$	-0.9087 $\pm 0.0126$	-0.8792 $\pm 0.0275$
$a_{22}^{(1)}$	-0.24	-0.2737 $\pm 0.0025$	-0.2757 $\pm 0.0025$	-0.2776 $\pm 0.0026$	-0.2738 $\pm 0.0038$	-0.2519 $\pm 0.0100$	-0.2975 $\pm 0.0151$	-0.2833 $\pm 0.0152$
$a_{11}^{(2)}$	0.57	0.4639 $\pm 0.0063$	0.4648 $\pm 0.0065$	0.4598 $\pm 0.0062$	0.4889 $\pm 0.0263$	0.5888 $\pm 0.0336$	0.5781 $\pm 0.0330$	0.5701 $\pm 0.0413$
$a_{12}^{(2)}$	-0.15	-0.0051 $\pm 0.0023$	-0.0098 $\pm 0.0024$	-0.0101 $\pm 0.0024$	-0.1194 $\pm 0.0235$	-0.1449 $\pm 0.0179$	-0.1138 $\pm 0.0162$	-0.0810 $\pm 0.0187$
$a_{21}^{(2)}$	-0.49	-0.4444 $\pm 0.0034$	-0.4425 $\pm 0.0034$	-0.4376 $\pm 0.0033$	-0.4406 $\pm 0.0060$	-0.4540 $\pm 0.0124$	-0.4123 $\pm 0.0152$	-0.4433 $\pm 0.0264$
$a_{22}^{(2)}$	-0.30	-0.1066 $\pm 0.0026$	-0.1085 $\pm 0.0025$	-0.1040 $\pm 0.0023$	-0.2247 $\pm 0.0103$	-0.3117 $\pm 0.0075$	-0.2720 $\pm 0.0140$	-0.2552 $\pm 0.0182$

has the largest MSE, while the MSE of the first and second pole is the smallest. Also, we note from Table 3.3 that the MSE of the modulus of the third and fourth poles are identically zeros. This is because these poles are real, and the estimated values are also real, and have the same sign as the true poles, which means equal modulus (i.e., zero angle for the positive poles and  $\pi$  for the negative poles).

Figure 3.1 is the plot of the average spectra and poles using the mentioned estimation methods. The estimated spectrum and poles are close to the true ones for NCYW equations, CC-Kalman filters and  $H_\infty$  filters, while they are biased in the case of SC-Kalman filters, ARFIT and YW equations. Figures 3.2 shows the plots of the true and estimated spectra and poles for 20 realizations. This figure shows that the estimated spectrum and poles has less variances and more close to the true values in the case of NCYW equations, CC-Kalman and CC- $H_\infty$  filters.

### 3.2.2 Large Sample Size

In this example, the simulations are carried out using the various methods to estimate the parameters of the synthetic M-AR process, whose coefficient matrices defined according

Table 3.2: The true and estimated poles at SNR=10dB based on 300 samples.

	Pole#1	Pole#2	Pole#3	Pole#4
True	0.4056 + 0.8491i	0.4056 - 0.8491i	0.5995	-0.4606
ARFIT [Neu01]	0.3857 + 0.8026i	0.3857 - 0.8026i	0.2413	-0.2637
SC-Kalman [Arn98]	0.3851 + 0.8022i	0.3851 - 0.8022i	0.2536	-0.2673
YW	0.3836 + 0.7996i	0.3836 - 0.7996i	0.2495	-0.2616
Hassan [Has03]	0.3940 + 0.8307i	0.3940 - 0.8307i	0.4749	-0.3778
NCYW	0.4015 + 0.8509i	0.4015 - 0.8509i	0.6130	-0.4499
CC-Kalman	0.4003 + 0.8496i	0.4003 - 0.8496i	0.5713	-0.4014
CC-H <sub>∞</sub>	0.4020 + 0.8466i	0.4020 - 0.8466i	0.5728	-0.4294

Table 3.3: MSE of modulus and argument of the estimated poles at SNR=10dB based on 300 samples.

	MSE of Pole#1		MSE of Pole#2		MSE of Pole#3		MSE of Pole#4	
	mod. (E-3)	arg. (E-6)	mod. (E-3)	arg. (E-6)	mod. (E-3)	arg. (E-6)	mod. (E-3)	arg. (E-6)
ARFIT	2.7422	299.285	2.7422	299.285	136.037	0	42.8073	0
SC-Kalman	2.8106	305.114	2.8106	305.114	127.145	0	41.3601	0
YW	3.1585	304.199	3.1585	304.199	129.818	0	43.4425	0
Hassan	1.0374	252.676	1.0374	252.676	252.676	0	16.3635	0
NCYW	0.22997	282.538	0.22997	282.538	3.66680	0	10.0017	0
CC-Kalman	0.20542	294.060	0.20542	294.060	4.05130	0	21.9942	0
CC-H <sub>∞</sub>	0.22583	273.526	0.22583	273.526	2.88410	0	11.8611	0

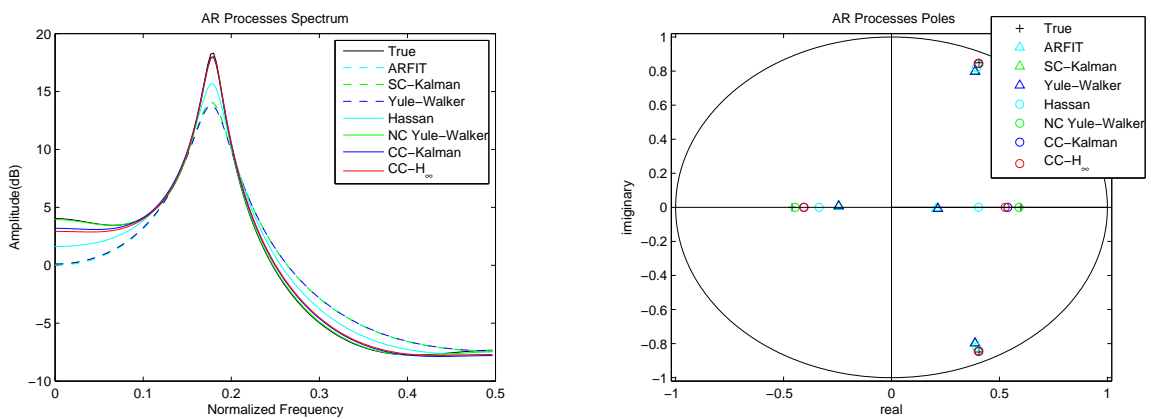


Figure 3.1: The average estimated spectrum and poles averaged over 200 realizations of synthetic M-AR process, at SNR=10dB based on 300 observations using various estimation methods.

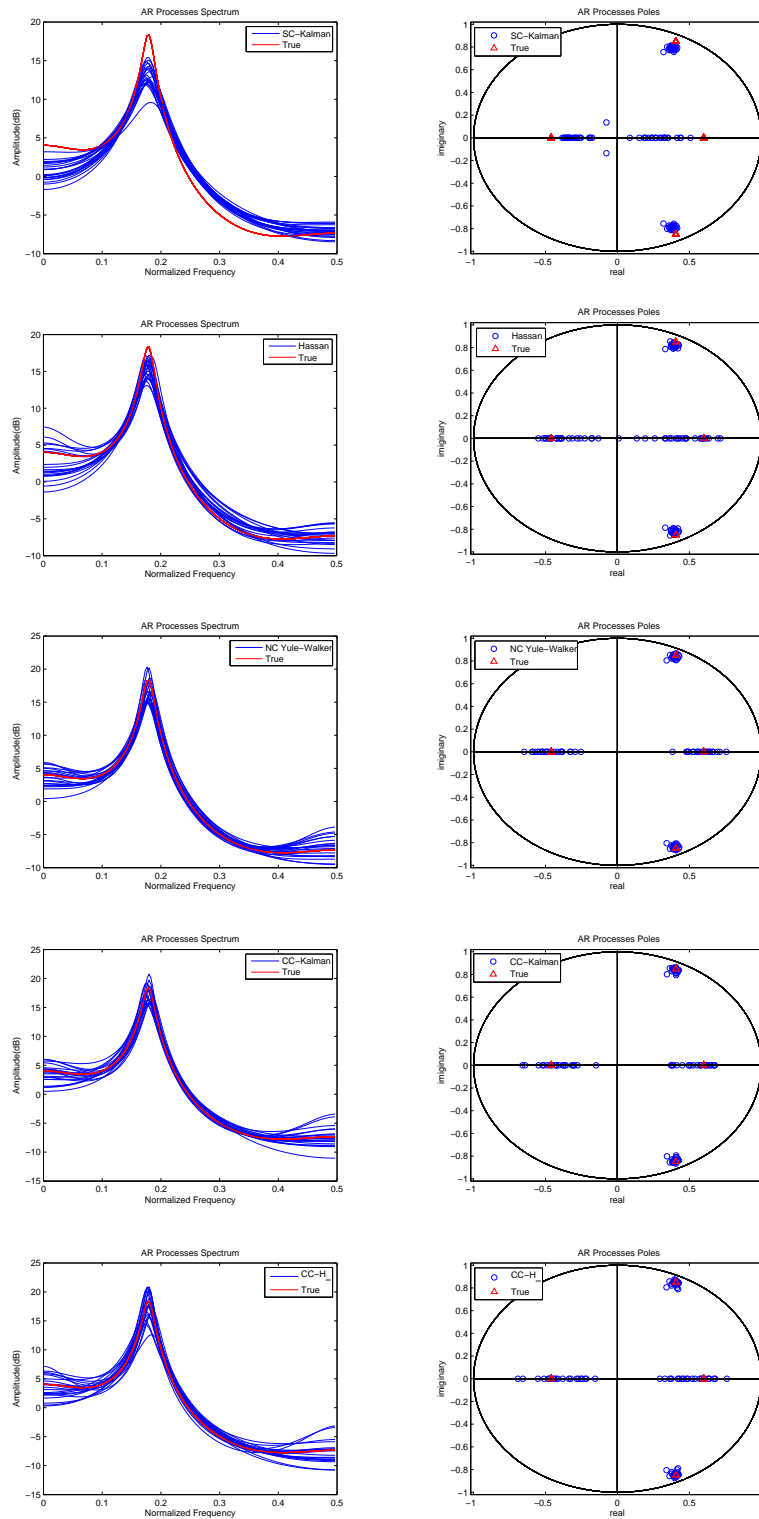


Figure 3.2: 20 realizations for the estimated spectrum and poles of synthetic M-AR process, at SNR=10dB based on 300 observations.

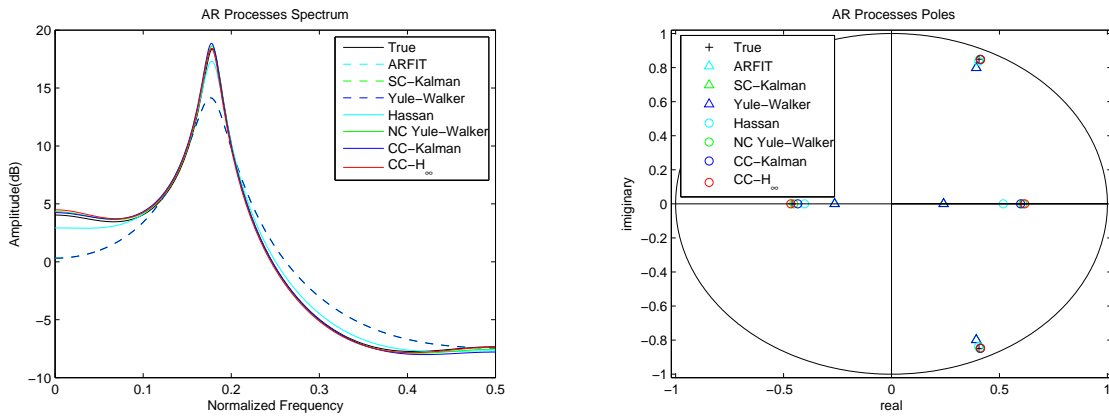


Figure 3.3: The average estimated spectrum and poles for synthetic M-AR process, at SNR=10dB based on 2000 observations using various estimation methods.

to the simulation protocol#1. In this case, 2000 samples are used to show the effect of using large sample size on the estimation process.

Table 3.4, 3.5 and 3.6 contains the estimated and the true parameters, poles and the MSE of the modulus and arguments, respectively.

We note from the tables that the estimated parameters in this case are more accurate than those in the previous example. This means that using large sample size improves the quality of the estimated parameters. In addition, the estimated parameters are close to each other and less deviate than using small sample size.

In addition, the same pattern as in example 1 repeated here. The worst estimated results obtained using SC-Kalman filters, ARFIT and YW equations. Better results are obtained using Hassan’s algorithm. But the difference here from the previous case, that the NCYW provides slightly better estimated results than CC-Kalman filters and CC- $H_\infty$  filters.

Figure 3.3 shows the average estimated spectrum and poles using the various methods. While, Figure 3.4 shows the plots of the average spectrum and poles for 20 realizations using SC-Kalman filters, Hassan’s algorithm, NCYW equations, CC-Kalman filters and CC- $H_\infty$  filters, respectively. The estimated spectrum and poles in these figures are much accurate with less variance than in the previous example.

Table 3.4: The true and estimated parameters at SNR=10dB based on 2000 samples.

	True	ARFIT [Neu01]	SC-Kalman [Arn98]	YW	Hassan [Has03]	NCYW	CC-Kalman	CC-H <sub>∞</sub>
$a_{11}^{(1)}$	-0.71	-0.4767 ±0.00029	-0.4770 ±0.00028	-0.4764 ±0.00028	-0.6861 ±0.0019	-0.7072 ±0.0006	-0.6929 ±0.0007	-0.6904 ±0.0009
$a_{12}^{(1)}$	0.32	0.3449 ±0.00046	0.3449 ±0.00045	0.3451 ±0.00045	0.3295 ±0.0064	0.3262 ±0.0025	0.3352 ±0.0070	0.3221 ±0.0067
$a_{21}^{(1)}$	-0.88	-0.6438 ±0.00064	-0.6439 ±0.00064	-0.6438 ±0.00063	-0.8524 ±0.0033	-0.8782 ±0.0010	-0.8746 ±0.0016	-0.8625 ±0.0016
$a_{22}^{(1)}$	-0.24	-0.2709 ±0.00031	-0.2712 ±0.00031	-0.2715 ±0.00032	-0.2396 ±0.0028	-0.2373 ±0.0014	-0.2697 ±0.0044	-0.2636 ±0.0051
$a_{11}^{(2)}$	0.57	0.4478 ±0.00046	0.4478 ±0.00046	0.4470 ±0.00046	0.5536 ±0.0060	0.5647 ±0.0027	0.5506 ±0.0070	0.5625 ±0.0066
$a_{12}^{(2)}$	-0.15	-0.015 ±0.00049	-0.0149 ±0.00048	-0.0148 ±0.00049	-0.1393 ±0.0038	-0.1509 ±0.0019	-0.1462 ±0.0036	-0.1358 ±0.0036
$a_{21}^{(2)}$	-0.49	-0.4617 ±0.00038	-0.4614 ±0.00039	-0.4605 ±0.00039	-0.4898 ±0.0030	-0.4902 ±0.0018	-0.4647 ±0.0049	-0.4733 ±0.0054
$a_{22}^{(2)}$	-0.30	-0.0956 ±0.00059	-0.0956 ±0.00059	-0.0954 ±0.00059	-0.2765 ±0.0044	-0.2990 ±0.0013	-0.2696 ±0.0041	-0.2645 ±0.0050

Table 3.5: The true and estimated poles at SNR=10dB based on 2000 samples.

	Pole#1	Pole#2	Pole#3	Pole#4
True	0.4056 + 0.8491i	0.4056 - 0.8491i	0.5995	-0.4606
ARFIT [Neu01]	0.3896 + 0.7995i	0.3896 - 0.7995i	0.2313	-0.2630
SC-Kalman [Arn98]	0.3896 + 0.7995i	0.3896 - 0.7995i	0.2320	-0.2630
YW	0.3895 + 0.7991i	0.3895 - 0.7991i	0.2316	-0.2626
Hassan [Has03]	0.4041 + 0.8455i	0.4041 - 0.8455i	0.5600	-0.4425
NCYW	0.4059 + 0.8494i	0.4059 - 0.8494i	0.5933	-0.4605
CC-Kalman	0.4062 + 0.8480i	0.4062 + 0.8480i	0.5733	-0.4231
CC-H <sub>∞</sub>	0.4059 + 0.8478i	0.4059 - 0.8478i	0.5652	-0.4229

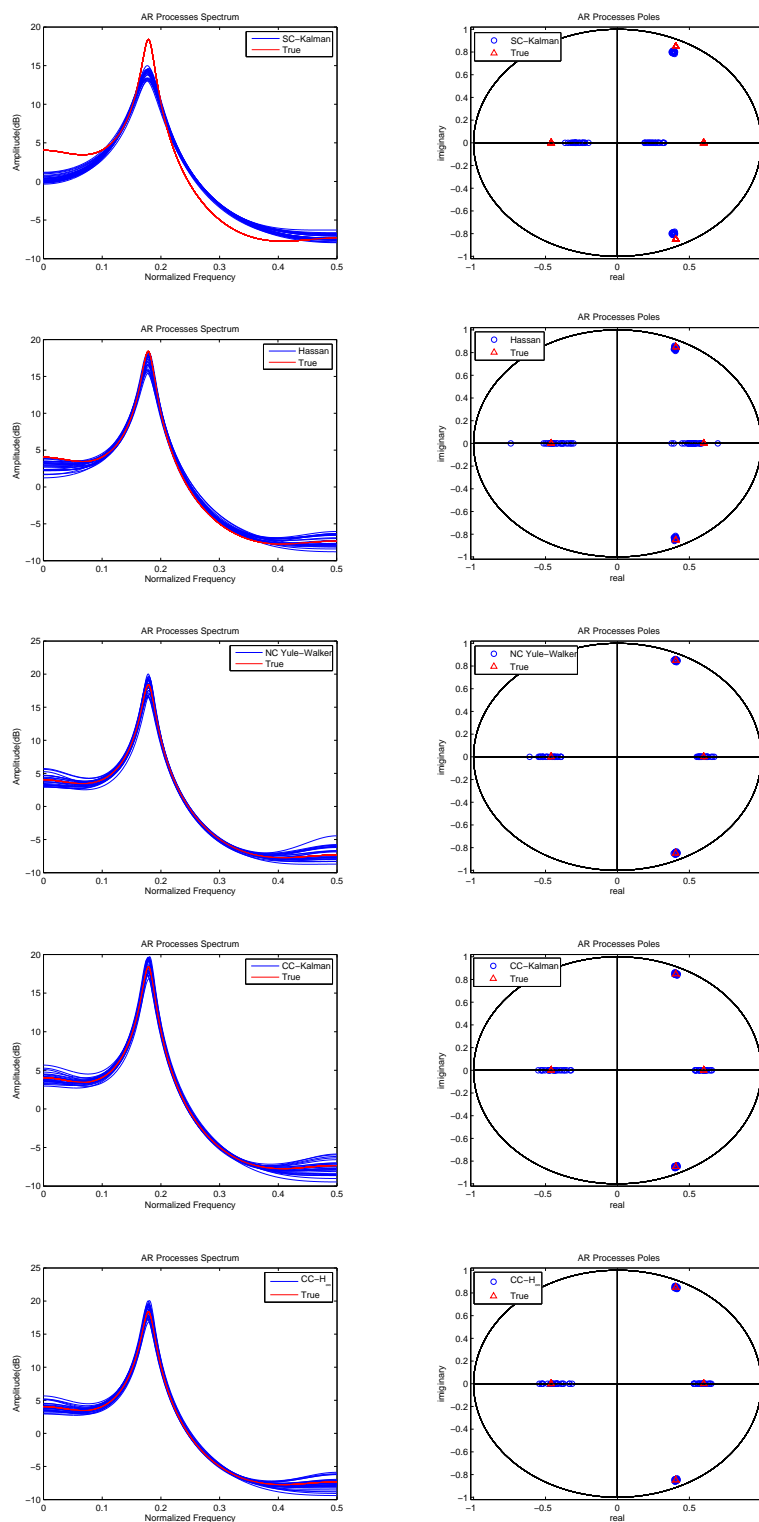


Figure 3.4: 20 realizations over 200 realizations of the estimated spectrum and poles of synthetic M-AR process, at SNR=10dB based on 2000 observations.

Table 3.6: MSE of modulus and argument of the estimated poles at SNR=10dB based on 2000 samples.

	MSE of Pole#1		MSE of Pole#2		MSE of Pole#3		MSE of Pole#4	
	mod. (E-3)	arg. (E-6)	mod. (E-3)	arg. (E-6)	mod. (E-3)	arg. (E-6)	mod. (E-3)	arg. (E-6)
ARFIT	2.7156	95.9868	2.7156	95.9868	138.804	0	40.8797	0
SC-Kalman	2.7218	95.6537	2.7218	95.6537	138.266	0	40.8478	0
YW	2.7651	97.1870	2.7651	97.1870	138.546	0	41.0099	0
Hassan	0.09061	33.4073	0.09061	33.4073	5.53450	0	4.61400	0
NCYW	0.04781	29.3603	0.04781	29.3603	29.3603	0	1.73870	0
CC-Kalman	0.04675	45.7556	0.04675	45.7556	1.6276	0	7.1652	0
CC-H <sub>∞</sub>	0.05129	42.0649	0.05129	42.0649	2.3626	0	8.5214	0

### 3.2.3 Comparative Study Between the CC-Kalman and CC-H<sub>∞</sub> Estimators

Here, we provide some simulation results to compare the performance of our approaches when using either the true values or the estimated values of the noise covariance matrices.

#### 3.2.3.1 Using True Values of the Noise Covariance Matrices

Figure 3.5 shows the average MSE of the arguments and modulus of the first estimated pole using YW equations, NCYW equations, CC-Kalman filter and CC-H<sub>∞</sub> filters at various number of samples ranging from (50-400) and SNR=10dB. While Figure 3.6 shows the MSE of the same poles. The simulations are performed at different values of SNR ranging from (2-16dB) based on 1000 samples.

According to Figure 3.5, the NCYW equations, CC-Kalman and CC-H<sub>∞</sub> filters provide approximately the same MSE. In addition, the YW equations provide high MSE. Moreover, the MSE decreases when the estimation process based on large number of samples. According to Figure 3.6, the same conclusions can be drawn. In addition, the MSE decrease when the SNR increases.

#### 3.2.3.2 Using Estimated Noise Covariance Matrices

To show the relevance of our approach, we provide simulation results for the estimation of the M-AR parameters using CC-Kalman filters, CC-H<sub>∞</sub> filters and NCYW equations. When using deviated values of the driving processes and additive noise covariance matrices  $\mathbf{Q}_u$  and  $\mathbf{R}_v$ , as follows:

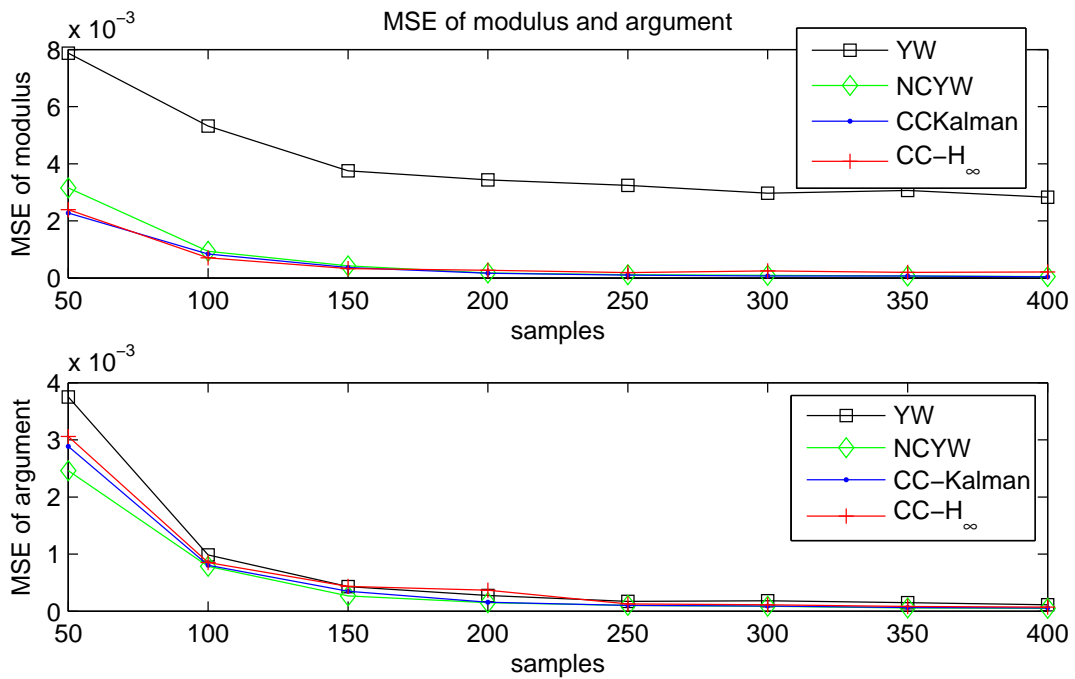


Figure 3.5: MSE of arguments and modulus for pole#1 based on different number of samples at SNR=10dB. True values of noise covariance matrices are used.

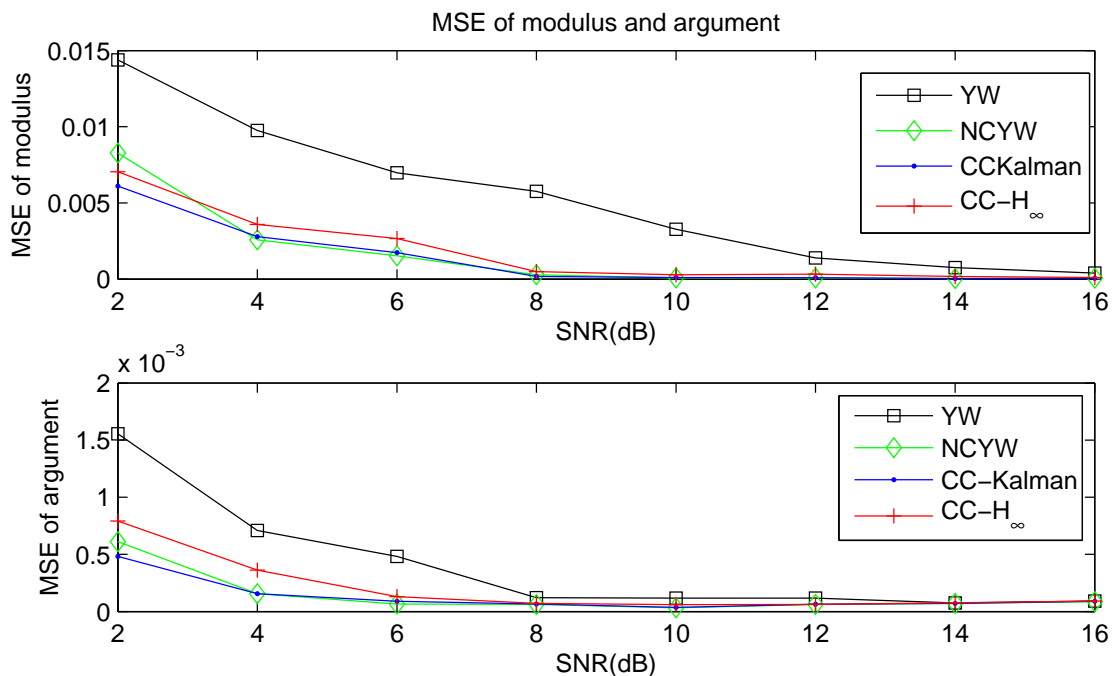


Figure 3.6: MSE of arguments and modulus for pole#1 at different SNR based on 1000 samples. True values of noise covariance matrices are used.

Table 3.7: The MSE of the arguments and the modulus of pole#1 for different  $\beta^{(i)}$  based on 1024 samples and SNR=[10,5]dB.

$\beta^{(i)}$	MSE of mod. of pole#1			MSE of arg. of pole#1		
	CC-Kalman	CC- $H_\infty$	NCYW	CC-Kalman	CC- $H_\infty$	NCYW
0.01	0.0043	0.0003	0.0051	0.0002	0.0001	0.0002
0.1	0.0027	0.0005	0.0033	0.0001	0.0003	0.0001
0.8	0.0003	0.0002	0.0003	0.0001	0.0001	0.0001
0.9	0.0003	0.0006	0.0002	0.0001	0.0001	0.0001
0.95	0.0002	0.0003	0.0001	0.0001	0.0002	0.0001
1	0.0003	0.0002	0.0001	0.0001	0.0001	0.0001
1.05	0.0002	0.0002	0.0001	0.0001	0.0001	0.0001
1.1	0.0002	0.0002	0.0002	0.0001	0.0002	0.0001
1.2	0.0002	0.0004	0.0004	0.0001	0.0003	0.0001
10	0.0014	0.0009	0.2679	0.0001	0.0011	0.0057
20	0.0016	0.0016	0.0105	0.0002	0.0044	0.8507

Let us introduce  $\beta$  whose  $i^{th}$  element is defined as follows:

$$\beta^{(i)} = \frac{\hat{\sigma}_{ui}^2}{\sigma_{ui}^2} = \frac{\hat{\sigma}_{vi}^2}{\sigma_{vi}^2} \quad (3.3)$$

Different values of  $\beta^{(i)}$  are used to study the influence of under estimate ( $\beta^{(i)} < 1$ ) and over estimate ( $\beta^{(i)} > 1$ ).

We use 1024 samples at SNR=10dB on the first channel and SNR=5dB on the second channel. The data are synthetically generated using the synthetic M-AR process described in simulation protocol#1.

The MSE of the arguments and the modulus of the first pole are provided in Table 3.7. The results of the other poles are omitted for convenience, as they produce approximately the same kind of results. According to this table, the MSE of arguments and modulus of the estimated poles are small for ( $0.8 < \beta^{(i)} < 1.2$ ), while they are large for ( $\beta^{(i)} > 1.2$  and  $\beta^{(i)} < 0.8$ ).

For high deviation ( $\beta^{(i)} > 1.2$  and  $\beta^{(i)} < 0.8$ ), the MSE is small when using CC- $H_\infty$  filters compared to CC-Kalman and NCYW. But, CC-Kalman filters outperforms the NCYW equations.

We can deduce the importance of using CC- $H_\infty$  filters, when there is a large deviation in the variances of the driving processes and the additive noise from the true values.

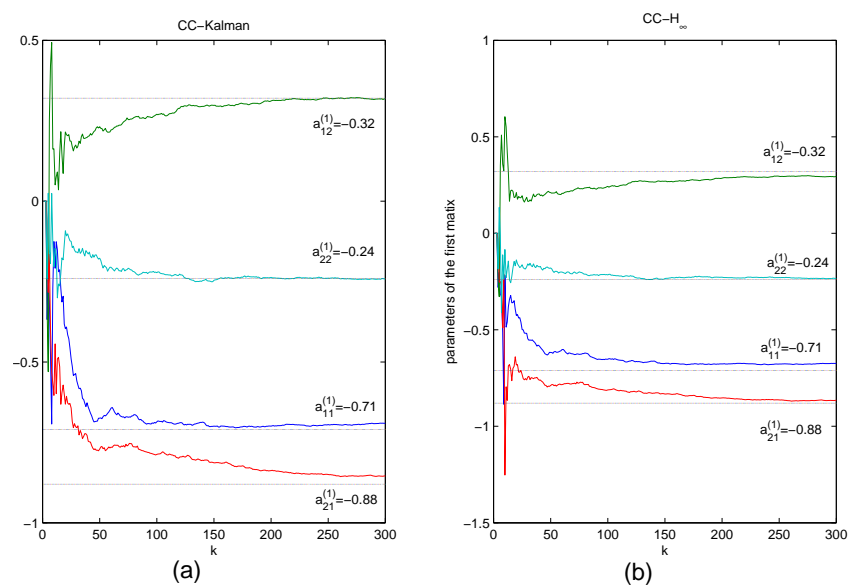


Figure 3.7: Convergence of the estimated parameters of the first matrix: (a) using CC-Kalman filters, (b) CC- $H_\infty$  filters.

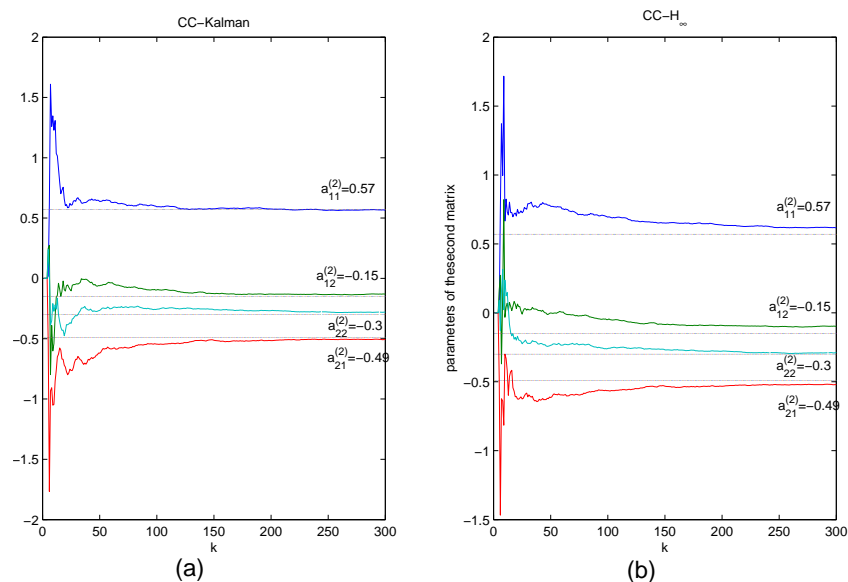


Figure 3.8: Convergence of the estimated parameters of the second matrix: (a) using CC-Kalman filters, (b) CC- $H_\infty$  filters.

### 3.2.3.3 Convergence Speed

In this section, we provide figures of the estimated parameters at each iteration when using CC-Kalman and CC- $H_\infty$  filters. We use the parameters that correspond to the synthetic M-AR process which described in the first protocol. The aim of these figures is to show the convergence speed for CC-Kalman and CC- $H_\infty$ .

Figure 3.7 shows the estimated parameters of the first matrix, while Figure 3.8 shows the estimated parameters of the second matrix. From these figures, we note that the cross-coupled filters adapt themselves rapidly to reach the convergence. Also, the CC-Kalman and CC- $H_\infty$  filters have the same speed of convergence. At 50 samples, they start to converge toward the true values and they provide better estimated parameters every new iteration. Moreover, accurate estimated parameters may be obtained at 150 samples.

## 3.3 Parameter Estimation of Mobile Fading Channels

In the previous section, the simulation is performed to estimate the parameter of a correlated synthetic M-AR process. The generated data are real and the correlation is due to the parameter matrices.

In this section, the simulation is carried out for the estimation of correlated mobile fading processes. The data are generated using the VAR method proposed by Baddour et al. [Bad04], which is described in chapter 1. The generated data are complex valued.

In the following subsections, the simulations are carried out based on 300 and 2000 samples at SNR=10dB.

### 3.3.1 Small Sample Size

In this examples, we generate 300 samples representing correlated fading processes based on simulation protocol#2.

Table 3.8 contains the true and the estimated parameters using the various M-AR parameter estimation methods. The estimated parameters are accurate when using CC-Kalman filters and CC- $H_\infty$  filters followed by the NCYW equations. These methods outperform Hassan's algorithm. The ARFIT, SC-Kalman filters and YW equations provide biased estimates.

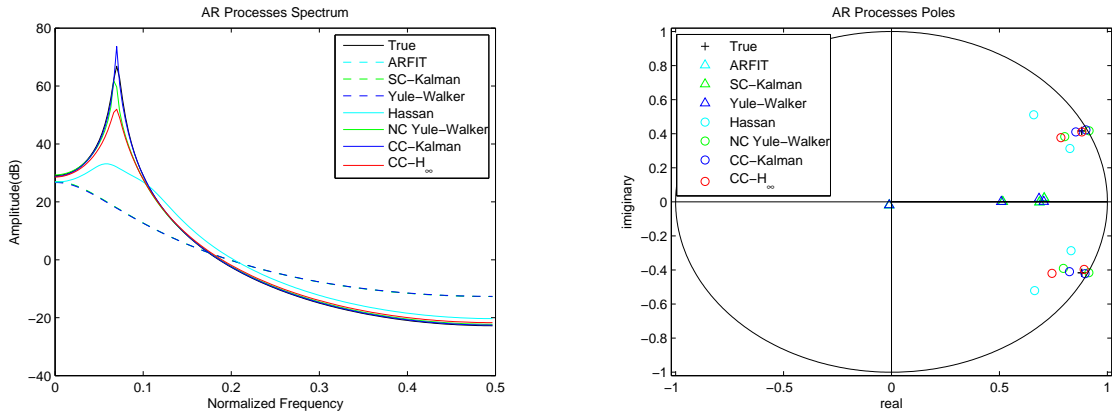


Figure 3.9: The average estimated spectrum and poles of fading channels, at SNR=10dB based on 300 observations using various estimation methods.

The M-AR poles that correspond to the estimated parameters are given in Table 3.9. According to this table, the estimated poles are accurate when using the CC-Kalman filters, CC-H<sub>∞</sub> filters and NCYW equations. While the estimated poles when using SC-Kalman filters, ARFIT and YW equations are inaccurate. Note that Hassan’s algorithm outperform the last three methods. These observations can be also deduced from Table 3.10, where it shows the MSE of the poles modulus and arguments.

Figure 3.9 shows the average estimated spectrum and poles using the various methods. According to this figure, we can note that the spectrum and poles are close to the true spectrum and poles when using CC-Kalman filters and CC-H<sub>∞</sub> filters followed by the NCYW equations. While they are inaccurate and far from the true plots when using the other methods. We can note that the estimated spectrum and poles that are obtained when using CC-Kalman filters and CC-H<sub>∞</sub> filters are slightly accurate than those obtained using NCYW equations. In addition, these methods outperform Hassan’s algorithm. The same conclusions can be also drawn from Figure 3.10, it shows the plots of 20 realization of the spectrum and poles for correlated fading processes generated based on the simulation protocol#2.

### 3.3.2 Large Sample Size

In this example, 2000 samples are used in the estimation process to show the effect of number of samples on the estimated results.

According to Tables 3.11, 3.12 and 3.13, the same conclusions can be drawn as example 1 in the previous subsection. The difference when using large samples that

Table 3.8: The true and estimated parameters at SNR=10dB based on 300 samples.

	True	ARFIT [Neu01]	SC-Kalman [Arn98]	YW	Hassan [Has03]	NCYW	CC-Kalman	CC-H <sub>∞</sub>
$a_{11}^{(1)}$	-1.7625	-0.9575 +0.0032i ±0.0023	-0.9577 +0.0032i ±0.0023	-0.9537 +0.0043i ±0.0023	-1.5228 +0.1533i ±0.3401	-1.7857 +0.0201i ±0.0285	-1.7369 +0.0023i ±0.1560	-1.7035 +0.0458i ±0.0458
$a_{12}^{(1)}$	0	-0.2280 -0.0080i ±0.0529	-0.2280 -0.0080i ±0.0031	-0.2243 -0.0094i ±0.0030	-0.0719 -0.1100i ±0.0545	0.0561 -0.0327i ±0.0356	-0.0570 -0.0092i ±0.0050	-0.0199 -0.0529i ±0.0241
$a_{21}^{(1)}$	0	-0.2450 +0.0120i ±0.0056	-0.2449 +0.0119i ±0.0056	-0.2417 +0.0146i ±0.0058	-0.1124 +0.1299i ±0.0962	0.0282 +0.0188i ±0.0524	-0.0651 +0.0188i ±0.0030	-0.0967 -0.0008i ±0.0277
$a_{22}^{(1)}$	-1.7625	-0.9392 -0.0049i ±0.0026	-0.9392 -0.0049i ±0.0026	-0.9328 -0.0068i ±0.0026	-1.4573 -0.1698i ±0.4035	-1.7517 -0.1698i ±0.0490	-1.7382 -0.0032i ±0.1540	-1.5991 -0.0164i ±0.1976
$a_{11}^{(2)}$	0.9503	0.2069 -0.0054i ±0.0036	0.2069 -0.0054i ±0.0036	0.2046 -0.0060i ±0.0035	0.7165 -0.1488i ±0.1568	0.9764 -0.0226i ±0.0276	0.9764 -0.0085i ±0.0276	0.8878 -0.0085i ±0.1090
$a_{12}^{(2)}$	0	0.1981 +0.0168i ±0.0050	0.1981 +0.0168i ±0.0049	0.1948 +0.0174i ±0.0047	0.0703 +0.1088i ±0.0497	-0.0552 +0.0342i ±0.0362	0.0572 +0.0162i ±0.0050	0.0063 +0.0911i ±0.0279
$a_{21}^{(2)}$	0	0.2056 +0.0016i ±0.0044	0.2057 +0.0016i ±0.0044	0.2024 -0.0001i ±0.0045	0.1140 -0.1146i ±0.0851	-0.0256 -0.0177i ±0.0527	0.0627 +0.0105i ±0.0527	0.0671 +0.0186i ±0.0291
$a_{22}^{(2)}$	0.9503	0.1917 -0.0008i ±0.0037	0.1916 -0.0008i ±0.0037	0.1872 +0.0006i ±0.0037	0.1872 +0.1611i ±0.2319	0.9377 +0.0186i ±0.0492	0.9300 -0.0042i ±0.0492	0.8010 +0.0042i ±0.1050

Table 3.9: The true and estimated poles at SNR=10dB based on 300 samples.

	Pole#1	Pole#2	Pole#3	Pole#4
True	0.8812 + 0.4167i	0.8812 - 0.4167i	0.8813 + 0.4167i	0.8813 - 0.4167i
ARFIT [Neu01]	0.7068 + 0.0224i	0.6851 - 0.0018i	0.5155 + 0.0005i	-0.0107 - 0.0195i
SC-Kalman [Arn98]	0.7073 + 0.0225i	0.6851 - 0.0018i	0.5156 + 0.0004i	-0.0109 - 0.0194i
YW	0.7052 + 0.0012i	0.6832 - 0.0189i	0.5085 + 0.0007i	-0.0103 - 0.0183i
Hassan [Has03]	0.8265 + 0.3129i	0.8316 - 0.2868i	0.6588 + 0.5113i	0.6632 - 0.5209i
NCYW	0.9644 + 0.4174i	0.9744 - 0.4159i	0.8023 + 0.3828i	0.7964 - 0.3908i
CC-Kalman	0.9007 + 0.4222i	0.8964 - 0.4220i	0.8537 + 0.4102i	0.8242 - 0.4095i
CC-H <sub>∞</sub>	0.8819 + 0.4107i	0.8925 - 0.3964i	0.7849 + 0.3764i	0.7433 - 0.4201i

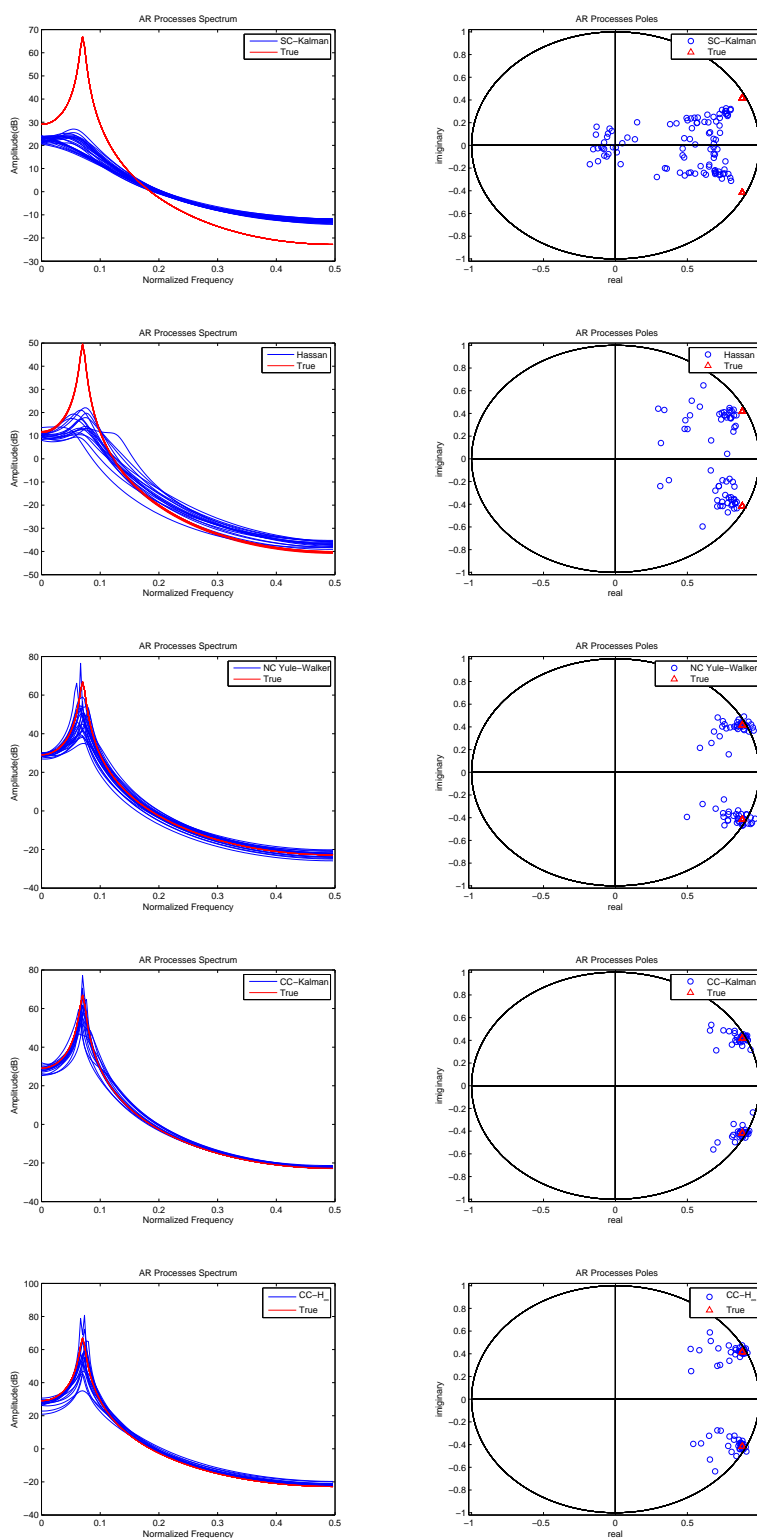


Figure 3.10: 20 realizations for the estimated spectrum and poles of multichannel fading processes, at SNR=10dB based on 300 observations.

Table 3.10: MSE of modulus and argument of the estimated poles at SNR=10dB based on 300 samples.

	MSE of Pole#1		MSE of Pole#2		MSE of Pole#3		MSE of Pole#4	
	mod. (E-3)	arg. (E-6)	mod. (E-3)	arg. (E-6)	mod. (E-3)	arg. (E-6)	mod. (E-3)	arg. (E-6)
ARFIT	62.5223	9.5711	67.5133	101.166	181.259	15.3069	789.881	2589.1
SC-Kalman	62.6081	9.6539	67.2771	101.214	181.248	15.3561	790.128	2592.1
YW	63.9646	9.9515	68.3888	101.504	188.015	15.8527	792.977	2541.6
Hassan	8.71240	24.210	8.23420	31.9666	15.6147	119.053	18.1981	83.833
NCYW	15.6521	5.0865	18.2306	4.25790	10.2816	1.55730	9.75360	1.3261
CC-Kalman	0.50481	0.2534	0.29635	0.14640	3.09220	0.76731	5.14000	4.4642
CC-H <sub>∞</sub>	0.46073	0.30731	0.57264	1.4765	26.2710	1.0921	19.5832	18.6622

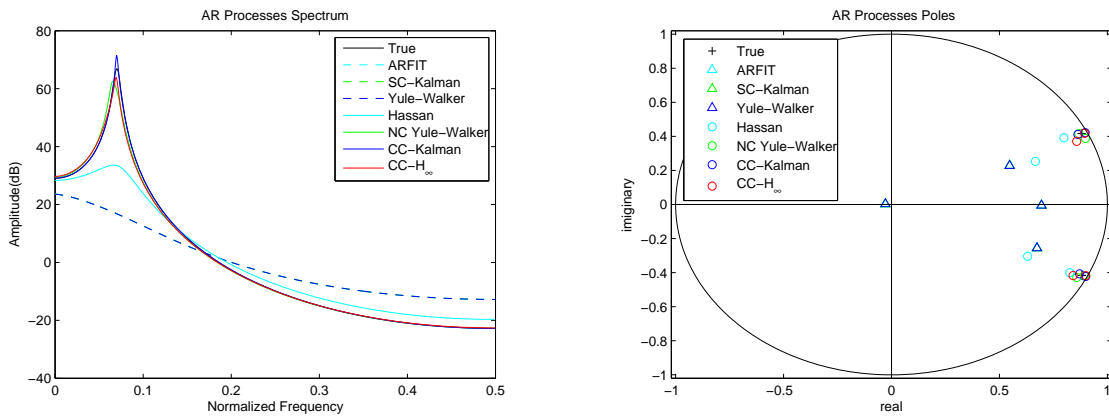


Figure 3.11: The average estimated spectrum and poles of fading channels, at SNR=10dB based on 2000 observations using various estimation methods.

the estimated parameters are more accurate than those when using small samples. In addition, the NCYW equations provide estimated parameters slightly more accurate than CC-Kalman filters and CC-H<sub>∞</sub> filters. Moreover, the divergence is reduced when using Hassan's algorithm.

Figure 3.11 shows the plots of the average spectra and poles while Figure 3.12 shows the plots of 20 realizations for the estimated spectrum and poles using the various estimation methods. According to these figures, we can note that the estimated poles and spectra are very close to the true values when using CC-Kalman filters, CC-H<sub>∞</sub> filters and NCYW equations. The three methods outperform Hassan's algorithm. The SC-Kalman filters provide the worst estimates.

Table 3.11: The true and estimated parameters at SNR=10dB based on 2000 samples.

	True	ARFIT [Neu01]	SC-Kalman [Arn98]	YW	Hassan [Has03]	NCYW	CC-Kalman	CC-H <sub>∞</sub>
$a_{11}^{(1)}$	-1.7625	-0.9669 -0.0021i ±0.0005	-0.9669 -0.0021i ±0.0005	-0.9659 -0.0024i ±0.0005	-1.5813 -0.0131i ±0.0406	-1.7545 -0.0010i ±0.0049	-1.7561 -0.0020i ±0.0010	-1.7296 -0.0238i ±0.0123
$a_{12}^{(1)}$	0	-0.2413 -0.0067i ±0.0018	-0.2413 -0.0067i ±0.0018	-0.2406 -0.0070i ±0.0018	-0.0882 +0.0001i ±0.0216	0.0005 -0.0074i ±0.0073	-0.0411 +0.0012i ±0.0013	-0.0535 +0.0012i ±0.0133
$a_{21}^{(1)}$	0	-0.2356 +0.0025i ±0.0024	-0.2356 +0.0025i ±0.0024	-0.2349 +0.0026i ±0.0024	-0.0816 -0.0115i ±0.0220	-0.0062 -0.0018i ±0.0100	-0.0327 -0.0000i ±0.0004	-0.0530 -0.0104i ±0.0080
$a_{22}^{(1)}$	-1.7625	-0.9711 +0.0002i ±0.0007	-0.9711 +0.0002i ±0.0007	-0.9696 +0.0001i ±0.0007	-1.5939 +0.0207i ±0.0376	-1.7530 +0.0034i ±0.0066	-1.7653 -0.0023i ±0.0003	-1.7513 +0.0050i ±0.0003
$a_{11}^{(2)}$	0.9503	0.2207 -0.9227 ±0.0008	0.2207 -0.0008i ±0.0008	0.2200 -0.0006i ±0.0008	0.7783 +0.0118i ±0.0384	0.9454 -0.0000i ±0.0052	0.9450 +0.0035i ±0.0016	0.9227 +0.0257i ±0.0125
$a_{12}^{(2)}$	0	0.1972 +0.0053i ±0.0306	0.1972 +0.0053i ±0.0020	0.1964 +0.0055i ±0.0020	0.0802 +0.0011i ±0.0020	-0.0020 +0.0089i ±0.0073	0.0418 -0.0034i ±0.0018	0.0483 -0.0306i ±0.0113
$a_{21}^{(2)}$	0	0.2093 -0.0018i ±0.0020	0.2093 -0.0018i ±0.0020	0.2086 -0.0018i ±0.0020	0.0816 +0.0144i ±0.0218	0.0071 +0.0046i ±0.0102	0.0354 +0.0005i ±0.0005	0.0406 +0.0168i ±0.0045
$a_{22}^{(2)}$	0.9503	0.0045 -0.0030i ±0.0009	0.2171 -0.0030i ±0.0009	0.2160 -0.0029i ±0.0009	0.7855 -0.0217i ±0.0009	0.9399 -0.0054i ±0.0009	0.9534 +0.0025i ±0.0004	0.9468 -0.0128i ±0.0173

Table 3.12: The true and estimated poles at SNR=10dB based on 2000 samples.

	Pole#1	Pole#2	Pole#3	Pole#4
True	0.8812 + 0.4167i	0.8812 - 0.4167i	0.8813 + 0.4167i	0.8813 - 0.4167i
ARFIT [Neu01]	0.6980 + 0.0124i	0.5731 - 0.0112i	0.6449 + 0.0044i	0.0219 - 0.0037i
SC-Kalman [Arn98]	0.6980 + 0.0124i	0.5732 - 0.0112i	0.6449 + 0.0044i	0.0219 - 0.0037i
YW	0.6975 + 0.0123i	0.5718 - 0.0110i	0.6445 + 0.0046i	0.0218 - 0.0037i
Hassan [Has03]	0.8375 + 0.3727i	0.8355 - 0.3722i	0.7553 + 0.4088i	0.7469 - 0.4168i
NCYW	0.9148 + 0.4211i	0.9122 - 0.4249i	0.8430 + 0.4060i	0.8375 - 0.4046i
CC-Kalman	0.8979 + 0.4257i	0.8983 - 0.4231i	0.8599 + 0.4111i	0.8653 - 0.4093i
CC-H <sub>∞</sub>	0.8985 + 0.4202i	0.8940 - 0.4186i	0.8416 + 0.4199i	0.8467 - 0.4027i

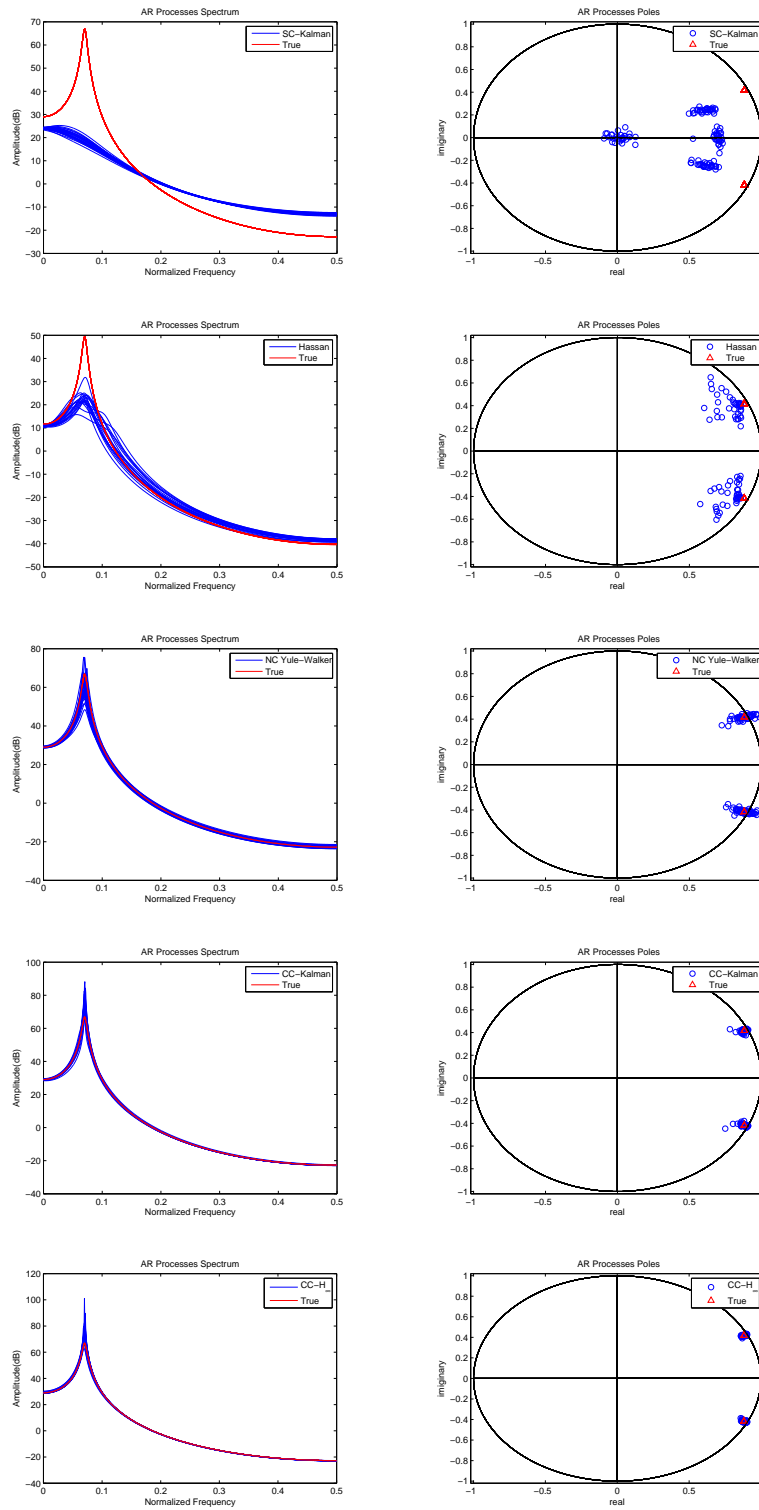


Figure 3.12: 20 realizations for the estimated spectrum and poles of multichannel fading processes, at SNR=10dB based on 2000 observations.

Table 3.13: MSE of modulus and argument of the estimated poles at SNR=10dB based on 2000 samples.

	MSE of Pole#1		MSE of Pole#2		MSE of Pole#3		MSE of Pole#4	
	mod. (E-3)	arg. (E-6)	mod. (E-3)	arg. (E-6)	mod. (E-3)	arg. (E-6)	mod. (E-3)	arg. (E-6)
ARFIT	81.8749	6.9206	75.1415	145.678	129.687	12.3388	839.599	1469.9
SC-Kalman	81.8911	6.9447	75.1038	145.691	129.702	12.3613	839.623	1471.3
YW	82.3296	7.1188	75.4344	145.869	130.909	12.0521	839.830	1473.2
Hassan	3.90410	2.6878	4.27760	3.52010	14.6799	13.2054	18.6557	9.1341
NCYW	1.8651	0.2812	1.70690	0.16059	2.43490	0.35338	3.58660	0.43124
CC-Kalman	0.38254	0.04121	0.33574	0.01916	1.1581	0.62337	0.73408	0.38262
CC-H <sub>∞</sub>	0.30647	0.04791	0.24477	0.06871	3.6085	9.9008	5.4135	4.3593

# Chapter 4

## Conclusions and Future Work

### Contents

---

4.1	Conclusions . . . . .	74
4.2	Future Work . . . . .	75

---

## 4.1 Conclusions

Multiple correlated data channels arise in many applications such as in wireless communications, biomedical engineering, radar systems, etc. In these applications, the multiple correlated channels are usually modeled by a M-AR process. This model is simple and contains few number of parameters. In the framework of mobile communications, the fading channels are usually modeled by a M-AR process for two main purposes. Firstly, this model is used to simulate correlated fading channels. Secondly, this model when combined with optimal filter such as Kalman or  $H_\infty$  filter can be used to estimate the fading channels [Bul98] [Cai04]. A key issue that is addressed in this thesis is to estimate the M-AR process parameters from the available noisy observations.

The M-AR parameter estimation methods can be classified as either off-line or on-line methods. Some of the off-line methods such as ARFIT and YW equations provide biased estimates. Other off-line methods such as NCYW equations, Hassan's algorithm, ILSV method and EIV based approach, they provide consistent estimation, as they compensate for the additive noise. However, they have high computational cost. In addition, some of them may diverge and result in unstable system.

When one observation is available at a time on-line methods can be used. On-line methods can be based on optimal filters such as Kalman or  $H_\infty$  filter. The so-called two serially-connected Kalman filters [Arn98] or the two serially-connected  $H_\infty$  filters [Cai04] provide biased parameter estimation, since they estimate the M-AR parameters directly from the noisy observations. The EKF and SPKF can jointly estimate the M-AR process and its parameters and provide consistent parameters estimates. However, the state vector to be estimated has large size. To avoid this drawback, we propose to extend the CC-Kalman filters [Lab06] initially proposed for speech enhancement to the multichannel case. This method provide consistent estimation of the parameters. However, Kalman filter requires that the driving processes and the additive noise to be white Gaussian with known variances. To relax these assumptions, we propose to extend the CC- $H_\infty$  filters [Lab07] to the multichannel case. This method provide robust estimation of the parameters in the case of under or over estimating the noise variances.

The accuracy of the estimated M-AR parameters are affected by several factors:

1. The SNR: the higher the SNR is the better the estimation accuracy.
2. The sample size: the larger sample size is the better the estimation accuracy.
3. The farness of the M-AR poles from the unit circle: the far the poles from the unit

circle the better the estimation accuracy.

4. The closeness of the initializations to the true values: the close initializations to the true values the better the estimation accuracy.

The effect of the above factors on the estimation accuracy depends on the estimation algorithm itself. According to the comparative simulation study we carried out, we can draw the following conclusions about the estimation algorithms studied in this thesis:

The estimated parameters produced by the ARFIT and YW equations are far from the true values, mainly, when complex processes are used. The SC-Kalman filters provide biased estimated parameters similar to the case of ARFIT and YW equations.

Hassan's algorithm provides more accurate estimates than ARFIT, YW equations and SC-Kalman filters, since it compensate for the additive noise variances. However, it may provide estimates which correspond to unstable systems, mainly at low SNR or small samples. In addition, it has high computational cost.

The NCYW equations, CC-Kalman filters and CC- $H_\infty$  filters provide accurate estimates when the true driving process and additive noise covariance matrices are used. However, when the driving process and the measurements covariance matrices are estimated (overestimated or underestimated), the accuracy of the estimated parameters degrades.

When the difference between the estimate and the true noise covariance matrices is large, then the accuracy of the estimated parameters will not be affected much when using the CC- $H_\infty$  filters. Thus, the CC- $H_\infty$  filters is robust to the deviation in the estimation of the noise covariance matrices. This is not the case when using CC-Kalman filters or the NCYW equations.

When comparing the CC-Kalman filters and CC- $H_\infty$  filters with the other exiting M-AR parameter estimation methods, they provide a compromise between the estimation accuracy and computational cost. If the driving processes and additive noise are Gaussian with known covariance matrices, we recommend to use the CC-Kalman filters. If these assumptions are violated, we recommend to use the CC- $H_\infty$  filters.

## 4.2 Future Work

In the thesis, we propose to extend the CC-Kalman filters and the CC- $H_\infty$  filters initially proposed for single channel applications to the multichannel case. We carried out a simulation using both synthetic M-AR process and realistic M-AR process corresponds

to mobile fading channels. The simulation results show that the CC-Kalman filters and CC- $H_\infty$  filters provide accurate estimates of the M-AR parameters.

Our recommendations for future work are as follows:

- The relevance of CC-Kalman filters and CC- $H_\infty$  filters for the estimation of time-varying fading channels, with application to OFDM systems have been investigated by Ahmad in [Abd08]. However, the author assumes that the fading channels are uncorrelated. In the case of correlated fading channels in OFDM systems, the fading processes should be modeled by M-AR process and could be estimated by the approach we developed in this thesis.
- The proposed methods can also be used for the estimation of correlated channels estimation when designing the diversity receivers for CDMA systems.

## Acronyms and Abbreviations

EEG	ElectroEncephaloGram
EEG	ElectroCardioGram
GPS	Global Position System
TAN	Terrain Aided Navigation
INS	Inertial Navigation System
LOS	Line-Of-Sight
WSS	Wide Sense Stationary
SSS	Strict Sense Stationary
ISI	Inter Symbol Interference
PDF	Probability Density Function
VAR	Vector AutoRegressive
MIMO	Multiple Input Multiple Output
ARMA	AutoRegressive Moving Average
MA	Moving Average
AR	AutoRegressive
M-AR	Multichannel AutoregRessive
OFDM	Orthogonal Frequency Division Multiplexing
OFDMA	Orthogonal Frequency Multiple Access
DS-CDMA	Direct-Sequence Code Division Multiple Access
3G	3rd Generation
WiMAX	Worldwide Interpretability for Microwave Access
ACF	AutoCorrelation Function
LQE	Linear Quadratic Estimation
CCF	Cross-Correlation Function
AWGN	Additive White Gaussian Noise
CLT	Central Limit Theorem
EIV	Errors-In-Variables
EKF	Extended Kalman Filter
SPKF	Segma Point Kalman Filter
UKF	Uncented Kalman Filter

LMS	Least Mean Square
LS	Least Square
ML	Maximum Likelihood
MMSE	Minimum Mean Square Error
MSE	Mean Square Error
NRYW	Newton-Raphson Yule-Walker
NCYW	Noise-Compensated Yule-Walker
NLMS	Normalized Least Mean Square
PSD	Power Spectral Density
RLS	Recursive Least Square
SNR	Signal-to-Noise Ratio
YW	Yule-Walker
CC-Kalman	Two Cross-Coupled Kalman
CC- $H_\infty$	Two Cross-Coupled $H_\infty$
ILSV	Improved Least Square for Vector Processes

# Notations

$\cdot$	matrices dot product
$E[\cdot]$	expectation operator
$\text{diag}[\cdot]$	diagonal matrix
$\det[\cdot]$	determinant
$\text{Re}(\cdot)$	real part
$\text{Im}(\cdot)$	imaginary part
$\delta(\cdot)$	dirac delta function
$\exp(\cdot)$	exponential function
$\otimes$	the matrices Kronecker product
$J_0(\cdot)$	zero-order Bessel function of the first kind
$\ \cdot\ $	Euclidean norm
$ \cdot $	absolute value
$\min(\cdot)$	minimum
$\max(\cdot)$	maximum
$\sup$	supremum
$(\cdot)^*$	complex conjugate
$(\cdot)^T$	transpose
$(\cdot)^H$	hermitian (complex conjugate transpose)
$(\cdot)^{-1}$	inverse
$\nabla$	gradient
$j$	$\sqrt{-1}$
$\hat{x}$	estimate of $x$
$\sigma_x^2$	variance of $x$
$\mathbf{x}$ or $\mathbf{X}$	vector or matrix
$\mathbf{0}_p$	zero vector of size $p \times 1$
$\mathbf{I}_p$	identity matrix of size $p \times p$
$T$	the periodic signal duration
$m_x(k)$	mean of $x(k)$
$\sigma_x^2(k)$	variance of $x(k)$
$C_x(k, l)$	autocovariance of $x(k)$

$R_x(k, l)$	autocorrelation of $x(k)$
$Y(z)$	the z-transform of $y(k)$
$H(z)$	the transfer function
$q$	MA model order
$\{b_l\}_{l=1, \dots, q}$	MA model parameter
$\mathbf{u}(k)$	driving processes vector
$\mathbf{v}(k)$	the additive noise vector
$\Sigma_u$	the driving processes covariance matrix
$\Sigma_v$	the additive noise covariance matrix
$\mathbf{Q}_u, \mathbf{R}_v$	weighting parameters in the $H_\infty$ filter
$\mathbf{V}$	cross-correlation matrix
$\mathbf{A}$	concatenation of M-AR model parameters
$\mathbf{G}$	the lower matrix of Cholesky factorization
$\mathbf{z}(k)$	white Gaussian noise
$\rho_{rs}$	the cross-correlation coefficient
$f_m$	Doppler rate
$\Delta w_{rs}$	the angular frequency separation
$\sigma_T$	delay spread of the wireless channel
$\Lambda$	the cross-correlation coefficient matrix
$\Delta$	the bandwidth of the base station
$\mathbf{A}(z)$	numerator of $\mathbf{H}(z)$
$\mathbf{B}(z)$	denominator of $\mathbf{H}(z)$
$T_m$	channel maximum delay spread
$B_c$	channel coherence bandwidth
$T_b$	bit duration
$1/T_b$	sample rate
$T_c$	chip duration of wide-band single-carrier DS-CDMA system
$W$	signal bandwidth
$W_M$	bandwidth of each carrier signal in MC-DS-CDMA system
$W_0$	bandwidth of wide-band single-carrier DS-CDMA system
$L_p$	number of resolvable paths in multi-path fading channel

---

$L_s$	number of scatterers in frequency-flat fading channel
$\nu$	mobile station speed
$\varphi$	angle of arrival
$f_c$	carrier frequency
$c$	light speed
$f_D$	Doppler frequency
$f_d$	maximum Doppler frequency
$f_i$	the $i^{th}$ carrier frequency
$f_d T_b$	Doppler rate
$W_0$	the total bandwidth of the transmitted signals
$f$	frequency
$T_c$	channel coherence time
$T_s$	symbol duration
$L_s$	maximum number of resolvable paths
$h_m(k)$	complex fading process at the $m^{th}$ carrier in the $k^{th}$ bit interval
$h_m^{(R)}(k)$	real part of the fading process
$h_m^{(I)}(k)$	imaginary part of the fading process
$\sigma_h^2$	fading process variance
$g_{ml}$	random amplitude associated with the $l^{th}$ scatterer and the $m^{th}$ carrier
$\varphi_{ml}$	random angle of arrival associated with the $l^{th}$ scatterer and the $m^{th}$ carrier
$\vartheta_{ml}$	random initial phase associated with the $l^{th}$ scatterer and the $m^{th}$ carrier
$\tilde{h}$	the envelope of fading process
$R_{hh}(i)$	the autocorrelation of the fading process at lag $i$
$p$	M-AR model Order
$M$	number of channels of M-AR process
$N$	number of available data samples
$\mathbf{h}(k)$	M-AR fading processes vector
$\mathbf{R}_{hh}$	M-AR model covariance matrix
$R_{hh}(k)$	ACF of the channel
$\Psi(f)$	PSD of the channel
$\tau_k$	time delay of the $k^{th}$ signal

$\epsilon$	very small positive constant
$\gamma$	disturbance attenuation level in the $H_\infty$ algorithm
$\{a_l\}_{l=1,\dots,p}$	AR model parameters
$\{\mathbf{A}^{(l)}\}_{l=1,\dots,p}$	M-AR model parameter matrices
$\boldsymbol{\theta}$	M-AR parameter vector
$\Phi$	Companion matrix containing the M-AR parameters
$\mathbf{b}(k)$	innovation processes
$\mathbf{h}(k)$	the state vector
$\hat{\mathbf{h}}(k/k-1)$	<i>a priori</i> estimate of $\mathbf{h}(k)$ given $k-1$ observations
$\hat{\mathbf{h}}(k/k)$	<i>a posteriori</i> estimate of $\mathbf{h}(k)$ given $k$ observations
$\mathbf{K}(k)$	Kalman filter gain at time $k$
$\underline{\mathbf{K}}(k)$	$H_\infty$ filter gain at time $k$
$\mathbf{P}(k/k-1)$	<i>a priori</i> covariance matrix of the state vector error
$\mathbf{P}(k/k)$	<i>a posteriori</i> covariance matrix of the state vector error
$\underline{\mathbf{P}}(k)$	the covariance matrix of the state vector error in the $H_\infty$ filter
$\{\sigma_{vi}^2\}_{i=1,\dots,M}$	measurement noise variances on the $i^{\text{th}}$ channel
$\{\sigma_{ui}^2\}_{i=1,\dots,M}$	driving processes variances
$\{\sigma_{hi}^2\}_{i=1,\dots,M}$	fading processes variances

## Appendix A

### Spatial correlation of MIMO system

Consider  $2 \times 2$  MIMO fading channel scenario involving transmission by a dual-antenna, under the assumption of 2-D isotropic scattering at the receiver antenna, the ACF for each channel is identically given by (1.36), and the CCFs are given as follows:

$$R_{h_{11}h_{21}}(m) = R_{h_{12}h_{22}}(m) = J_0(\{a^2 + b^2 - 2ab \cos(\beta - \varrho)\}^{\frac{1}{2}}) \quad (4.1)$$

$$R_{h_{11}h_{12}}(m) = R_{h_{21}h_{22}}(m) = J_0(\{a^2 + c^2\Delta^2 - 2ac\Delta \sin(\alpha) \sin(\varrho)\}^{\frac{1}{2}}) \quad (4.2)$$

$$R_{h_{11}h_{22}}(m) = R_{h_{12}h_{21}}(m) = J_0(\{a^2 + b^2 + c^2\Delta^2 - 2ab \cos(\beta - \varrho) - 2c\Delta \sin(\alpha)[a \sin(\varrho) - b \sin(\beta)]\}^{\frac{1}{2}}) \quad (4.3)$$

where  $a = 2\pi f_d |k|$ ,  $b = 2\pi d/\lambda$ ,  $c = 2\pi\delta/\lambda$ ,  $d$  denotes the distance between the receiver antennas,  $\delta$  denotes the separation between base antennas,  $\Delta$  specifies the bandwidth at the base, and  $\alpha, \beta$  and  $\varrho$  are angles which specify the orientation of the base station, mobile arrays and the direction of user motion, respectively.

## Appendix B

**Property:**

The M-AR parameter matrices are diagonal when the cross correlation matrix is symmetric (i.e.,  $\rho_{rs} = \rho_{sr}$ ).

**Proof:**

Assume first order M-AR fading processes and  $\rho_{rs} = \rho_{sr}$ , the following two equations hold:

$$R_{h_r h_s}(0) = R_{h_s h_r}(0) = \begin{cases} 1, & \text{if } r = s \\ \rho_{rs}, & \text{if } r \neq s \end{cases} \quad (4.4)$$

$$R_{h_r h_s}(1) = R_{h_s h_r}(1) = \begin{cases} J_0(2\pi f_d), & \text{if } r = s \\ \rho_{rs} J_0(2\pi f_d), & \text{if } r \neq s \end{cases} \quad (4.5)$$

Writing Yule-Walker equation for this system using (1.41) as follows:

$$\underbrace{\begin{pmatrix} 1 & \rho_{12} & \cdots & \rho_{1M} \\ \rho_{12} & 1 & \cdots & \rho_{2M} \\ \vdots & \vdots & \ddots & \vdots \\ \rho_{1M} & \rho_{2M} & \cdots & 1 \end{pmatrix}}_{\mathbf{\Lambda}} \underbrace{\begin{pmatrix} a_{11}^{(1)} & a_{12}^{(1)} & \cdots & a_{1M}^{(1)} \\ a_{21}^{(1)} & a_{22}^{(1)} & \cdots & a_{2M}^{(1)} \\ \vdots & \vdots & \ddots & \vdots \\ a_{M1}^{(1)} & a_{M2}^{(1)} & \cdots & a_{MM}^{(1)} \end{pmatrix}}_{\mathbf{A}} = -J_0(2\pi f_d) \underbrace{\begin{pmatrix} 1 & \rho_{12} & \cdots & \rho_{1M} \\ \rho_{12} & 1 & \cdots & \rho_{2M} \\ \vdots & \vdots & \ddots & \vdots \\ \rho_{1M} & \rho_{2M} & \cdots & 1 \end{pmatrix}}_{\mathbf{\Lambda}} \quad (4.6)$$

Compute  $\mathbf{A}$  using the above equation as follows:

$$\mathbf{A} = -J_0(2\pi f_d) \mathbf{\Lambda}^{-1} \mathbf{\Lambda} = -J_0(2\pi f_d) \mathbf{I}_M \quad (4.7)$$

where  $\mathbf{I}_M$  is  $M \times M$  identity matrix.

We can note that the parameter matrix  $\mathbf{A}$  is diagonal.













# Bibliography

- [Abd08] Ahmad Z. Abdo. – *Estimation of autoregressive time-varying fading channels: application to OFDM systems*, M.Sc. Thesis, Al-Quds University, Jerusalem-Palestine, 2008.
- [Arn98] Matthias Arnold, Wolfgang H.R. Miltner, Herbert Witte, Reinhard Baur, Christoph Braun. – Adaptive AR modeling of nonstationary time series by means of Klamann filtering. *IEEE Trans. on Biomedical Engineering*, vol. 45, no.5, May 1998, pp. 553–562.
- [Bad04] Kareem E. Baddour, Norman C. Beaulieu. – Accurate simulation of multiple cross-correlated Rician fading channels. *IEEE Trans. on Communications*, vol. 52, no.11, November 2004, pp. 1980–1987.
- [Bad05] Kareem E. Baddour, Norman C. Beaulieu. – Autoregressive modeling for fading channel simulation. *IEEE Trans. on Wireless Communications*, vol. 4, no.4, July 2005, pp. 1650–1662.
- [Bek06] Ilya Bekkerman, Joseph Tabikyan. – Target detection and localization using MIMO radar and sonar. *IEEE Trans. on Signal Processing*, vol. 54, no.10, October 2006, pp. 3873–3883.
- [Bob07] W. Bobillet, R. Diversi, E. Grivel, R. Guidorzi, M. Najim, U. Soverini. – Speech enhancement combining optimal smoothing and errors-in-variables identification of noisy ar processes. *IEEE Trans. on Signal Processing*, vol. 55, no.2, 2007, p. 5564–5578.
- [Bul98] Selaka B. Bullumulla, Saleem A. Kassam, Santosh S. Venkatesh. – An adaptive diversity receiver for OFDM in fading channels. *Proceeding of IEEE-ICC98*, pp. 325–329, Georgia, Atlanta, June 1998.

- [Cai04] Jun Cai, Xuemin Shen, Jon W. Mark. – Robust channel estimation for OFDM wireless communication systems-an  $H_\infty$  approach. *IEEE Trans. on Wireless Communications*, vol. 3, no.6, November 2004, pp. 2060–2071.
- [Che99] Zuo. Dian Chen, Ruey-Feng Chang, Wen-Jia Kuo. – Adaptive predictive multiplicative autoregressive model for medical image compression. *IEEE Trans. on Medical Imaging*, vol. 18, no.2, February 1999, pp. 181–184.
- [Che04] Wei Chen, Ruifeng Zhang. – Estimation of time and frequency selective channels in OFDM systems: A Kalman filter structure. *Proceeding of IEEE-GLOBECOM*, pp. 800–803, Dallas, Texas, December 2004.
- [Cla68] R. H. Clarke. – A statistical theory of mobile radio reception. *Bell Labs System Technical Journal*, vol. 47, July-August 1968, pp. 957–1000.
- [Dav01] Carlos E. Davila. – On the noise-compensation Yule-Walker equations. *IEEE Trans. on Signal Processing*, vol. 49, no.6, June 2001, pp. 1119–1121.
- [Fer04] Adam C. Ferguson, Curt H. Davis, Joseph E. Cavaugh. – An autoregressive model for analysis of ice sheet elevation change time series. *IEEE Trans. on Geoscience and Remote Sensing*, vol. 42, no.11, November 2004, pp. 2426–2436.
- [Gib74] Jerry D. Gibson, Stephen K. Jones, James L. Melsa. – Sequentially adaptive prediction and coding of speech signals. *IEEE Trans. on Wireless Communications*, vol. 22, no.11, November 1974, pp. 1789–1797.
- [Gon06] Junbin Gong, Hongbo Xu, Jinwen Tian, Hua Cheng, Zhang. – Adaptive fused Kalman filter based on imaging lasar radar for TAN. *Proceeding of SPIE-ISSN*, Wuhan, China, November 15–17 2006.
- [Gul01] Inan Guler, M. Kemal Kiyimik, Mehmet Akin, Ahmet Alkan. – AR spectral analysis of EEG signals by using maximum likelihood. *Computers in Biology and Medicine*, vol. 31, no.6, 2001, pp. 441–450.
- [Has93] Babak Hassibi, Ali Sayed, T. Kailath. – LMS is  $H_\infty$  optimal. *Proceeding of IEEE-32nd Conference on Decision and Control*, pp. 74–80, San Antonio, Texas, December 1993.

- [Has03] Md. Kamrul Hassan, Md. Jahangir Hossain, Md. Aynal Haque. – Parameter estimation of multichannel autoregressive processes in noise. *Signal Processing*, vol. 83, no.3, March 2003, pp. 603–610.
- [Hay96] Monson Hayes. – *Statistical Digital Signal Processing and Modeling*, Wiley, 1996.
- [Hay00] Simon Haykin. – *Communication Systems*, Wiley, 4th edition, 2000.
- [Hay02] Simon Haykin. – *Adaptive Filter Theory*, Prentice Hall, 4th edition, 2002.
- [Jak94] William C. Jakes. – *Microwave Mobile Communications*, Wiley-IEEE Press, January 1994.
- [Jam07a] Ali Jamoos. – *Contribution on receiver design and channel estimation for multi-carrier DS-CDMA mobile systems*, PHD dissertation, Bordoux University, France, 2007.
- [Jam07b] Ali Jamoos, Ahmad Abdo, Hanna Abdel Nour. – Estimation of OFDM time-varying fading channels based on two-cross-coupled Kalman filters. *Springer*, December 2007, pp. 287–292.
- [Jam08] Ali Jamoos, Eric Grivel, Nicolai Christov. – Estimation of autoregressive fading channels based on two cross-coupled  $H_\infty$  filters. *SIViP*, November 2008.
- [Jam09] Ali Jamoos, Eric Grivel, Nidal Shakarneh, Hanna Abdel Nour. – Dual  $H_\infty$  vs dual Kalman filters for parameter estimation from noisy observations. *Accepted to European Signal Processing Conference (EUSIPCO)*, Glasgow, Scotland, August 2009.
- [Kay79] Steven M. Kay. – The effects of noise on the autoregressive spectral estimator. *IEEE Trans. on Acoustics, Speech, and Signal Processing*, vol. 27, no.5, October 1979, pp. 478–485.
- [Kay80] Steven M. Kay. – Noise compensation for autoregressive spectral estimation. *IEEE Trans. on Acoustics, Speech, and Signal Processing*, vol. 28, no.3, June 1980, pp. 292–303.
- [Lab06] D. Labarre, E. Grivel, Y. Berthoumieu, E. Todini, M. Najim. – Consistent estimation of autoregressive parameters from noisy observations based on two interacting Kalman filters. *Signal Processing*, vol. 86, 2006, pp. 2863–2876.

- [Lab07] David Labarre, Eric Grivel, Mohamad Najim, Nicolai Christov. – Dual  $H_\infty$  algorithm for signal processing application to speech enhancement. *IEEE Trans. on Signal Processing*, vol. 55, no.11, November 2007, pp. 5195–5208.
- [Mah08] Alimorad Mahmoudi, Mahmood Karimi. – Estimation of the parameters of multichannel autoregressive signals from noisy observations. *Signal Processing*, vol. 88, no.11, November 2008, pp. 2777–2783.
- [Neu01] Arnold Neumaier, Tapio Schnieder. – Estimation of parameters and eigenmodes of multivariate autoregressive models. *ACM Trans. on Mathematical Software (TOMS)*, vol. 27, no.1, March 2001, pp. 27–57.
- [Nis04] Mauri Nissila, Subbarayan Pasupathy. – Joint estimation of frequency offset and fading rate in multipath fading channel using autoregressive channel modeling. *Proceeding of IEEE-VTC04*, pp. 1063–1067, Milan, Italy, May 17–19, 2004.
- [Per04] Eduardo Hornandez Perez, Juan L. Navarro Mesa, Maria J. Millan Munoz. – An approach to maximum likelihood identification of autoregressive marine mammal sources by passive sonar. *Proceeding of IEEE-IGARSS04*, pp. 1435–1438, Anchorage, Alaska, September 2004.
- [Pet09a] J. Petitjean, R. Diversi, E. Grivel, R. Guidrozi, P. Roussilhe. – Recursive error-in-variables approach for ar parameter estimation from noisy observations. application to radar sea clutter rejection. *Proceeding of IEEE-ICASSP09*, pp. 3401–3404, Taipei, Taiwan, January 2009.
- [Pet09b] Julien Petitjean, Eric Grivel, William Bobillet, Patrick Roussilhe. – Multichannel AR parameter estimation from noisy observations as an error-in-variable issue. *Signal, Image and Video Processing Journal, Springer*, March 2009, pp. 1863–1711.
- [Pie04] Mathieu St. Pierre, Denis Gingras. – Comparison between the unscented Kalman filter and the extended Kalman filter for the position estimation module of an integrated navigation information system. *Proceeding of IEEE-Intelligent Vehicles*, pp. 831–835, Parma, Italy, June 2004.
- [Pop01] Maruis F. Pop, Norman C. Beaulieu. – Limitations of sum-of-sinusoids fading channel simulators. *IEEE Trans. on Communications*, vol. 49, no.4, April 2001, pp. 699–708.

- [Pro00] Riccardo Provsì, Gain Antonio Zanetta. – The extended Kalman filter in the frequency domain for the identification of mechanical structures excited by sinusoidal multiple inputs. *Mechanical Systems and Signal Processing*, vol. 14, no.3, May 2000, pp. 327–341.
- [Rab89] Lawrence R. Rabiner. – A tutorial on hidden Markov models and selected application in speech recognition. *Proceeding of IEEE*, vol. 77, no.2, February 1989, pp. 257–286.
- [She97] Xuemin Shen, Li Deng. – Game theory approach to discrete  $H_\infty$  filter design. *IEEE Trans. on Signal Processing*, vol. 45, no.4, April 1997, pp. 1092–1095.
- [Sk197] Bernard Sklar. – Rayleigh fading channels in mobile digital communication systems part I: Characterization. *IEEE Communications Mag.*, vol. 35, no.7, July 1997, pp. 90–100.
- [Sor06] Siamak Sorooshyari, David G. Daut. – On the generation of correlated Rayleigh fading envelopes for accurate simulation of diversity channels. *IEEE Tran. on Communications*, vol. 54, no.8, August 2006, pp. 1381–1386.
- [Tra05] Le Chung Tran, Tadeusz A. Wysocki, Alfred Mertins, Jennifer Seberry. – A generalized algorithm for the generation of correlated Rayleigh fading envelopes in wireless channels. *EURASIP Journal on Wireless Communications and Networking*, vol. 5, July 2005, pp. 801–815.
- [Ube08] Elif Derya Ubelyi, Dean Cvetkovic, Irena Cosmic. – AR spectral analysis technique for human PPG, ECG and EEG signals. *Journal of Medical Systems*, vol. 32, no.3, June 2008, pp. 201–206.
- [Xia06] Chengshan Xiao, Yahong Rosa Zheng, Norman C. Beaulieu. – Novel sum-of-sinusoids simulation models for Rayleigh and Rician fading channels. *IEEE Trans. on Wireless Communications*, vol. 5, no.12, December 2006, pp. 3667–3679.
- [Xu09] Zhemin Xu, Sana Sfar, Rick S. Blum. – Analysis of MIMO systems with receive antenna selection in specially correlated Rayleigh fading channels. *IEEE Trans. on Vehicular Technology*, vol. 58, no.1, January 2009, pp. 251–262.
- [Zei98] Rodger E. Zeimer, William H. Tranter, D. Ronald Fannin. – *Signals and Systems: Continuous and Discrete*, Tom Robbins, Fourth edition, 1998.

- [Zhe05] Wei Xing Zheng. – Fast identification of autoregressive signals from noisy observations. *IEEE Trans. on Circuit and Systems II: Express Briefs*, vol. 52, no.1, January 2005, pp. 43–48.